Scattering of Radio Waves

by High Atomic Rydberg States

by
Thomas Smid

as published in
Radio Science 28,3,361,S93-001,1993

For enquiries go to http://www.plasmaphysics.org.uk/feedback.htm

Contents **page**

Abstract

The scattering coefficient of highly excited atomic levels formed by recombination from a plasma and energetically broadened by plasma field fluctuations is determined. For this purpose, the population of the levels is calculated from a detailed balance equation which is solved consistently together with the corresponding equation for the free electron spectrum. All relevant quantum mechanical cross sections and decay constants as well as the elastic electron scattering cross sections are hereby derived from first principles in a form directly suitable for numerical application.

A special emphasis in the theoretical treatment is laid on the problem of the determination of the energetical level broadening for a given plasma density and -energy , because the spectral line width of a discrete transition is the crucial quantity affecting the resultant scattering coefficient as a function of frequency, and because usual theoretical approaches concerning Stark broadening are either inconsistent or insufficient for the present purpose. Furthermore, as a new aspect concerning the interaction of radiation with atoms, the effect of a finite wave field strength (compared to the plasma fluctuation field) and the wave coherence on the photoionization cross section is considered as an important mechanism which has to be taken into account in a complete and consistent theory.

Numerical results are obtained for initial values appropriate for ionospheric conditions. The solution proves to be in no way related to LTE- situations, therewith invalidating usual treatments of the problem, which are not consistently based on a detailed balance approach.

With the present theory, the scattering coefficient for radio waves (in particular for frequencies < 100 MHz) turns out to depend sensitively on the electron impact- and (radio-)photo -ionization frequencies since they determine the level population for high quantum numbers (this offers for instance a straightforward explanation for the so called ionospheric 'short wave fadeout' which is observed in connection with solar radio bursts).

The theoretical result for the equilibrium coefficient for resonant scattering of radio waves by Rydberg atoms is consistent with experimental data obtained from the ionosphere. This suggests that the considered mechanism is exclusively responsible for the scattering of radio waves in particular and electromagnetic radiation in general.

1. Introduction

Though being generally of little importance for the overall energy and radiation budget in natural plasmas, atoms in highly excited states may become significant and observable if energies very small compared to the average plasma energy are being examined.
From a variety of astrophysical objects for example, such as HII-regions, planetary nebulae and galaxies, line transitions up to quantum numbers as high as n=350 have been detected by means of radio telescopes. These observations are being used to derive physical properties of these objects like density and temperature.
The observed line radiation related to the excited states is generally due to spontaneous decay to lower lying states, whereby the intensity of the lines is proportional to the level population (the usual designation of these lines as 'recombination lines' is therefore somewhat inaccurate, since one is not dealing with photons related to the radiative recombination process (bound-free transitions) but to bound-bound transitions following radiative capture into high levels).
On the other hand, the non-zero density of atoms in high levels also provides the chance that radiation with a frequency corresponding to the energy difference between those states may be resonantly scattered exactly analogous to transitions involving the ground state. This possibility has so far been neglected in the literature concerning the physics of highly excited atomic states.
Several aspects have to be considered for calculating the scattering efficiency of Rydberg states correctly:
a) for the determination of the production rate for each level: a non-LTE calculation of the energy distribution of free plasma electrons for energies as small in value as the energy of this bound state; the radiative recombination cross sections and decay constants for those continuum energies and discrete levels; the rate of elastic collisions interfering with the recombination process and cascading between the bound states ;
b) for the loss processes: knowledge of the life time of each level with regard to radiative decay to lower levels; collisional -and photo -ionization out of these states;
c) determination of the level broadening by plasma field fluctuations which enables line scattering even if the wave frequency does not match the transition frequency to within a natural or Doppler linewidth;
d) the resonance scattering cross section involving two states;
e) a weighted summation of the resultant scattering coefficient over all broadened states;
f) (in connection with b)): the dependence of the photoionization cross section upon the field strength and coherence of the wave field .
In the present literature, points a) and b) are usually treated only by methods relating to LTE-approximations**.**
For the case of low density plasmas and quantum states $n \leq 10$, it has however already been shown by means of a detailed balance approach (Smid, 1987) that the LTE- concept lacks completely a physical justification. The method developed there will be extended for the present purpose to the appropriate energy range and quantum numbers.
Some confusion exists presently still also about the degree of line broadening by plasma

field fluctuations, which is for instance reflected in the discussion of corresponding astronomical observations. This indicates also the necessity for a different theoretical approach to this problem.
Since a consistent theoretical treatment of the relevant atomic processes (photoionization, radiative recombination, resonance scattering) is not available in the generally accessible literature, it is given here in suitable form in a separate appendix section, based on the approach used in the thesis of Smid (1987). The same holds for the problem of elastic electron- electron -(Coulomb-) scattering which is relevant for calculating the free-free and bound-free collision rates.

Numerical results are primarily obtained for physical situations corresponding to scattering of radio waves in the ionosphere and (where it is possible) compared to experimental data, but there is also a reference to astrophysical plasmas since transitions between high Rydberg states are a more or less well known phenomenon in this area of research and numerous high resolution measurements of the radio emission of astronomical objects exist which can aid as a test of the theory.

2. Theory

2.1 Determination of the Level Population in Detailed Balance Equilibrium

In detailed balance equilibrium, the density of atoms in the excited state n (where n=1 shall designate the atoms ground state, i.e. n is the effective quantum number) is given by the quotient of the production rate and loss (depopulation) frequency

$$N_n = q_n/\nu_n^{loss} \quad . \qquad \textbf{(1)}$$

The production rate consists of the primary production rate due to radiative recombination q_n^{Rec} and a secondary rate due to cascading from higher levels, that is

$$q_n = q_n^{Rec} + q_n^{casc} \quad . \qquad \textbf{(2)}$$

Induced excitation from lower levels by radiation or collisions is neglected here because the cross section for a resonant transition from level n-Δn to n (n>>1; Δn<<n) decreases like $(\Delta n)^{-3}$ (as it follows from Eq.**(A.1.15)**) and limits thus eventual transitions to neighboring states for which, however, the production and loss rates will be almost the same (at least for natural conditions) so that the effect cancels out.

In the absence of collisions interfering with the recombination process, the first term in Eq.**(2)** is given by

$$q_n^{Rec,0} = \eta_n^{Rec} \cdot \mathcal{N}_p \cdot \int_0^\infty d\varepsilon \; \mathcal{N}_e(\varepsilon) \cdot \sigma_n^{Rec}(\varepsilon'(\varepsilon,\varepsilon_I)) \cdot v'(\varepsilon,\varepsilon_I) \quad , \qquad \textbf{(3)}$$

where ε is a dimensionless energy variable characterizing the energy of the free plasma electron in the laboratory system (as defined by the center of mass of the ions), $\mathcal{N}_p$ the total plasma (ion) density which is related to the energy specific electron density distribution function $\mathcal{N}_e(\varepsilon)$ by the condition of quasi neutrality of the plasma

$$\mathcal{N}_p = \int_0^\infty d\varepsilon \; \mathcal{N}_e(\varepsilon) \quad . \qquad \textbf{(4)}$$

Furthermore, $v'(\varepsilon,\varepsilon_I)$ is the relative velocity between the recombining electron and an ion of average energy ε_I in the laboratory system, $\sigma_n^{Rec}(\varepsilon'(\varepsilon,\varepsilon_I))$ the recombination cross section into level n for the corresponding relative kinetic energy ε' (see Eqs.**(11)** and **(12)**) and η_n^{Rec} a reduction factor which takes the Stark broadening of the level n into account if this becomes comparable to the level energy (see Sect.2.3, Eq.**(79)**).

However, Eq.**(3)** neglects the fact that the recombination process does not proceed infinitely fast but within a finite time given by the effective quantum mechanical decay constant (see Appendix A, Eq.**(A.2.19)**)

$$A_n^{Rec} = 7 \cdot 10^4 \cdot n^{-3.4} \qquad [sec^{-1}] \qquad \textbf{(5)}$$

and can thus be interrupted by energy changing collisions with the other plasma electrons. In order to describe this effect correctly, one has to make assumptions about the details of the recombination process, because it represents a fundamental problem that the decay time of the continuum electron into a bound state is many orders of magnitude larger than the time the electron spends in the vicinity of the ion (as given by the quantum mechanical wave function for the level n).
It is therefore assumed here that the electron first 'recombines' radiationless into a 'pre-bound' state η ($|n| = |\eta|$) within a sufficiently short time and then decays into the actual state n according to the constant A_n^{Rec} under emission of a photon with a frequency corresponding to the energy difference between the initial energy of the free electron and the bound level n (it is beyond the scope of this paper and requires further basic theoretical work to answer the question, how energy is conserved during this two stage process; it should be obvious, however, that this model is the only physically reasonable one considering the different time scales involved in the problem).
The density in the 'pre-bound' state η is then given by

$$N_\eta = q_n^{Rec,0} / (A_n^{Rec} + \nu_\eta^c) \quad . \qquad \textbf{(6)}$$

Apart from the decay to the actual bound state n (determined by A_n^{Rec}), a further loss for the 'level' η is assumed here to arise from elastic scattering by the bulk of plasma electrons (of density N_p and average energy ε_p) back into the continuum, which (for large n) occurs with a collision frequency

$$\nu_\eta^c = 1.2 \cdot 10^{-8} \cdot (N_p/\varepsilon_p) \cdot n \qquad [sec^{-1}] \quad , \qquad \textbf{(7)}$$

if one assigns classically to the state η the energy of the related actual quantum level n (Eq.**(7)** corresponds thus to the frequency for collisional ionization by electrons from the atomic level n; see Appendix B, Eq**.(B.20)**).
The recombinative production rate for level n is then

$$q_n^{Rec} = N_{//} \cdot A_n^{Rec} =$$
$$= \alpha_n^{Rec,c} \cdot q_n^{Rec,0} \quad , \qquad \textbf{(8)}$$

where

$$\alpha_n^{Rec,c} := A_n^{Rec} / (A_n^{Rec} + \nu_{//}^{c}) \qquad \textbf{(9)}$$

is the recombinative - collisional 'branching- ratio' for 'level' n (see also Fig.1 for a schematic illustration of this 'two-step' recombination model).

The relative quantities v' and ε' in Eq.**(3)** can usually be identified with the velocity and energy of the electron because of the small velocity of the ions related to their higher mass , and only for electron velocities within the core of the ion velocity distribution function does the latter become relevant. Since the velocity ratio between the ion of mass M and the electron of mass m is connected to their kinetic energy ratio through

$$v_I / v_e = \sqrt{ (m/M \cdot \varepsilon_I / \varepsilon) } \quad , \qquad \textbf{(10)}$$

and because v_I and ε_I shall represent here an average ion velocity and energy (as given by their thermal values for instance), one can therefore adopt in a simplifying manner

$$\varepsilon'(\varepsilon,\varepsilon_I) = \begin{cases} \varepsilon & \text{for } \varepsilon > \varepsilon_I.m/M \\ \varepsilon_I.m/M & \text{for } \varepsilon \le \varepsilon_I.m/M \end{cases} \quad , \qquad \textbf{(11)}$$

to which v' is related by

$$v'(\varepsilon,\varepsilon_I) = v_0 \cdot \sqrt{ \varepsilon'(\varepsilon,\varepsilon_I) } \quad , \qquad \textbf{(12)}$$

where

$$v_0 := v_e(\varepsilon=1) \qquad \textbf{(13)}$$

is the normalizing electron velocity (=$2.2 \cdot 10^8$ cm/sec if ε is in units of Rydberg).

With this, the recombination rate into level n becomes

$$q_n^{Rec} = \alpha_n^{Rec,c} \cdot \eta_n^{Rec} \cdot \mathcal{N}_p \cdot v_0 \cdot \int_0^{\infty} d\varepsilon \; \mathcal{N}_e(\varepsilon) \cdot \sigma_{\perp}^{Rec}(\varepsilon'(\varepsilon,\varepsilon_I)) \cdot \sqrt{\varepsilon'(\varepsilon,\varepsilon_I)} \quad . \qquad \textbf{(14)}$$

By assuming the integrand constant within subintervals $\varepsilon_{k-1}, \varepsilon_k$ (ε_0=0), one can finally write the discrete sum approximation

$$q_n^{Rec} = \alpha_n^{Rec,c} \cdot \sum_{k=1}^{\infty} \mathcal{N}_{e,k} \cdot v_{\perp,k}^{Rec,0} \quad , \qquad \textbf{(15)}$$

with

$$\mathcal{N}_{e,k} = (\varepsilon_k - \varepsilon_{k-1}) \cdot \mathcal{N}_e(\varepsilon_k) \qquad \textbf{(16)}$$

and

$$v_{\perp,k}^{Rec,0} = \mathcal{N}_p \cdot v_0 \cdot \sigma_{\perp}^{Rec}(\varepsilon'_k) \cdot \eta_n^{Rec} \cdot \sqrt{\varepsilon'_k} \quad , \qquad \textbf{(17)}$$

where the explicit argument of ε' has been dropped here .

Since the recombination cross section in Eq.**(17)** is a known quantity (see Appendix A.2) and the associated reduction factor due to excessive level broadening is independently derived in Sect.2.3 (Eq.**(79)**), the only unknown in Eq.**(15)** is the electron spectrum $\mathcal{N}_e(\varepsilon_k)$ which is determined in the separate Section 2.2 (although actually a set of coupled equations describing the densities in the discrete (N_n) and continuous energy region is being solved).

The loss frequency for the excited state n is given by the sum of the total spontaneous decay probability to lower levels A_n and the collisional (v_n^c) and photoionization (v_n^*) frequencies out of this state, that is

$$v_n^{loss} = A_n + v_n^c + v_n^* \quad , \qquad \textbf{(18)}$$

where

$$A_n = \sum_{m=1}^{n-1} A_{m,n} \quad ; \quad (n \geq 2) \qquad . \qquad \textbf{(19)}$$

The decay constant for a dipole transition from the upper level n to the lower level m can be numerically approximated by

$$A_{m,n} \approx 1.3 \cdot 10^9 \cdot m^{-1.8} \cdot (n-1)^{-3.2} \cdot \mathrm{Min}[1, m/(n-1)^{0.75}] \qquad [\mathrm{sec}^{-1}] \quad , \qquad \textbf{(20)}$$

where the last factor is a correction for contributions of higher angular momentum values considering the initial population of the level n due to recombination (see Appendix A.1, Eq.**(A.1.14)** and App.A.2, Eq.**(A.2.10)**).
(in the case n=2, Eq.**(20)** holds of course only for the 2p state, since the 2s level is metastable with regard to a decay into the (1s) ground state).
An explicit numerical evaluation of Eq.**(19)** shows that the total decay probability from level n can be approximated by

$$A_n \approx 1.1 \cdot 10^9 \cdot (n-1)^{-3.6} \qquad [\mathrm{sec}^{-1}] \qquad \textbf{(21)}$$

(one should note,however, that only Eq.**(19)** itself gives exact consistency with the cascading scheme Eq.**(30)**).

The collision frequency for ionization by plasma electrons is given by Eq.**(7)** (or Eq. **(B.20)**) and the photoionization frequency for level n is

$$\nu_n^* = \eta_n^{\mathrm{Ion}} \cdot \int_{f_n}^{\infty} df \; F^{\mathrm{ph}}(f) \cdot \sigma_n^{\mathrm{Ion}}(f) \qquad , \qquad \textbf{(22)}$$

where F^{ph} is the ionizing radiation flux at frequency f in photons/unit area/sec/unit frequency interval (f_n being the minimum (threshold) frequency for ionization of level n) and σ_n^{Ion} the ionization cross section for level n for which the symmetry property holds (see also Appendix A.2)

$$\sigma_n^{\mathrm{Ion}}(f) = \sigma_n^{\mathrm{Rec}}(\varepsilon(f)) \qquad , \qquad \textbf{(23)}$$

with

$$\varepsilon(f) = f/f_0 - \varepsilon_n \qquad ; \quad f \geq f_n \qquad \textbf{(24)}$$

where

$$\varepsilon_n = f_n / f_0 \quad , \qquad \textbf{(25)}$$

and f_0 is a unit frequency which provides the conversion to the dimensionless energy unit ε . It is convenient to choose f_0 to be the threshold frequency for ionization of the ground state of hydrogen ($3.2898 \cdot 10^{15}$ Hz) which normalizes ε to the energy of 1 Rydberg (13.6058 eV).
In the case of hydrogen, ε_n is then given by the Rydberg formula

$$\varepsilon_n^{H} = 1/n^2 \quad , \qquad \textbf{(26)}$$

which can also be considered to be a good approximation for other elements if n>>1, since highly excited states are hydrogenlike due to the large distances of the electron orbit from the atomic nucleus and the other atomic electrons (Eq.**(26)** holds for the case of singly excited neutrals (recombination of a singly ionized gas), which is the assumption throughout this paper; otherwise a factor Z^2, where Z is the degree of ionization, would occur).
The factor η_n^{Ion} in Eq.**(22)** takes into account that the ionization efficiency of a given radiation field may depend on its degree of coherence, its field strength and on disturbances by collisions with other particles during the ionization process. Because this topic has to go beyond the usual perturbation theory used for calculating the ionization cross section, it is discussed in the separate section 2.4 where the appropriate form for η_n^{Ion} is derived (Eq.**(91)**).

Eq.**(22)** can be discretized by transforming to the excess energy unit ε defined by Eq. **(24)** and assuming the integrand constant over subintervals $\varepsilon_{k-1}, \varepsilon_k$, so that

$$\nu_n^{*} = \eta_n^{Ion} \cdot \sum_{k=1}^{\infty} (\varepsilon_k - \varepsilon_{k-1}) \cdot F^{ph}(\varepsilon_k) \cdot \sigma_n^{Ion}(\varepsilon_k) \quad , \qquad \textbf{(27)}$$

where the normalization is now such that the photon flux has to be taken per energy interval $\Delta\varepsilon$, i.e.

$$F^{ph}(\varepsilon) = F^{ph}(f) \cdot f_0 \quad , \qquad \textbf{(28)}$$

as it follows from Eq.**(24)** (if $f_0 = 3.2898 \cdot 10^{15}$ Hz, $F^{ph}(\varepsilon)$ is thus in units of photons/Rydberg ; if the energy flux of the radiation is given instead of the photon flux, the former has to be transformed by means of Eq.**(94)**).

Through Eqs.**(1),(2),(15),(18),(21),(7)** and **(27)**, N_n is therefore determined if the production due to cascading is negligible, which is true for sufficiently high quantum numbers, because the decay constant becomes rapidly smaller with increasing n and ,on the other hand, the collision frequency increases.
Defining a quantum number n_0 such that the level population for $n=n_0+1$ can be determined without considering cascading, the cascading rate into level n_0 becomes thus

$$q_{n_0}^{casc} = \sum_{m=n_0+1}^{\infty} N_m \cdot A_{n_0,m} \quad , \qquad \textbf{(29)}$$

where $A_{n_0,m}$ is the spontaneous decay constant for transitions from level m to n_0 as given by Eq.**(20)** (note however the interchange of the variables designating the lower and upper state respectively, which arises from the convention used throughout this paper that the first subscript always indicates the lower state).
Repeating this procedure recursively for values $n=n_0-1$, n_0-2 ....etc. yields then the cascading rate into each level n via Eqs.**(1)** and **(2)** and

$$q_n^{casc} = \sum_{m=n+1}^{\infty} N_m \cdot A_{n,m} \quad . \qquad \textbf{(30)}$$

It should already be noted that, because of the very low densities N_m and the small cascading probabilities implied by Eq.**(20)** for high quantum numbers, q_n^{casc} tends to be much smaller than the primary production rate q_n^{Rec} . Only for sufficiently small values of n, for which the level population decreases strongly because of the rapidly increasing probability of decay to lower levels (Eq.**(21)**) and the resulting decreasing importance of collisions, does cascading become significant.

Compared to cascading, induced redistribution of the electrons (either by radiation or collisions) among the levels can be neglected, because , as already indicated below Eq. **(2)**, transitions are effectively limited to neighboring states for which (under natural conditions) the initial production and loss rates and therewith the occupation numbers are almost the same, so that the net effect of induced transitions between those states will be zero. Only for an extremely selective, coherent and powerful excitation, which can be achieved in laser applications for instance, could this process become significant.
One should also note that the collisional ionization of each level has been assumed here to be only due to free plasma electrons, i.e. the contribution of ions and neutrals to the loss

frequency (Eq.**(18)**) is considered as insignificant. This simplification is justified, because for all atomic levels of interest here the orbital velocity of the bound electron is much higher than the thermal velocity of ions and neutrals, which makes energy changing collisions with the latter very ineffective (see also Appendix B, Eq.**(B.25)**). In the case of neutrals, the ionization efficiency is especially small since the collision cross section is much smaller than for Coulomb scattering where σ_n^c increases proportional to the quantum number n due to the unscreened potential of the colliding particles (see Eq. **(B.15)**) .
Only if a very high neutral/plasma density ratio compensates for the small collision cross section, may the excited atom density be controlled by neutral constituents. With regard to the earths ionosphere, this may happen at D-region heights and below.

Concerning the applicability of the results obtained with a detailed equilibrium approach, one should be aware that one is essentially limited to situations where there is no variation in the physical parameters over the longest characteristic time scale entering into the problem, which is here given by the recombination constant A_n^{Rec} (Eq.**(5)**) and the elastic collision frequency ν_0^c (see Eq.**(B.23)**). Because this amounts up to many hours for those atomic levels and plasma densities of interest here, a relatively small increase in the loss frequencies ν_n^c or ν_n^* may lead to a considerable decrease in the level population N_n during a time interval small compared to this. A quantitative determination of these short term variations of N_n is therefore only possible by means of a time dependent consideration of the problem. On the other hand, the detailed balance approach may be applied in a quantitative sense even to non-stationary situations if only long term (several hours in this context) integrals or averages are being considered (see also Sect.3.5 and the discussion of the theoretical and experimental radar scattering coefficients in Sect.3.4.3).

2.2 Determination of the Plasma Electron Distribution Function

The energy distribution functions of the plasma electrons can be calculated from a balance equation including the production and loss rates due to photoionization, radiative recombination and inelastic and elastic collision processes. For ionospheric conditions and energies $\varepsilon>0.01$ ($\varepsilon=1 \cong 1$ Ry =13.6058 eV), it is almost exclusively determined by the first three processes, elastic (electron-electron) collisions being only of a secondary nature. Above approximately 3 eV ($\varepsilon\approx0.2$) inelastic collisions (with neutral constituents) constitute the main loss mechanism determining the electron spectrum, whereas for smaller energies the strongly increasing cross section for radiative recombination into high levels (see Appendix A.2) leads to a rapidly decreasing value of $\mathcal{N}_e^*(\varepsilon)$ (Smid,1987).
For the energies considered in Smid(1987) ($\varepsilon\geq0.01$; corresponding to $n\leq10$ (see Eq. **(26)**)), the individual recombination process is fast enough ($A_{10}^{Rec}\approx 28$ sec^{-1} ; see Eq.**(5)**) to neglect interfering elastic collisions ($\nu_{//}^c \approx 2.6\cdot10^{-2}$ sec^{-1} (see Eq.**(7)** for n=10, $\varepsilon_p=0.5$ and a plasma density of $\mathcal{N}_p^*=10^5$ cm^{-3})). For much smaller energies, however, elastic collisions will eventually limit the actual recombination rate because of the rapidly decreasing value of $\alpha_n^{Rec,c}$ ($\sim n^{-4.4}$) if $\nu_{//}^c>A_n^{Rec}$ (Eq.**(9)**). One can find the quantum state n* where the transition from the collisionally undisturbed to the disturbed recombination occurs by equating Eqs.**(5)** and **(7)**, with the result

$$n^* = (5.4\cdot10^{12}\cdot\varepsilon_p/\mathcal{N}_p^*)^{0.23} \quad , \qquad \textbf{(31)}$$

where the plasma density $\mathcal{N}_p^*$ has to be taken in [cm^{-3}] and the average plasma energy ε_p in units of Rydberg (for $\mathcal{N}_p^*=10^5$ cm^{-3} and $\varepsilon_p=0.5$, n*=51) (the numerical results will show that the excited atomic densities N_n have a maximum value just for a state n which is close to n*).
For continuum energies $\varepsilon<1/n^{*2}$ (in units of Rydberg), the interference of elastic collisions with the recombination process will therefore lead to a saturation of the electron spectrum $\mathcal{N}_e^*(\varepsilon)$, whereas for higher energies the latter reflects basically the energy dependence of the total recombination frequency $\nu_7^{Rec,0}(\varepsilon)$; see Appendix A.2, Eq.**(A.2.17)** and Sect.3.2).

A further possible mechanism affecting $\mathcal{N}_e^*(\varepsilon)$ even at very low energies could be inelastic scattering of photoelectrons of higher energy (impact- ionization and -excitation of atoms or molecules) .
A detailed knowledge of the relationship between photoelectron energy and the energy loss spectrum related to the relevant inelastic transitions (including the associated cross sections) would be necessary in order to treat the problem consistently, which is beyond present theoretical understanding of inelastic collision processes. On the other hand, experimental data concerning inelastic scattering usually have a spectral resolution of not

much better than 0.01 Ry, which is by far insufficient for the present consideration which deals with energies and energy differences as small as 10^{-6} Ry and less.
However, from the energy loss data published in Massey (1969) (Chpts.11 and 13) and Rees (1989) (pp.114 , 272-273) one can conclude that the cross section for inelastic collisions involving an energy loss comparable to the electron energy itself ('near threshold excitation') is very small, i.e. only very few electrons will end up with an energy as close to zero as indicated above. For the case of the earth's ionosphere, computations show (Smid, 1987) that the frequencies for the elastic and inelastic collisions are comparable in magnitude at energies corresponding to the maxima of the continuous cross section curves for the latter process (>1 Ry) (although elastic collisions are insignificant below a height of 500 km for the shape of the electron distribution function because the related changes in the production and loss rates partially compensate and the life time with regard to radiative recombination is not long enough for 'thermalization' to occur).
Because the 'near threshold' cross section for an inelastic collision can be expected to be several orders of magnitudes smaller than the maximum value, one can thus assume that the corresponding production rate at very small energies is smaller by this factor if compared to the production due to elastic collisions.
For the present purpose, it has therefore been decided to neglect the effect of inelastic collisions completely, because also below about 10^{-3} Ry there is no significant energy loss due to excitation of rotational, vibrational or fine structure transitions .

With this assumption, the balance equation for the production and loss rates determining the density $\mathcal{N}_{e,k}$ of free electrons in the energy interval ε_{k-1}, ε_k (Eq.**(16)**) can be written as

$$p_{1,k} + \sum_{\substack{i=1 \\ \neq k}}^{M} \mathcal{N}_{e,i} \cdot \nu_{i,k}^{c} + \sum_{n=2}^{\infty} N_n \cdot \nu_{n,k}^{c} + \sum_{n=2}^{\infty} N_n \cdot (\nu_{n,k}^{c} + \nu_{n,k}^{*}) =$$

$$= \mathcal{N}_{e,k} \cdot \left(\sum_{\substack{i=1 \\ \neq k}}^{M} \nu_{k,i}^{c} + \sum_{n=1}^{\infty} \nu_{n,k}^{Rec,0} \right) \quad ; \quad k=1,M \quad , \qquad \textbf{(32)}$$

where the summation over the energy index of the plasma electrons has now been limited to a maximum value M rather than infinity as in Eq.**(15)**, therewith restricting the energy spectrum from $\varepsilon_k = 0....\varepsilon_M$.
The various collision frequencies are (see Fig.1) :
$\nu_{i,k}^{c}$ is the frequency for elastic free-free (Coulomb-) scattering of electrons from the

energy range $\varepsilon_{i-1}, \varepsilon_i$ into $\varepsilon_{k-1}, \varepsilon_k$ ($\nu_{k,i}^c$ indicates the inverse process), assuming that there is no scattering within the interval $\varepsilon_{k-1}, \varepsilon_k$ itself (i.e. $i \neq k$) (see Appendix B , Eq. **(B.17)**),

$\nu_{n,k}^c$ is the frequency for elastic collisions from the bound level n (electron impact ionization) into the continuum energy range $\varepsilon_{k-1}, \varepsilon_k$, $\nu_{n',k}^c$ the (numerically identical) frequency for the 'pre-bound' level n', (Appendix B , Eq.**(B.19)**) and

$$\nu_{n,k}^* = \eta_n^{Ion} \cdot F^{ph}(\varepsilon_k) \cdot \sigma_n^{Ion}(\varepsilon_k) \qquad \textbf{(33)}$$

is the photoionization frequency from level n (see Eq.**(27)**) (note that it is assumed in Eq. **(32)** that there is no photoionization from the 'pre-bound' level n').

The recombination frequency $\nu_{n',k}^{Rec,0}$ into the pre-bound level n' is given by Eq.**(17)** and $p_{1,k}$ is the primary production due to ionization of the ground state of neutrals, which is taken here separately as an external boundary condition (note that the ground state n=1 (and n'=1) has been excluded from the sum describing collisional and photoionization from the individual levels) and is assumed to be of the form

$$p_{1,k} = p_0 \cdot (\varepsilon_k - \varepsilon_{k-1}) \quad , \qquad \textbf{(34)}$$

that is, the production function $p_1(\varepsilon_k)$ is taken as const. = p_0 , which is a reasonable approximation in view of the fact that the photoionization cross section for the ground state decreases from its maximum value roughly as $\sqrt{\varepsilon}$ for $\varepsilon \to 0$ (see Appendix A.2), whereas on the other hand the cross section for electron impact ionization (which contributes nearly the same amount to the total production rate as photoionization (Smid, 1987)) varies in the inverse manner (see Appendix B, Eq.**(B.20)**).

Rather than calculating p_0 explicitly from the local density of neutrals and the ionizing radiation flux, it is a more convenient method here to define it implicitly by noting that in equilibrium the total ionization rate from the ground state must equal the recombination rate (including cascading from higher levels) into the ground state, that is

$$\sum_{k=1}^{M} p_{1,k} = p_0 \cdot \varepsilon_M = q_1 \qquad \textbf{(35)}$$

(where q_1 is given by Eq.**(2)**,**(15)** and **(30)**) and imposing instead the external boundary condition of a given plasma density $\mathcal{N}_p^*$ over the normalizing equation (see Eq.**(4)**)

M

$$\sum_{k=1} \mathcal{N}_{e,k} \;=\; \mathcal{N}_p \qquad . \qquad \textbf{(36)}$$

In this form, Eq.**(32)** reduces to a system of equations determining the normalized electron distribution function

$$\begin{aligned} f_e(\varepsilon_k) \;&:=\; \mathcal{N}_e(\varepsilon_k)/\,\mathcal{N}_p \;= \\ &=\; \mathcal{N}_{e,k}\,/(\varepsilon_k-\varepsilon_{k-1})\,/\,\mathcal{N}_p \qquad , \end{aligned} \qquad \textbf{(37)}$$

i.e. Eq.**(32)** becomes

$$q_1\cdot\Delta\varepsilon_k/\varepsilon_M \;+\mathcal{N}_p\cdot\sum_{\substack{i=1\\ \neq k}}^{M}\Delta\varepsilon_i\cdot f_e(\varepsilon_i)\cdot\nu_{i,k}^{\,c} \;+\sum_{\nu=2}^{\infty}\mathcal{N}_\nu\cdot\nu_{\nu,k}^{\,c} \;+\sum_{n=2}^{\infty}N_n\cdot(\nu_{n,k}^{\,c}+\nu_{n,k}^{\,*})=$$

$$=\; \mathcal{N}_p\cdot\Delta\varepsilon_k\cdot f_e(\varepsilon_k)\;\cdot\;[\;\nu_{k,L}^{\,c}\;+\nu_{\mathcal{T},k}^{\,Rec,0}\;] \qquad ;\;\; k=1,M \qquad , \qquad \textbf{(38)}$$

where

$$\nu_{k,L}^{\,c} \;=\; \sum_{\substack{i=1\\ \neq k}}^{M}\nu_{k,i}^{\,c} \qquad \textbf{(39)}$$

(see Eq.**(B.18)**),

$$\nu_{\mathcal{T},k}^{\,Rec,0} \;=\; \sum_{\nu=1}^{\infty}\nu_{\nu,k}^{\,Rec,0} \qquad \textbf{(40)}$$

(see Eqs.**(17)**, **(A.2.17)** ,

and

$$\begin{aligned} \Delta\varepsilon_k \;&=\varepsilon_k-\varepsilon_{k-1} \qquad , \\ \Delta\varepsilon_i \;&=\varepsilon_i-\varepsilon_{i-1} \qquad . \end{aligned} \qquad \textbf{(41)}$$

Eq.**(38)** is a system of M equations for the M unknowns $f_e(\varepsilon_k)$. Together with Eq.**(1)**,**(2)**, **(6)** and **(15)** , which determine the recombination rate q_1 and the atomic level densities N_n and $\mathcal{N}_\nu$, they represent a consistent set of coupled equations for the discrete and

continuous electron spectrum (see also Fig.1, where the transitions between the various electronic states are illustrated through a schematic energy level diagram (using the definitions of this chapter)).

2.3 Stark Broadening of Atomic Levels by Plasma Field Fluctuations

For atomic transitions related to small quantum numbers it is usually (under natural conditions) sufficient to calculate the corresponding line profile only from the apparent natural and Doppler broadening involved (see Appendix A1. Eq.**(A.1.4)** and following). In order to obtain the correct frequency dependent scattering cross section for transitions between highly excited states, it is however essential to consider the explicit energetical shift or broadening of the atomic levels by external perturbations, because disturbing fields which are insignificant for small quantum numbers may become important for higher states. This is due to the strongly decreasing values for the natural broadening $A_{m,n}$ (Eq.**(A.1.14)**, Doppler broadening (if transitions between neighboring states are being considered; Eq.**(A.1.6)** and Eq.**(A.1.10)**) and the level separation (Eq.**(A.1.10)** with increasing m,n.

On the other hand, the energy shift caused by external fields is at least independent of the quantum number (as for the magnetic field; Zeeman effect). In the case of an electric field (Stark effect) it increases even for higher states, which is evident from considering the work a homogeneous static electric field does on an electron in level n during one revolution in its orbit, namely

$$(\delta W)_{n,S}^{Static} = \pm\, e \cdot |E_{\|}| \cdot 2 \cdot \langle r \rangle_n =$$

$$= \pm\, e \cdot |E_{\|}| \cdot r_0 \cdot n^2 \quad , \qquad \textbf{(42)}$$

with e the elementary charge , $E_{\|}$ the average electric field amplitude in the orbital plane of the electron, $\langle r \rangle_n$ the expectation value for the radius of the electron orbit in state n>>1 (Eq.**(A.1.12)**), r_0 the Bohr radius and the $\pm$ sign arises from the circumstance that during one half of the orbit the electron gains this energy, while on the other half it looses the same amount.

(Note added later: Eq.(42) effectively assumes a linear Stark effect. This is justified here because high Rydberg states can be considered to be hydrogen-like. Additionally, the electric microfield due to the plasma is not static but varies on a time scale which is practically for all cases much shorter than the time required to polarize the atomic charge distribution (which should be given by the linear Stark frequency). The present treatment should therefore also be applicable to low lying states of multi-electron atoms).

In the case of a static (the conditions under which a field can be considered as static will become evident below) and macroscopically directed electric field of strength |E|, the projected field is classically simply given by

$$|E_{\|}| = |E| \cdot \cos\alpha \quad , \qquad \textbf{(43)}$$

where $\alpha = 0...\pi/2$ is the angle between the electric field vector and the orbital plane of the

electron. If the latter is randomly orientated in space, α would, for a large number of atoms, classically take on all possible continuous values. Because of directional quantization, however, only certain discrete values are allowed. From the observation of spectral lines, one finds for level n the n possibilities

$$\cos\alpha_p = (n-p)/n \quad ; \quad p=1...n \quad . \qquad \textbf{(44)}$$

This gives the splitting scheme of the atomic level n in a static electric field of strength $|E|$

$$(\delta W)_{n,S}^{Static} = \pm\, e\cdot|E|\cdot r_0 \cdot n\cdot(n-p) \quad ; \quad p=1...n \quad . \qquad \textbf{(45)}$$

In the case of a time dependent electric field $E_{\|}(t)$ fluctuating with (an average) period Δt_f (defined by the average time between two zero crossings of $E_{\|}(t)$), each shifted level will additionally be broadened according to the associated change of work ({ }= time average)

$$(\delta W)_{n,B} = \pm\, e\cdot\{|dE_{\|}(t)/dt|\}\cdot\Delta t_w \cdot \{|dr/dt|\}\cdot\Delta t_w \quad , \qquad \textbf{(46)}$$

where

$$\Delta t_w = \Delta t_f\cdot T_n / (\Delta t_f + T_n) \qquad \textbf{(47)}$$

is the average period of the work done on the electron due to the field fluctuation period Δt_f and the angular period of revolution of the electron in state n

$$T_n = 1/\omega_n = \sqrt{m/e}\cdot\langle r\rangle_n^{3/2} \approx \approx 8.6\cdot10^{-18}\cdot n^3 \quad [\text{sec}] \quad , \qquad \textbf{(48)}$$

as one obtains classically by considering the circular frequency of an electron with orbital radius $\langle r\rangle_n$ in a neutral atom.

If the field variation is equal in magnitude to the field amplitude, then the average change of work becomes

$$\{|dE_{\|}(t)/dt|\} = 2\cdot\{|E_{\|}|\}/\Delta t_f \quad . \qquad \textbf{(49)}$$

Furthermore , the projected velocity of the electron is

$$|dr/dt| = 2\cdot\langle r\rangle_n / T_n = r_0 \cdot n^2 / T_n \quad , \qquad \textbf{(50}$$

so that the energetical broadening of level n becomes

$$(\delta W)_{n,B} = \pm\, e \cdot 2\cdot\{|E_{\|}|\}\cdot r_0 \cdot n^2 \cdot \zeta_n \quad , \qquad \textbf{(51)}$$

with

$$\zeta_n = \Delta t_f \cdot T_n / (\Delta t_f + T_n)^2 \quad . \qquad \textbf{(52)}$$

Note that ζ_n has a maximum for $\Delta t_f = T_n$ and decreases linearly with the ratio of the time constants in both limits $\Delta t_f >> T_n$ and $\Delta t_f << T_n$. As a consequence (see Eq.**(48)**), $(\delta W)_{n,B}$ increases $\sim n^5$ in the first limit ('small' n) but decreases $\sim n^{-1}$ in the second ('large' n) with increasing n.

Due to the fluctuating field, the actual level shift $(\delta W)_{n,S}$ will be reduced compared to its static limit given by Eq.**(42)** or **(45)** . Assuming that the relevant time scale which defines a static field is T_n , and that in the limit of $\Delta t_f << T_n$ the reduction is determined by the ratio of the squares of the fluctuation field gradient $\{|E_{\|}|\}/\Delta t_f$ to the characteristic gradient $\{|E_{\|}|\}/T_n$ (thus relating it to the associated (dynamical) field energies rather than the field values), one can adopt the relative splitting (or shift) factor

$$\mu_n = 1/(1+(T_n/\Delta t_f)^2) \quad . \qquad \textbf{(53)}$$

For the present problem, the electric field is neither uniquely determined nor macroscopically directed, since it is produced by the superposition of the fields of all charged particles in the plasma which are distributed randomly in space and furthermore are in constant motion.
Therefore, the zero order static field (obtained by integrating over a homogeneous density distribution) vanishes at any time instant t and only statistical fluctuations around this quasi-neutrality situation occur.
If deviations from the purely statistical field due to close encounters of charged particles with the considered atom are being neglected, the (unnormalized) distribution about this mean value is a Gaussian probability function

$$\wp(E_{\|}(t)) = \exp[-(E_{\|}(t)/\Delta E_p)^2] \quad . \qquad \textbf{(54)}$$

The dispersion value ΔE_p is the first order electric field which a single charged particle produces at a distance corresponding to the average separation

$$r_p = (4\pi/3 \cdot \mathcal{N}_p^{\circ})^{-1/3} \qquad \textbf{(55)}$$

of two particles in the plasma, that is

$$\begin{aligned} \Delta E_p &= e/r_p^2 = \\ &= e \cdot (4\pi/3 \cdot \mathcal{N}_p^{\circ})^{2/3} = \\ &= 1.25 \cdot 10^{-9} \cdot \mathcal{N}_p^{\circ 2/3} \qquad [\text{statvolt/cm} = 3 \cdot 10^4 \text{ V/m}] \end{aligned} \qquad \textbf{(56)}$$

if the plasma density $\mathcal{N}_p^{\circ}$ is in [cm^{-3}] .

The average field fluctuation period associated with Eq.**(55)** (which replaces Δt_f in Eq. **(52)** and **(53)**) is given by

$$\Delta t_{p,i} = 2\, r_p / v_i \quad , \qquad \textbf{(57)}$$

where v_i is the average velocity of the charged particle species i relative to the considered atom (the factor 2 arises from the circumstance that a particle has to travel twice the average distance r_p in order for the resultant field to change sign).

The Gaussian field distribution Eq.**(54)** for species i transforms now over Eq.**(51)** and the energy-frequency relationship

$$(\delta W)_{n,B,i} = h \cdot (\delta f)_{n,B,i} \qquad \textbf{(58)}$$

(with h the Planck constant) into the frequency broadening function for level n

$$\varphi_{n,i}(\delta f) = \exp [- (\delta f / (\Delta f)_{n,B,i})^2] \quad , \qquad \textbf{(59)}$$

where

$$(\Delta f)_{n,B,i} = 2/\sqrt{\pi} \cdot (\Delta f)_0 \cdot n^2 \cdot \zeta_{n,i} \quad , \qquad \textbf{(60)}$$

with $\zeta_{n,i}$ given by Eq.**(52)** for $\Delta t_f = \Delta t_{p,i}$ and

$$(\Delta f)_0 = 0.49 \cdot \mathcal{N}_p^{\circ 2/3} \qquad [\text{Hz}] \qquad \textbf{(61)}$$

if $\mathcal{N}_p$ is again in [cm^{-3}] (the factor $1/\sqrt{\pi}$ in Eq.**(60)** arises from the field average in Eq.**(51)** with the distribution function Eq.**(54)**).
One should be aware that Eq.**(52)** will lead to a quite inaccurate representation of the line profile in the wings ($\delta f >> (\Delta f)_{n,B,i}$) because of the neglection of close encounters in Eq. **(54)**. The exact statistical field distribution would however make an analytical treatment impossible, and the Gaussian profile, adequate in the line core, yields still a sufficiently accurate approximation for the overall behaviour of the scattering coefficient in the region of blended lines as well as giving correct values for the equivalent widths of the individual lines.

The presence of a second species j of charged particles causes a further, independent dispersion for each of the possible values of δf, so that the resulting field distribution function is obtained by folding the individual distributions, i.e.

$$\varphi_n(\delta f) \sim \int_{-\infty}^{\infty} df' \; \varphi_{n,i}(f') \cdot \varphi_{n,j}(f'-\delta f) \quad =$$

$$= \exp\left[- (\delta f / (\Delta f)_{n,B})^2 \right] \quad , \qquad \textbf{(62)}$$

where

$$(\Delta f)_{n,B} = 2/\sqrt{\pi} \cdot (\Delta f)_0 \cdot n^2 \cdot \sqrt{(\zeta_{n,i}^{\,2} + \zeta_{n,j}^{\,2})} \quad . \qquad \textbf{(63)}$$

The generalization to more than two species is obviously achieved by adding the further contributions under the square root in Eq.**(63)**.
(Note that $\varphi_n(\delta f)$ has been taken as an unnormalized function here because the normalizable quantity is the product of the distributions for the two levels involved in a radiative transition).

For a plasma consisting of electrons and a single species of ions (both of density $\mathcal{N}_p$), the field fluctuation period Eq.**(57)** attains the numerical values (respectively)

$$\Delta t_e = 2 r_p / v_e(\varepsilon_p) =$$
$$= 5.6 \cdot 10^{-9} \; / \mathcal{N}_p^{\,1/3} \; / \sqrt{\varepsilon_p} \qquad [\text{sec}] \qquad \textbf{(64)}$$

and

$$\Delta t_I = 2r_p/v_I =$$
$$= 9.4 \cdot 10^{-5} / \mathcal{N}_p^{1/3} / \sqrt{(T/A)} \qquad [\text{sec}] , \qquad \textbf{(65)}$$

with $\mathcal{N}_p$ the plasma density in [cm^{-3}] , ε_p the average electron plasma energy in units of Rydberg , T the ion temperature in ^oK and A the ion mass number.
With these values inserted into Eq.**(52)** for each species, the frequency dispersion of level n becomes

$$(\Delta f)_{n,B} = 2/\sqrt{\pi} \cdot (\Delta f)_0 \cdot n^2 \cdot \sqrt{(\zeta_{n,e}^2 + \zeta_{n,I}^2)} \quad . \qquad \textbf{(66)}$$

Assuming now a lower level m with broadening $(\Delta f)_m$ and an upper level n with broadening $(\Delta f)_n$ while the centers of the Stark shifted levels are separated by the frequency $f_{m,n}'$, the atomic line absorption profile in dependence of the given frequency f and a fixed level shift can therefore be written as

$$\varphi_{m,n}(f) = 1/\sqrt{\pi} / (\Delta f)^*_B \cdot \int_{-\infty}^{\infty} df' \, \varphi_m(f') \cdot \varphi_n(f'-f+f_{m,n}') \quad , \qquad \textbf{(67)}$$

with

$$(\Delta f)^*_B = (\Delta f)_{m,B} \cdot (\Delta f)_{n,B} / \sqrt{((\Delta f)_{m,B}^2 + (\Delta f)_{n,B}^2)} \quad . \qquad \textbf{(68)}$$

Evaluation of the integral yields

$$\varphi_{m,n}(f) = \exp [- (f - f_{m,n}')^2 / (\Delta f)_B^2] \quad , \qquad \textbf{(69)}$$

where now the abbreviation

$$(\Delta f)_B = \sqrt{((\Delta f)_{m,B}^2 + (\Delta f)_{n,B}^2)} \qquad \textbf{(70)}$$

has been introduced for the microscopic line broadening.
One should note that the atomic absorption profile $\varphi_{m,n}(f)$ is normalized to the line center ($f = f_{m,n}'$) rather than the integral over frequency because of the normalization of $\int df' \, \varphi_m(f') \cdot \varphi_n(f')$.

The frequency separation of the levels $f_{m,n}'$ depends on degree of static splitting of each

of the levels which is determined by the quantities μ_m and μ_n (Eq.**(53)**) for the combined (reduced) fluctuation period for the fields of electrons and ions (replacing Δt_f there)

$$\Delta t_{e,I} = \Delta t_e \cdot \Delta t_I / (\Delta t_e + \Delta t_I) \quad . \qquad \textbf{(71)}$$

For a level n, the absolute frequency shift of the level centers is then

$$(\delta f)_{n,S} = \pm (\Delta f)_0 \cdot n^2 \cdot \mu_n \cdot E/\Delta E_p \quad , \qquad \textbf{(72)}$$

with $(\Delta f)_0$ (the normal frequency shift for the ground state in a field ΔE_p) given by Eq. **(61)**.
Assuming that only those sub-states with the same sign of displacement contribute significantly to the transition cross section, the frequency separation between the centers of two Stark shifted levels m,n can therefore be written as

$$f_{m,n}' = f_{m,n} \pm (\Delta f)_0 \cdot \gamma_{m,n} \cdot E/\Delta E_p \quad , \qquad \textbf{(73)}$$

where $f_{m,n}$ is the original (unshifted) transition frequency between the two levels and

$$\gamma_{m,n} = n^2 \cdot \mu_n - m^2 \cdot \mu_m \quad . \qquad \textbf{(74)}$$

The macroscopic frequency scattering profile is now obtained by averaging Eq.**(69)** over the Gaussian probability distribution for the plasma fluctuation field (ensemble average) , i.e.

$$\phi_{m,n}(f) = \langle \varphi_{m,n}(f) \rangle = 1/\sqrt{\pi}\,/\Delta E_p \cdot c_{m,n} \cdot \int_{-\infty}^{\infty} dE \; e^{-(E/\Delta E_p)^2} \cdot \varphi_{m,n}(f) \quad , \quad \textbf{(75)}$$

where $c_{m,n}$ is a normalization constant which makes the integral of $\phi_{m,n}(f)$ over frequency equal to 1 in the limit of zero microscopic line broadening $(\Delta f)_B$ (thus normalizing only the macroscopic (ensemble) part of the profile due to the line splitting $(\Delta f)_S$ since only this is connected to the given volume density of scatterers and has therefore to be normalized).
After substitution of Eq.**(73)** into **(69)** and elementary integration one obtains the result

$$\phi_{m,n}(f) = 1/\sqrt{\pi}\,/(\Delta f)_S \cdot \exp[\, -(f - f_{m,n})^2 \,/\, (\,(\Delta f)_B^2 + (\Delta f)_S^2\,)\,] \quad , \quad \textbf{(76)}$$

where now the abbreviation

$$(\Delta f)_S = (\Delta f)_0 \cdot \gamma_{m,n} \qquad \textbf{(77)}$$

has been introduced for the static line splitting.

$\phi_{m,n}(f)$ represents the actual macroscopic absorption profile for resonance scattering of a wave of frequency f by the statistically Stark broadened and shifted states m and n under neglection of further Doppler and natural broadening (with the restriction mentioned below Eq.**(61)**).
One should be aware of the different physical origin of the two contributions to its width $(\Delta f)_B$ and $(\Delta f)_S$, since the continuous broadening associated with the latter is only a result of the macroscopic (volume) averaging process, whereas the former is an actual continuous broadening of the level of an individual atom (due to a time average rather than a volume average) and therefore resembles more the natural broadening of spectral lines .
For this reason, the emitted (in contrast to the absorbed) line is only represented by $\phi_{m,n}(f)$ in case of a spontaneous transition between levels n and m or for scattering of a wave with a sufficiently broad frequency spectrum. The line profile of an initially monochromatic signal scattered by Stark broadened and shifted states is however different from the absorption profile $\phi_{m,n}(f)$ because the scattering is coherent in the atoms frame and (at least if the atomic broadening $(\Delta f)_B$ dominates) only the Doppler effect connected to the velocity distribution of the scattering atoms will affect the line width. The inclusion of the latter line broadening mechanism and the natural broadening into the absorption profile, which has been neglected in this chapter since it is not related to the Stark broadening , is performed separately in the next Section 2.4 where the actual scattering cross section is derived by folding $\phi_{m,n}(f)$ with the corresponding distributions and finally adding the contributions of all quantum states in order to get the total scattering coefficient for a wave of a given frequency.

A further consequence of Stark broadening should be a reduction of transition cross sections if the level width is not small compared to the transition frequency.
For recombination into a given level n one has to assume that it is reduced if either the average broadening $(\Delta f)_{n,B}$ or the average splitting (see Eq.**(72)**)

$$(\Delta f)_{n,S} = (\delta f)_{n,S}\,(E=\Delta E_p) \qquad \textbf{(78)}$$

becomes comparable and greater than the threshold ionization frequency f_n (Eq.**(25)**,**(26)** and **(A.1.11)**) from this level, because then the discrete level becomes energetically undefined and blends into the continuum. Assuming an exponential reduction of the

corresponding recombination cross section with the ratio of the total level broadening to the threshold ionization frequency, one gets the reduction factor for recombination

$$\eta_n^{Rec} = \exp[- f_n /(\Delta f)_n] \quad , \qquad \textbf{(79)}$$

with

$$(\Delta f)_n = \sqrt{((\Delta f)_{n,B}^2 + (\Delta f)_{n,S}^2)} \quad . \qquad \textbf{(80)}$$

In the case of discrete transitions, i.e. for resonance scattering, the efficiency factor is given by the degree of (non)-overlap of the two states m and n involved, which yields the expression

$$\eta_{m,n}^{sc} = 1 - \exp[- f_{m,n}^2 / ((\Delta f)_B^2 + (\Delta f)_S^2)] \quad . \qquad \textbf{(81)}$$

2.4 Effect of External Perturbations and Wave Coherence on the Photoionization Cross Section

The cross section for photoionization (Eq **(A.2.4)**) is derived from the assumption of an ideal radiative transition, i.e. an atom interacting with an ideally coherent photon (infinitely long sinusoidal wavetrain) with no time dependent perturbations by other electrostatic or electromagnetic sources.
It is however obvious that the ionization efficiency can not stay the same if either the duration (coherence length) of the wave train is shorter than the characteristic transition time for this process or if the electric field strength of the photon is not large compared to disturbing fields varying irregularly on a similar time scale, because (in contrast to a pure scattering process) actual work must be done on the atomic electron by the wave field in order to transfer it to the free electron spectrum.
The plasma fluctuation field (see Sect.2.3) will therefore affect the photoionization process if it becomes comparable in magnitude to the field strength of the incident wave. Assuming that the corresponding reduction will be determined by the field energy (i.e. the square of the field strengths) rather than the field strengths themselves, one can adopt the efficiency factor

$$\beta_n(E_w) = E_w^2 / (E_w^2 + \Delta\{E\}_n^2) \quad , \qquad \textbf{(82)}$$

where E_w is the field strength of the incident wave and

$$\Delta\{E\}_n = \Delta E_p \cdot \sqrt{(\zeta_{n,e}^2 + \zeta_{n,I}^2)} \qquad \textbf{(83)}$$

the effective plasma fluctuation field for the level n from which the transition originates (Sect.2.3,Eqs.**(56)**, **(66)**).
It is in general (although not for the results of the present paper) important that by taking the field strength dependence of the photoionization cross section into account, one obtains a finite optical depth over infinite path lengths for this radiative process. This is because the square of the field strength of the original wave decreases in an absorbing (scattering) medium with distance from the centre of emission as

$$E_w^2(s) = E_w^2(s_0) \cdot e^{-\tau_n(s-s_0)} \cdot (s_0/s)^2 \quad . \qquad \textbf{(84)}$$

The last factor is the usual inverse square law behaviour in vacuum conditions and the exponential takes an absorption process related to level n into account characterized by the optical depth

$$\tau_n(s-s_0) = \sigma_n^0 \cdot \int_{s_0}^{s} ds'\, N_n(s') \cdot \beta_n(E_w(s') \cdot \chi_{Ion}(E_w(s'))) \quad , \qquad \textbf{(85)}$$

with N_n the density in level n and σ_n^0 the cross section in the absence of plasma fluctuations (χ_{Ion} is an additional reduction factor taking coherence effects into account and is derived below (Eq.**(90)**).
Since β_n is itself dependent on the optical depth through Eqs.**(82)** and **(84)**, Eq.**(85)** constitutes an integral equation in τ_n which can be solved numerically.
The result is shown in Fig.2 as a function of the field independent optical depth τ_n^0 (β_n=1) for various values of the ratio

$$\Gamma = E_w / \Delta\{E\}_n \qquad \textbf{(86)}$$

(only the effect due to β_n has been considered here, i.e. it was assumed that χ_{Ion}=1; it is evident from Eq.**(90)** below that the dependence on χ_{Ion} produces analogous effects with regard to the ratio $T_w^{coh}/T_{Ion}(E_w(s_0))$). For simplicity, the 'geometrical factor' s_0/s has hereby been assumed as constant=1, i.e. the results correspond effectively to the case of the propagation of a plane wave. Because in this case the asymptotic solution of Eq.**(85)** for sufficiently large distances is logarithmic (as is easily verified), the optical depth over infinite path lengths is also infinite (with the power of the wave decreasing inversely proportional with distance). For realistic geometries with a finite divergence of the plane of propagation of the signal,however, $E_w^2(s)$ decreases faster than $1/s^2$ and the statement above Eq.**(84)** holds.

The second aspect of importance for the photoionization efficiency is the coherence of the wave field. Assuming the oscillating electron always to be in phase with the incident wave of field strength E_w , one obtains the time T_{Ion} required for photoionization by substituting the classical relationship

$$\Delta v = a(E_w) \cdot T_{Ion} = \\ = e/m \cdot E_w \cdot T_{Ion} \qquad \textbf{(87)}$$

into the (correspondence-like) energy equation

$$m/2 \cdot (\Delta v)^2 = h \cdot f_w \qquad \textbf{(88)}$$

where f_w is the effective frequency of the ionizing wave (see Eq.**(97)**).
After inserting the numerical values of the physical constants, one gets therefore

$$T_{Ion} = 7.2 \cdot 10^{-18} \cdot \sqrt{f_w} / E_w \qquad [sec] \qquad , \qquad \textbf{(89)}$$

with f_w in [Hz] and E_w in cgs-units (statvolt/cm $= 3 \cdot 10^4$ V/m).

As long as T_{Ion} is small compared to the coherence time T_w^{coh} of the wave (time during which a sinusoidal waveshape is maintained to within one cycle) , the ionization process should not depend on T_w^{coh} and the ionization efficiency in this case be given by Eq. **(82)**. Otherwise, it will be further reduced by a factor which in the opposite limit should be the square of the ratio of T_w^{coh} and T_{Ion} since the ionization cross section (Eq. **(A.2.4)**) depends on the square of the dipole moment which for a classical oscillator is proportional to the field strength of the incident wave. Over Eq.**(89)** this implies therefore also a quadratic dependence on the time scales involved and one can thus adopt the coherence efficiency factor for photoionization

$$\chi_{Ion}(f_w, E_w) = 1/[\,1 + (T_{Ion}/T_w^{coh})^2\,] \qquad . \qquad \textbf{(90)}$$

*Note added later: this result is only applicable if the field strength E_w of the wave is obtained from the intensity of light over the classical relationship Eq.**(96)**; in this case, one can still make the technical assumption of the ionization time given by Eq.**(89)**; if E_w is given explicitly however, the ionization time takes on a different dependence on field strength and frequency (see http://www.plasmaphysics.org.uk/photoionization.htm) .*

An additional dependence of the ionization efficiency on the corresponding quantum mechanical transition constant (which by symmetry arguments should be identical to the recombination constant A_n^{Rec} ; see Appendix A.2) can not be logically excluded with certainty by means of theoretical arguing ; from experimental results it is however evident that even if $T_w^{coh} << 1/A_n^{Rec}$, the photoionization cross section remains unaffected (each photon produced by a discrete atomic transition has a coherence time which is about 4 orders of magnitude smaller than the characteristic time for bound-free transitions (cf. Eq.**(5)** and **(20)**); the ionization efficiency for those 'discrete' photons is however not known to be accordingly smaller than for 'continuous' photons produced by radiative recombination (in fact, experimental photoionization cross sections are usually derived by measuring the attenuation of certain discrete spectral lines by the examined gas and they are also consistent with ionization efficiencies of continuous spectral radiation)). Although this evidence might in principle be due to the circumstance that the electric field strength of the radiation field was high enough so that the classical coherence criterion is valid ($\chi_{Ion} \approx 1$, which might be a sufficient but not necessary condition for ionization to occur with maximum efficiency), it is somewhat physically unreasonable to assume that the quantum mechanical transition constant is a further independent reference quantity for the coherence time of the wave , since this would mean that even for a vanishingly small field strength E_w , ionization occurs with

maximum efficiency as long as $T_w^{coh} >> 1/A_n^{Rec}$.
Therefore, one can take Eq.**(90)** as the actual efficiency factor for ionization with regard to wave coherence , so that the total relative efficiency factor (considering the combined effects of plasma field fluctuations and wave coherence) is obtained as

$$\eta_n^{Ion}(f_w,E_w) = \beta_n(E_w) \cdot \chi_{Ion}(f_w,E_w) \quad . \qquad \textbf{(91)}$$

(the cross section for resonance scattering between discrete states, on the other hand, does not depend on the wave coherence, since the wave is re-radiated instantaneously in a coherent way by the atomic electron and no work in a quantum mechanical sense is done on the latter).

If the radiation field does not consist of a monochromatic wave but a more or less extended energy spectrum, the effective field strength E_w and frequency f_w can be derived by considering the amount of energy flux which the atomic transition 'cuts' out of the available spectrum according to the frequency characteristics of the corresponding cross section.
For photoionization from level n, the total effective energy flux is given by

$$\mathbf{F}_n = 1/\boldsymbol{\sigma}_n^{Ion} \cdot \int_{f_n}^{\infty} df \; P_n^{Ion}(f) \quad , \qquad \textbf{(92)}$$

where

$$P_n^{Ion}(f) = F(f) \cdot \sigma_n^{Ion}(f) \qquad \textbf{(93)}$$

is the power of photoionization at frequency f . The associated energy flux F(f) relates to the photon flux used in Eq.**(22)** by

$$F(f) = F^{ph}(f) \cdot h \cdot f \qquad \textbf{(94)}$$

with h designating Planck's constant.

The average effective cross section for photoionization is hereby determined through

$$\boldsymbol{\sigma}_n^{Ion} = \int_{f_n}^{\infty} df \;\; \sigma_n^{Ion}(f) \cdot P_n^{Ion}(f) \;\; / \;\; \int_{f_n}^{\infty} df \;\; P_n^{Ion}(f) \qquad . \qquad \textbf{(95)}$$

From Eq.**(92)** , the effective field strength is then derived by means of the well known relationship of electrodynamics

$$E_w = \sqrt{(\mathbf{F}_n \cdot 8\pi/c)} \qquad , \qquad \textbf{(96)}$$

with c the velocity of light.

The average effective frequency f_w of the ionizing radiation , which goes into Eq.**(89)** is also determined by using the ionizing power as a weighting function, that is

$$f_w = \int_{f_n}^{\infty} df \;\; f \cdot P_n^{Ion}(f) \;\; / \;\; \int_{f_n}^{\infty} df \;\; P_n^{Ion}(f) \qquad . \qquad \textbf{(97)}$$

For the resonance scattering process, on the other hand, the field strength and frequency are assumed to be known here, since one considers the scattering of (nearly) monochromatic waves.

The only unknown left (in connection with determining the photoionization efficiency) is the effective coherence time of the radiation field T_w^{coh} . Since generally this quantity is not provided by measurements of natural radiation sources (the solar radiation field for instance), one has to make assumptions about the generation of the radiation with regard to its coherency, i.e. the atomic decay times for the relevant transitions and the effect of interfering collisions, and rely on the conservation of the coherence time if many sources are being superposed, even if the latter are distributed randomly in space and time (numerical calculations of the field resulting from the superposition of many overlapping wavetrains with random relative phase shifts indicate in fact that the effective coherence time of the total wave field is (approximately) identical with the coherence time of the individual waves, despite the fact that the superposition is statistical and the total amplitude increases only with the square root of the number of wavetrains).

2.5 Total Scattering Coefficient

The actual macroscopic frequency profile for resonance scattering between states m and n can be found be folding the Stark broadening function $\phi_{m,n}(f)$ with the Doppler and natural profile H(a,w) (Eq.**(A.1.7)**). As a result one obtains the function

$$\Phi_{m,n}(f) = 1/\sqrt{((\Delta f)_S^2 + (\Delta f)_D^2)} \cdot H(a,w(f)) \quad , \qquad \textbf{(98)}$$

where

$$w(f) = (f - f_{m,n})/\Delta f \quad , \qquad \textbf{(99)}$$

$$a = A_{m,n}/ 4\pi /\Delta f \qquad \textbf{(100)}$$

with

$$\Delta f = \sqrt{((\Delta f)_B^2 + (\Delta f)_S^2 + (\Delta f)_D^2)} \quad , \qquad \textbf{(101)}$$

i.e. the the widths of the individual Gaussian components simply add in the usual way.
The normalization of $\Phi_{m,n}(f)$ takes into account that Δf consists of a microscopic (atomic, coherent) broadening $(\Delta f)_B$ and the macroscopic (ensemble, incoherent) broadenings $(\Delta f)_S$ and $(\Delta f)_D$ of which only the latter component has to be normalized (see below Eq.**(75)**).

The cross section related to $\Phi_{m,n}(f)$ is obtained by substituting it into Eq.**(A.1.4)** for the function $1/(\Delta f)_D \cdot H(a,w)$. This yields the result

$$\sigma_{m,n}(f) = 2\pi^{5/2} \cdot e^2/h \cdot \sqrt{(M/2kT)} \cdot \langle r \rangle_{m,n}^2 \cdot g_{m,n} \cdot \eta_{m,n}^{sc} \cdot H(a,w(f)) \, , \qquad \textbf{(102)}$$

with

$$g_{m,n} = 1/\sqrt{(1 + (\Delta f)_S^2 /(\Delta f)_D^2)} \qquad \textbf{(103)}$$

and the dimensionless efficiency factor $\eta_{m,n}^{sc}$ (which takes the dependence of the scattering cross section on the energetical overlap of the Stark broadened states into account) given by Eq.**(81)**.
It is important that only the Stark splitting and Doppler broadening determines the absolute (peak) magnitude of the cross section, the atomic Stark broadening $(\Delta f)_B$ leading only to an increase of the line width by affecting the scale of w (note that $H(a,w) = e^{-w^2}$

for a<<1, which holds in most cases of practical interest) (it should again be emphasized (see Sect.2.3 below Eq.**(61)**) that a Gaussian or Voigt profile has in the first instance been chosen for the sake of convenience and does not represent the actual profile in the collisional line wings).

Inserting now the approximate expression for $\langle r \rangle_{m,n}$ for large quantum numbers (Eq. **(A.1.13)**), one obtains the generalized form of Eq.**(A.1.15)**

$$\sigma_{m,n}(f) \approx 5.1 \cdot 10^{-12} \cdot [1/m^2 - 1/n^2]^{-3} \cdot m^{-1.8} \cdot (n-1)^{-3.2} \cdot \sqrt{(A/T)} \cdot g_{m,n} \cdot \eta_{m,n}^{sc} \cdot H(a,w(f))$$

$$[cm^2] \qquad (m,n >>1) \ , \quad \textbf{(104)}$$

with A the atomic mass number and T the atom temperature in ^{o}K.
Note again that, apart from the explicitly labelled quantities, also the line profile parameters a and w depend upon the quantum numbers m and n, in particular through the line broadening Δf.
The scattering coefficient related to $\sigma_{m,n}(f)$ is now given by

$$\kappa_{m,n}(f) = N_m \cdot \sigma_{m,n}(f) \quad , \quad \textbf{(105)}$$

and the total scattering coefficient at the given frequency f is

$$\kappa_0(f) = \sum_{m=1}^{\infty} \sum_{n=m+1}^{\infty} \kappa_{m,n}(f) \quad . \quad \textbf{(106)}$$

The index 0 shall indicate that the contributions of the individual atoms are assumed to superpose linearly to the total scattering coefficient ('incoherent' superposition). This assumption will however fail if the total effective density of scatterers for the wave of frequency f

$$N_{eff}(f) = \kappa_0(f) / \boldsymbol{\sigma}(f) \quad , \quad \textbf{(107)}$$

where

$$\boldsymbol{\sigma}(f) = 1/\kappa_0(f) \cdot \sum_{m=1}^{\infty} \sum_{n=m+1}^{\infty} \sigma_{m,n}(f) \cdot \kappa_{m,n}(f) \quad , \quad \textbf{(108)}$$

is such that the related average distance of scatterers

$$d_{eff}(f) = (4\pi/3 \cdot N_{eff}(f))^{-1/3} \quad \textbf{(109)}$$

is less than one wavelength $\lambda=c/f$, i.e. if the scattering is specular (or 'coherent'). In this case the scattering coefficient can be expected to increase in a non-linear way analogously to the total energy of a wave if the individual sources are being superposed in phase rather than incoherently.
Assuming a quadratic dependence on the parameter

$$\delta(f) = \lambda / d_{eff}(f) = c/f/ d_{eff}(f) \quad , \quad \textbf{(110)}$$

the total macroscopic (effective) scattering coefficient can be written as

$$\kappa(f) = \kappa_0(f) \cdot (1 +\delta^2(f)) \quad \textbf{(111)}$$

(in the following results section, $\kappa(f)$ will be referred to as 'effective' or 'coherent' scattering coefficient, whereas for $\kappa_0(f)$ 'atomic' or 'incoherent' scattering coefficient will be used).

One should note that apart from affecting the total (integrated) scattered power as given by $\kappa(f)$, the quantity $\delta(f)$ determines also the characteristics of the scattered wave field by the well known principles of interference optics (e.g. the so called magnetic aspect sensitivity (orthogonality effect) which is observed with the scattering of radar signals from the ionosphere (as a necessary condition for the magnetic field to affect the scattering characteristics of electromagnetic waves, it is reasonable to assume that the local gyrofrequency exceeds the natural width of the atomic states involved in the scattering and eventually the frequency of disturbing collisions with other atoms ; in the radio wave region and for ionospheric conditions this is certainly always the case due to the small values of $A_{m,n}$ and ν_n^c for the associated quantum numbers (see Eqs.**(20)** and **(7)**)).

3. Numerical Results

3.1 Details of the Computational Method

The coupled system of equations determining the free electron energy spectrum and the density of neutral atoms in excited states (see Sect.2.1 and 2.2) was solved iteratively with the numerical grid for the free electron energy scaled like the discrete atomic levels, that is, the energy values ε_k in Eq.**(38)** were determined by

$$\varepsilon_k = 1/k^2 \quad ; \; k = 1....k_{max} \quad . \qquad \textbf{(R.1)}$$

(in order to achieve a better resolution at high energies, additional non-integer values k=1.1 ,1.2....1.9 were added)
The maximum energy of the free electrons was therefore assumed to be 1 Rydberg and the minimum energy was given by the highest quantum number considered which was in this case $k_{max}=7000$, i.e. $\varepsilon_{min} = 2 \cdot 10^{-8}$.
This numerical scaling symmetry between the continuous and discrete electron spectrum is justified by the functional dependence of the recombination cross section (which determines the free electron spectrum) on the bound level quantum number n and the continuous energy ε (see Appendix A.2).
The circumstance that Eq.**(R.1)** implies only a relatively low resolution of the free electron spectrum at high energies is not important here, since one is interested in the recombination into states with n>>1 which is primarily due to low energy electrons (k>>1) although the latter constitute only a small fraction compared to the bulk of higher energy plasma electrons.
Because a matrix of 7000·7000 coefficients is inconvenient to handle numerically and the physical quantities determining them vary only relatively slowly with the bound level quantum number n if n is large (at least for natural conditions), the whole grid has been divided into four regions with different grid resolutions, namely

$$\begin{aligned} \Delta n &= 1 \quad \text{if} \quad 1 \le n < 10 \\ \Delta n &= 2 \quad \text{if} \quad 10 \le n < 40 \\ \Delta n &= 20 \quad \text{if} \quad 40 \le n < 2000 \\ \Delta n &= 100 \quad \text{if} \quad 2000 \le n < 7000 \end{aligned} \qquad \textbf{(R.2)}$$

and the same division was taken for the continuous energy numbers k, Δk (with the exception k<2; see below Eq.**(R.1)**).
With the coefficients and densities assumed constant between two points, this defines a step function of 173 intervals for the discrete and 182 for the continuous energy spectrum, which turns out to result in a relative error for the electron density distribution function $f_e(\varepsilon)$ and the excited atom densities N_n of about 20% at each point (this corresponds to the change of the densities within one unresolved interval Δn; a higher numerical

accuracy could be achieved by decreasing Δn accordingly, but this would be pointless here considering the fact that the numerical expressions for the atomic cross sections and decay constants have been derived by means of inter- and extrapolations of only a few explicitly calculated values and are unlikely to be more accurate than this throughout (see Appendix A)).
About 10 iterations were necessary in order to make the solution converge numerically to within an error of less than 10%.
It should be mentioned that for all calculations presented in this paper, the free electron spectrum turned out to depend only on the 'pre-bound' densities $N_{//}$ but not the actual level densities N_n (with n>=2) which are too low to cause any significant production of free electrons due to ionization at any energy. In principle, the bound levels could have been therefore excluded from the iteration procedure (calculations for some extreme (although unrealistic in this context) ionizing radiation flux spectra showed however that under certain circumstances there can be some effect at certain energies of the free electron spectrum, therewith justifying the formal coupling of the whole system of equations as illustrated by Fig.1). Due to the course grid resolution implied by Eq.**(R.2)** , conservation of electrons within the cascading scheme given by Eqs.**(19)** and **(30)** could not be achieved with a sufficient accuracy. The total recombination rate into the ground state q_1 , which defines the ionization equilibrium through Eq.**(35)**, was therefore simply determined by adding up the initial recombination into all levels, that is $q_1=\Sigma q_n^{Rec}$, taking advantage of the above mentioned circumstance that only a negligible amount of the total number of recombined electrons become re-ionized before having cascaded into the ground state.

The final summation of the contributions from all levels to the total atomic scattering coefficient(Eq.**(106)**) was performed by first adding up all transitions between states n,n+1 (n1- or nα-transitions) then with n,n+2 (n2 or nβ) and so on. This method provides a better convergence, since the scattering cross section decreases rapidly with increasing m for n,m transitions (as it follows from Eq.**(104)**). The actual number of transitions which has to be taken into account in order to achieve a given accuracy depends strongly on the assumed physical parameters, in particular the plasma density and the related level broadening as well as the considered wave frequency. If the latter is in the continuous region of the scattering coefficient (which is for instance the case for f<1GHz if $N_p^* = 10^5$ cm^{-3} ; see Sect.3.4, Fig.12), it is sufficient to add up n1-n3 transitions in order to achieve an error of less than 10%, whereas in the line region (f>500 MHz if $N_p^* = 10^4$ cm^{-3} ; see Fig.11) n1-n10 transitions have to be taken into account (the general tendency is therefore an increase in the number of contributing transitions with decreasing plasma density and increasing wave frequency).

In order to avoid confusion when discussing the dependence of the results on the total plasma density N_p^* , the values for the mass and temperature of neutrals and ions (which are assumed to be identical) have been kept constant throughout, namely A=32 and

T=300 ^{o}K. This is appropriate for the lower ionosphere from where the measurements of scattering coefficients used for comparison with the theoretical results have been obtained. The circumstance that these values are not in any case consistent with the assumed plasma densities if referred to the ionosphere is only of minor importance because the results are only weakly dependent on A and T. For ionospheric F2- region conditions for instance (A=16, T=1200 ^{o}K), the only effect would be to reduce the scattering coefficient by a constant factor 0.6 due to an according depletion in the excited atom densities.

3.2 Plasma Electron Distribution Function

Fig.3 shows the normalized electron energy spectrum $f_e(\varepsilon)$ (as defined in Sect. 2.2) appropriate for lower ionospheric conditions ($\mathcal{N}_p = 10^5$ cm^{-3} , ε_p=0.5 Ry, T=300^{o}K, A=32; see also remarks at the end of Sect.3.1) (thick solid step function). The dashed step function gives the electron spectrum when neglecting all elastic collisions, i.e. only the primary production rate q_1 and the (undisturbed) recombination frequency $\nu_{T,k}^{Rec,0}$ (thin solid curve, left ordinate) are hypothetically assumed to determine the spectrum (see Eq. **(38)**). It is evident that elastic collisions are the dominant production mechanism apart from the highest energies (ε>0.1) where the primary production q_1 (photo- and electron impact ionization) dominates. Within the elastic scattering domain, one can further differentiate into free-free scattering of electrons and scattering out of the 'pre-bound' state *n*. The former is dominant for energies greater than the characteristic energy corresponding to the quantum number n* (Eq.**(31)**) where the recombination constant A_n^{Rec} (dashed-dotted line, left ordinate) and the elastic collision frequency ν_n^c (thin dashed line) become equal (the upper abscissa gives the quantum number scale which is related to the energy scale through $\varepsilon=1/n^2$), whereas the latter is dominant for energies smaller than this. Only in this region does $f_e(\varepsilon)$ depend on the total plasma density at all (i.e. is the specific electron density $\mathcal{N}_e(\varepsilon)$ a non-linear function of the total plasma (electron) density $\mathcal{N}_p$). A comparison with Figs.4 and 5 ($\mathcal{N}_p = 10^4$ cm^{-3} and 10^6 cm^{-3} respectively) indicates a dependence $f_e(\varepsilon) \sim \mathcal{N}_p^{0.23}$ (which can be attributed to the function $\alpha_n^{Rec,c}$, see Eq.**(31)**) in the energy region where recombination is not yet affected by plasma field fluctuations (see Sect.2.3) and $\sim \mathcal{N}_p^{0.4}$ for energies even smaller than this (corresponding to the saturation region of the recombination frequency $\nu_{T,k}^{Rec,0}$).

One should furthermore note that for energies $\varepsilon<<1$, $\nu_{T,k}^{Rec,0}$ is (for the given ion mass and temperature; see Eq.**(A.2.17)**) always large compared to the elastic collision frequency ν_n^c (which is effectively equal to the free-free loss frequency $\nu_{k,L}^c$ (Eq. **(B.18)**)), i.e. the loss rates at a given electron energy are almost exclusively determined by recombination. This means that the differences in $f_e(\varepsilon)$ for different plasma densities are only caused by differences in the production rates due to elastic scattering out of the 'pre-bound' state *n*. Only for much higher ion temperatures and/or smaller masses does the recombination cross section become small enough so that elastic collisions dominate the loss rates also for $\varepsilon<<1$ with the consequence of $f_e(\varepsilon)$ being much closer to 1 in this region.

3.3 Excited Atom Densities

With knowledge of the plasma electron distribution function $f_e(\varepsilon)$ (or equivalently the specific electron density $\mathcal{N}_e(\varepsilon)$) the production rate q_n and thus the excited atom density N_n can be calculated (Sect.2.1). For the conditions valid for Fig.3 ($\mathcal{N}_p = 10^5$ cm^{-3}) the result is shown in Fig.6.

The thin solid curve gives the production rate q_n (left ordinate, to be multiplied by 10^5) as a function of n (lower abscissa, taken as a continuous variable here), with the close dashed-dotted curve showing the initial production rate q_n^{Rec} (i.e., neglecting the cascading rate q_n^{casc})

One can distinguish two regions of the production rate function : for levels n lower than n* (see Eq.**(31)** and previous paragraph 3.2; n*≈50 here), the recombination rate decreases approximately in proportion with the narrowing of the continuum energy range from which electrons can recombine into level n ($\Delta\varepsilon \sim 1/n^2$), whereas for higher levels, where collisions become important, the recombination rate decreases even much more rapidly with increasing n due to the additional reduction factor $\alpha_n^{Rec,c}$ ($\sim n^{-6.4}$) (see Eqs. **(9)** and **(14)**).

The loss frequency ν_n^{loss} is given by the thick short dashed curve (right ordinate). It is the sum of the decay constant A_n (long dashed) which is dominant below a quantum number of n≈350 in this case, the collisional ionization frequency ν_n^c (short-dashed line) which dominates for n>350 and the photoionization frequency ν_n^* (dotted curve) corresponding to an average (quiet conditions ; F_{sol} =1) solar radiation flux which turns out to be unimportant for all n although at about n=300 it comes close in order of magnitude to both A_n and ν_n^c .

By taking the ratio of the production rate and the loss frequency, one obtains the level population N_n (thick solid curve). It increases from n=2 to n=n* because the decay constant A_n decreases more rapidly with n than the production rate (the steep increase from n=2p to n=1 indicates only schematically the much higher density in the ground state with A_1=0, since it is not self-consistently contained in the level rate equations). Only in this region does q_n^{casc} become significant (the cascading rate is of the same order of magnitude here as the primary production rate q_n^{Rec}), because the rapid increase in N_n with n can compensate for the low densities and small cascading probabilities.

A comparison with the solution for other plasma densities (Figs.7 and 8, note the absolute scale) shows that $N_n \sim \mathcal{N}_p^2$ for n<n*, $N_n \sim \mathcal{N}_p$ for n*<n<n_c (where n_c is the level at which the collisional ionization frequency ν_n^c becomes dominant (≈350 $\mathcal{N}_p = 10^5$ cm^{-3})) and N_n independent of $\mathcal{N}_p$ for n>n_c .

It is important that with a solar radio flux much higher than the quiet sun flux (as it occurs for instance during a solar burst), the photoionization frequency ν_n^* can become the main loss process for high quantum numbers (where usually collisions are dominant) and

the dependence of N_n on $\mathcal{N}_p$ will then also be linear there (Fig.9 shows the photoionization frequency and corresponding excited atom density for the strongest observed solar bursts (F_{sol}^{Burst} =1, 'Type IV', see Fig.10) for a plasma density of $\mathcal{N}_p = 10^5$ cm^{-3} (compare to the quiet solar conditions of Fig.6)) (note that this is an equilibrium consideration and that much smaller changes in the radiation flux may be sufficient to produce short term non-equilibrium variations of the same magnitude; this argument holds also for the collisional ionization frequency ν_n^c ; see Sect.3.5 for a more detailed discussion of the non- equilibrium aspect).

In both cases (quiet and enhanced solar flux), the efficiency factor for photoionization (Eq.**(90)**) was calculated by assuming the coherence time T_w^{coh} of the solar radiation flux to be determined by elastic collisions in a plasma of a density $\mathcal{N}_p^{sol} = 10^8$ cm^{-3} which is appropriate for the lower solar corona. Since the frequency f_w of the emitted radiation is approximately related to the quantum number n over (twice) the threshold frequency f_n (Eqs.**(25)**,**(26)**), the coherence time is therefore given by the associated collision frequency ν_n^c (Eq.**(7)**) for the plasma density $\mathcal{N}_p^{sol}$, i.e.

$$T_w^{coh}(f_w) = 1/\nu_n^c(\mathcal{N}_p^{sol})$$
$$= 7.7\cdot 10^7 \cdot\sqrt{(f_w/6.6\cdot 10^{15})}\cdot \varepsilon_p/\mathcal{N}_p^{sol} \quad [\text{sec}] \quad , \quad \textbf{(R.3)}$$

where f_w (as defined by Eq.**(97)**) has to be taken in [Hz] and $\mathcal{N}_p^{sol}$ in [cm^{-3}]. The average plasma (electron) energy was chosen to be identical with the ionospheric value ε_p= 0.5.

For frequencies higher than about 10^4 MHz, the quiet sun radiation flux of Fig.10 was extrapolated by means of the the power law $F(f) \sim f^{1.85}$ (see Eq.**(94)**) which yields consistency with measurements of the solar spectrum in the optical region (Unsöld, 1955, p.34). A crude exponential interpolation was then applied between the maximum of the solar spectrum and the far UV -region, where the flux for the latter was taken from Rees (1989) (p. 9). With this, the photoionization frequency ν_n^* (Eq.**(22)**) could be calculated consistently for all states n=2.

As a general aspect arising from the results presented in the last two sections, one should note that both for the continuous and discrete electron energies, the derived densities are in no way related to some kind of thermal equilibrium. In the light of the consistent detailed equilibrium theory developed in this paper, it is in fact hard to see how approaches based on Saha-Boltzmann statistics, which are widely if not exclusively used in areas as astrophysics, plasma physics etc., could be connected to it and yield any physically reasonable approximation to the true situation or only order of magnitude estimates thereof. Such concepts should therefore be abandoned and replaced by detailed equilibrium approaches like the one presented in this paper. In the case that one has to consider time dependent situations which vary significantly within the longest time scale

entering into the problem , it becomes of course even necessary to generalize the rate equations to time dependent expressions (see end of Sect.2.1 and Sect.3.5 for a qualitative discussion of the non-equilibrium aspect).

3.4 Equilibrium Scattering Coefficient for Radio Waves

3.4.1 Atomic (Incoherent) Scattering Coefficient

The total atomic scattering coefficient for a radio wave of frequency f is obtained from the excited atom densities calculated in Sect.3.3 via Eqs.**(105)** and **(106)** (and preceding formulae). In Figs.11, 12, and 13 the result for $\kappa_0(f)$ (thick short-dashed curve, left ordinate) is plotted for radar frequencies from 820 KHz to 1.9 GHz for those plasma densities discussed in Sects.3.2 and 3.3 (undisturbed conditions).
The frequency dependence of the atomic scattering coefficient is strongly determined by the line frequency broadening , which is shown here by the thin solid curve (right ordinate) for the case of $n\alpha$ ($n\rightarrow n+1$) -transitions as a function of n (upper abscissa, which is scaled such that the frequency of the related $n\alpha$ -transition matches the radar frequency (lower abscissa)).
Three different domains can be distinguished (see in particular Fig.11):
1) an almost frequency independent region corresponding to scattering by states which are broadened in excess of the level separation (long-short-dashed line, right ordinate) (level continuum);
2) a f^{-2} region related to levels which are well separated but broader than the frequency difference between two neighboring ($n\alpha$, $(n+1)\alpha$) -lines (long-dashed line) (line continuum);
3) a region where the broadening is smaller than the line separation and the individual lines become visible (discrete line region).
The functional behaviour in region 2 is explained by the increasing number of lines able to get into resonance with the given frequency f as the latter decreases and probes higher (i.e. more closely spaced) levels with an increasing collisional broadening.
Once the frequency (long-short-dashed line) gets smaller than the level broadening, however, all lines with a resonance frequency below this 'critical' frequency scatter the wave and the atomic scattering coefficient becomes constant (region 1 ; this is effectively the limit $f<<f_{m,n}<<\sqrt{((\Delta f)_B^2+(\Delta f)_S^2)}$ in Eq.**(76)**, which makes the scattering profile ϕ independent of f ; it should be noted in this context that for the considered frequencies, i.e the corresponding states n, the line broadening is only determined by the component $(\Delta f)_B$ which is related to the actual collisional level broadening , whereas the apparent line broadening due to a further static level shift $(\Delta f)_S$ (see Sect.2.3) is only dominant for much smaller quantum numbers (=60 for the conditions considered here) and therefore higher frequencies).
In region 3, the dominant lines are formed by the $n\alpha$-transitions, which have the largest scattering cross section ($\sigma_{n,n+\Delta n}\sim\Delta n^{-3}$, as it follows from Eq.**(104)**) and the smallest broadening (because they are associated with smaller quantum numbers than $n\beta$- and higher order transitions in the same frequency region). With increasing radar frequency, the number of orders of lines ($n\alpha$, $n\beta$....) which become visible increases, the rest of the lines forming a quasi-continuum with the lower order lines superposed (see Fig.14 for a

frequency range of 900-1000 MHz and a plasma density of 10^4 cm^{-3} ($\kappa_0(f)$ and $\kappa(f)$ coincide here); the small peaks at 975.6 MHz and 988 MHz are for instance due to the 237β- and 236β- transitions respectively; note however that the wings of the lines are quantitatively not correctly reproduced by a Gaussian profile; the actual scattering coefficient may therefore be somewhat higher between the line peaks (see Sect.2.3 below Eq.**(61)**)
One should note that the 'continuum' formed by the blended higher order lines shows also the $\sim f^{-2}$ decrease with frequency which is characteristic for region 2, whereas the completely resolved lines have approximately equal peak amplitude in this frequency region, because for quantum numbers n>n* (see Eq.**(31)**) the increase in the scattering cross section with increasing n ($\sim n^4$ for transitions between neighboring states) is just compensated by the decrease of the level densities N_n (see Fig.7).

Concerning the dependence of the atomic (incoherent) scattering coefficient on the total plasma density, it is evident from Figs.11, 12, 13 that $\kappa_0(f)$ shows an (approximate) proportionality to $\mathcal{N}_p$ only for frequencies near the transition from region 1 to 2 (≈50 - 200 MHz for those densities considered here).
In region 1, κ_0 is a weaker function of $\mathcal{N}_p$ ($\sim\mathcal{N}_p^{0.4}$) since the density N_n of the responsible (high) levels is almost invariable (the relevant levels are within the collisionally determined regime; see Sect.3.3, Figs.6, 7, 8), but also because the increased broadening with higher $\mathcal{N}_p$ is assumed here to lead to a reduction in the scattering cross section if the levels are blended into each other (as it is just the case in region 1).
In region 2 , on the other hand, the dependence is stronger than linear ($\sim\mathcal{N}_p^{1.4}$). For frequencies located between the dominant line peaks in region 3 (that is, in its 'continuum' part) the dependence may be even stronger because the increase in the line broadening related to an increase in $\mathcal{N}_p$ can bring the frequency point from the line wing close to the line center of the dominant line, an effect which adds to the $\sim\mathcal{N}_p^{0.7}$ increase of κ_0 in the line center (see Figs.14 and 15 where κ_0 increases by about 2 orders of magnitude between the nα- line peaks as $\mathcal{N}_p$ changes from 10^4 to 10^5 cm^{-3} (as already mentioned above , the line profile differs significantly from the assumed Gaussian function in the line wings (see Sect.2.3, below Eq.**(61)**) and the actual relative increase may therefore be somewhat less)).

Fig.16 has been added here in order to justify the above argumentative use of the nα-transitions to explain the behaviour of κ_0 with frequency. It shows that they contain in fact all the features of the total scattering coefficient and amount at least to 50% of its absolute magnitude apart from frequencies between the nα- peaks in region 3 (compare to Fig.12).

3.4.2 Effective Density of Excited Atoms at a Given Frequency

The scattering coefficient $\kappa_0(f)$, as given by Eq.**(106)** and discussed in the previous section, is related to an effective density of excited atoms for the wave of frequency f through Eqs.**(107)** and **(108)**.
From the results displayed in Figs.11, 12 and 13 one derives in this way the effective density $N_{eff}(f)$ as shown in Figs.17, 18 and 19 respectively (thick solid curve, left ordinate). It is evident that for frequencies in region 1 and 2 (that is, in the 'continuum ' part of the scattering coefficient where the line broadening (thin solid curve in **Figs.11-13**) exceeds the line separation (long-dashed line in **Figs.11-13**)) the effective density at frequency f is much higher than the number density N_n (thin solid curve in **Figs.17-19**) of those levels n associated to f by the frequency relationship for $n\alpha-$ transitions (upper abscissa). In region 2, the ratio of the two curves for a given point on the abscissa can thus be interpreted as the number of levels able to scatter the wave of the given frequency (this is not possible in region 1, since scattering is here by all states higher than the state where the level broadening exceeds the level separation, and quantum number n and frequency f are therefore not directly related anymore).

The 'scattering coherence' parameter $\delta(f)$ (Eq.**(110)**) is shown in **Figs.17-19** as the dashed curve (right ordinate). Remarkably, the transition between the optically different regions of 'incoherent' ($\delta(f) <1$) and 'coherent' (specular) scattering ($\delta(f) >1$) occurs just within the frequency range considered here, i.e. for frequencies usually applied for probing the ionosphere. With increasing plasma density the critical frequency shifts to higher frequencies (≈250 MHz if $\mathcal{N}_p = 10^4$ cm^{-3} , 700 MHz if $\mathcal{N}_p = 10^5$ cm^{-3}, 2 GHz if $\mathcal{N}_p = 10^6$ cm^{-3}). Relatively small variations of $\mathcal{N}_p$ may therefore bring a given frequency from one characteristic region into the other and change the backscatter efficiency considerably in a non-linear way.
One should again be aware, however, that these are considerations based on the assumption of a time independent equilibrium situation and that changes in the plasma density will not immediately be reflected in the scattering coefficient since it takes a considerable time until the additional free electrons have recombined into excited atomic states. More important are therefore probably time dependent non-equilibrium effects due to increases in the loss frequencies ν_n^c and (or) ν_n^* (see end of Sect.2.1 and Sect.3.5).

3.4.3 Effective (Coherent) Scattering Coefficient

The effective (coherent) scattering coefficient $\kappa(f)$ is obtained from the atomic (incoherent) scattering coefficient $\kappa_0(f)$ (see Sect.3.4.1) and the parameter $\delta(f)$ (see Sect.3.4.2) by means of Eq.**(111)**. In Figs.11, 12, 13 it is shown as the thick solid curve. It is evident that $\kappa(f)$ becomes strongly enhanced over $\kappa_0(f)$ with decreasing frequency due to the increasing value of $\delta(f) > 1$. The existence of three different regions (see Sect.3.4.1) is still preserved, with the constant region 1 of $\kappa_0(f)$ changing to a f^{-2} slope and the f^{-2} behaviour of $\kappa_0(f)$ in region 2 to f^{-4}. In region 3 both curves coincide, which is due to the accidental circumstance that $\delta(f)$ becomes smaller than 1 at about the same frequency where the line separation begins to exceed the line broadening.
It is furthermore evident from the figures that $\kappa(f)$ depends much stronger on the plasma density than $\kappa_0(f)$ because of the additional dependence of $\delta(f)$ on $\mathcal{N}_p$ ($\sim\mathcal{N}_p^{1.2}$ in region 1 , $\sim\mathcal{N}_p^{2.2}$ in region 2 and between the $n\alpha$ -lines in region 3 and $\sim\mathcal{N}_p^{0.9}$ in the centers of the $n\alpha$-lines in region 3).
Interestingly, $\kappa(f)$ yields an optical depth >1 for the ionosphere for frequencies in the HF region and lower (f< a few MHz) (for $\mathcal{N}_p = 10^5$ cm^{-3} and f=4 MHz, τ_{sc}=1 would be reached within a distance of 10 km). This means that for those frequencies the ionosphere becomes opaque and (in the limit of large optical depths) totally reflective.

A comparison of $\kappa(f)$ with the experimental determination by Moorcroft (1987) (Fig.20, the absolute values can be compared directly) shows quite a good agreement for frequencies from 30 MHz to 1.2 GHz if one drops Moorcrofts assumption that $\kappa(f)$ can be represented by a simple power law and includes the measured values for the lowest and highest frequencies which have been excluded from Moorcrofts least square fit. One should hereby note that an exact agreement would be rather accidental, because the experimental determination is subject to several uncertainties (note Moorcrofts title 'Estimates of...'). In particular is the assumption of an isotropic scattering phase function not consistent with the 'orthogonality effect' (magnetic aspect angle dependence) which is always associated with radar backscatter as long as one has 'specular' scattering ($\delta(f)>1$) . This could lead here to an overestimation of the backscatter coefficient by a few (up to 4, most likely 2-3) orders of magnitude. On the other hand, destructive interference of the contributions of scattering atoms along the line of sight could reduce the received power by a similar amount which only accidentally would cancel with the first effect.
In view of the compatibility of the theoretical (as obtained with the present approach) and experimental determinations of $\kappa(f)$, it seems therefore to be doubtful that any other mechanism than resonant scattering by atomic Rydberg states (i.e. the well known diverse 'coherent' and 'incoherent' backscatter 'theories') could be relevant at all for explaining the scattering of radio waves in general.

3.4.4 Further Discussion of the Level Broadening

It is worthwhile to have a closer look at the level broadening as a function of the quantum number (thin solid curve in Figs.11, 12, 13), since this is the crucial quantity determining the scattering coefficient. As indicated at the end of Sect.3.4.1, the broadening (which is only due to the component $(\Delta f)_B$ for those n values of interest here (see remarks in Sect.3.4 and Eq.**(76)** and following)) increases strongly with n ($\sim n^5$) if n is small enough so that T_n is small compared to the shortest plasma fluctuation time scale which is in this case Δt_e (Eq.**(64)**). If only electrons would be present, the broadening should reach a maximum with increasing n at a quantum number where the usual $\sim n^2$ increase of the broadening is just compensated by the function ζ_n (see Eq.**(60)**; this happens at about $2 \cdot n_e$ if n_e is the state where $T_{n_e} = \Delta t_e$) and then decrease with a $\sim 1/n$ behaviour in the limit $T_n >> \Delta t_e$ as it follows from Eqs.**(52)** and **(60)**. The presence of ions, however, changes this picture since an additional characteristic fluctuation period Δt_I (Eq.**(65)**) is introduced, which leads to a superposition of the individual broadenings as given by Eq.**(66)** with the consequence of a strong increase in the broadening as soon as the ion component becomes dominant. If n becomes so large that $T_n > \Delta t_I$, also the ion broadening becomes saturated and eventually decreases again $\sim 1/n$ if $T_n >> \Delta t_I$ (for the plasma densities considered here, the ion broadening exceeds the electron broadening for quantum numbers of the order of n>1000 which is here however without any significant consequence for the scattering coefficient at the corresponding nα-transition frequencies, since the broadening exceeds the level separation already for smaller n (> 500-700) so that all lines corresponding to levels higher than this contribute anyway with their (close to -) line center cross section. Apart from this, scattering by levels blended into each other because of collisional broadening is here supposed to be strongly reduced (see discussion in Sect.3.4.1 concerning the interpretation of the atomic (incoherent) scattering coefficient in region 1)).
It should be noted that it is of course only accidental that the electron dominated broadening reaches its maximum close to the same quantum number where it exceeds the level separation (at about n≈500 for $\mathcal{N}_p^* = 10^5$ cm^{-3}). With a different bulk energy of the plasma electrons than 0.5 Rydberg for instance , the maximum shifts to different values of n because the fluctuation period Δt_e (Eq.**(64)**) changes.

With regard to astrophysical applications, it is interesting that the observed width of emission lines in the radio spectrum of HII - regions has about the same value as one would expect from the Stark broadening due to plasma field fluctuations for those conditions. This is evident from Fig.21 which shows the H157α - line at 1.6832 GHz emitted from the Orion nebula (Pankonin, 1980, p. 121) (the halfwidth corresponds to about 100 kHz if transformed into frequencies) and Fig.22 giving the theoretical scattering profile for this line as one would expect it from Stark broadening in a plasma of $\mathcal{N}_p^* = 2 \cdot 10^3$ cm^{-3} (this is thought to be the highest plasma density in the Orion nebula

(Lang, 1974, p.121)). Note that the resultant (half) line width of about 75 kHz is solely due to the Stark broadened atomic levels , since a temperature of 10 ^{o}K has been assumed here which yields a negligible thermal Doppler broadening compared to this. It is therefore likely that the commonly accepted interpretation of the line broadening in HII- regions as a thermal effect (which implicates temperatures of about 10^4 ^{o}K) is at least in some cases incorrect.

3.4.5 Dependence of the Scattering Coefficient on the Ionizing RadiationFlux

As already indicated in Sect.3.3, the excited atom density N_n, and therewith also the scattering coefficient κ, depends on the ionizing radiation flux if the latter leads to photoionization frequencies ν_n^* which are greater than the decay constant A_n and the collisional ionization frequency ν_n^c. For the case of the earths ionosphere, the solar radiation flux corresponding to quiet (normal) conditions is just not strong enough to affect the equilibrium densities significantly (see Fig.6) (only for plasma densities as low as $\mathcal{N}_p^* = 10^4$ cm^{-3} it might become moderately relevant; see Fig.7 for quantum numbers n=500-1000). During times of enhanced solar activity however, the radio flux increases by orders of magnitude in particular at low frequencies (see Fig.10) and the resultant photoionization becomes the dominant loss process for levels n≥300, thus reducing N_n for those states. Fig.23 shows the result for $\kappa_0(f)$ and $\kappa(f)$ for the strongest (Type IV) solar bursts observed and a plasma density of $\mathcal{N}_p^* = 10^5$ cm^{-3} (that is, corresponding to Fig.9)) which has to be compared to the quiet conditions scattering coefficient of Fig.12. It is evident that the scattering coefficient is significantly reduced for f<200 MHz (by about a factor 0.5 for f =100 MHz and a factor 0.2 if f =1 MHz). With a plasma density of $\mathcal{N}_p^* = 10^4$ cm^{-3} (which may be even more appropriate for the lower ionosphere), the effect is even more dramatic and results in a more than 2 orders of magnitude decrease in $\kappa(f)$ for f<10 MHz with the related optical depth changing from optically thick to thin for frequencies around 1 MHz (see Fig.24 in comparison to Fig.11).

Since $\kappa(f)$ is a direct measure of the reflectivity of the ionosphere, it is a straightforward conclusion to relate this effect to the so called short wave fadeout which is observed for the transmission of radio waves between frequencies of 500 kHz and 10 MHz after the onset of a solar flare (burst) (Mitra, 1974; pp. 5, 27) . The almost simultaneous fading of the signal with the increase of the solar radio flux at frequencies f≥600 MHz (Fig.25) is in fact consistent with the assumption that photoionization of highly excited states is responsible for this effect, since the photoionization frequencies are so high (see dotted curve in Fig.9) that the Rydberg atoms become ionized within fractions of a second for the strongest bursts. It is therefore not a 'curious requirement' (Mitra, 1974, p.93) that a threshold solar radio flux is needed for 'Sudden Ionospheric Disturbances' to occur, but an expression of the fact that only above a certain value of the radio flux the photoionization frequency ν_n^* is high enough (in comparison to the collisional ionization frequency ν_n^c) to affect the population number of atoms in high Rydberg states significantly and cause the reflectivity of the ionosphere to change.

Obviously, the same 'fadeout' effect can be achieved artificially by illuminating the relevant region of the ionosphere with a sufficiently powerful radio signal of the appropriate frequency. In this sense, Fig.26 gives (in comparison to Fig.12) the scattering coefficient for a plasma of density $\mathcal{N}_p^* = 10^5$ cm^{-3} subject to an ionizing microwave radiation with a frequency of $f_w^* = 35$ GHz and a field strength of $E_w^* = 0.2$ V/m at the

location of scattering. For frequencies f<200 MHz the scattering coefficient is here reduced by about 2 orders of magnitude because of the strong additional loss of electrons in states n higher than the threshold level $\sqrt{(3.2898 \cdot 10^{15}\ \text{Hz} / f_w^*)}$ (≈300 here) (Fig.27, thin solid curve in comparison to Fig.18 ; see Eq.**(24)** and following for the relation between threshold frequency and quantum number (the small scale variations in the curve for n>300 are not real but of a numerical nature due to the finite grid resolution and the almost monochromatic microwave frequency spectrum).

It should again be emphasized that these are equilibrium results, i.e. in both cases (natural or artificial) will the observed effects be even much stronger if one considers times after the increase of the radiation flux which are short compared to the equilibrium relaxation time (this is of the order of several hours for ionospheric plasma densities and the frequencies considered here; see Sect.3.5). For this reason, only a relatively small increase in the ionizing radiation flux is needed to produce a short term non- equilibrium reduction of the scattering coefficient comparable in magnitude to the equilibrium effects shown here.

3.5 Non- Equilibrium Considerations

All numerical results presented in chapter 3 are based on the initial assumption of a detailed balance equilibrium. As already indicated at the end of Sects.2.1 , 3.3, 3.4.2 and 3.4.5, they are therefore only strictly valid if the considered physical conditions vary slowly compared to the longest characteristic time constant entering into the problem. It is obvious that for instance a variation in the total density of free plasma electrons $\mathcal{N}_p$ will not lead to a different scattering coefficient for radio waves until it causes a corresponding change in the level densities N_n . On the other hand, a sudden removal of electrons in the excited atomic states (by means of photo- or electron impact - ionization for instance) will be related to an instantaneous drop in the scattering coefficient which will then only gradually return to its equilibrium value as the states are re-populated from the free electron spectrum. For level n this takes (on the statistical average) a time $1/A_n^{Rec}$ (Eq.**(5)**) which amounts from about 1 to many hours for the states of interest here. With variations in the bulk plasma parameters (total electron density and mean energy), there is even a further delay $1/\nu_0^c$ (see Appendix B, Eq.**(B.23)**) until the change becomes apparent (by means of elastic collisions) at electron energies which are responsible for the recombination into those levels n of interest here. For ionospheric plasma densities, the collisional time scale becomes dominant if n<150, whereas for larger n (which covers those states relevant for the numerical results for the scattering coefficient presented in this work), the recombination time scale is larger and determines therefore the time dependent behaviour (one should again realize that $1/A_n^{Rec}$ is the duration of the quantum mechanical recombination process (the effective life time of the 'pre-bound' level n, see Sect.2.1 and Fig.1) which has to be distinguished from the recombinative collision time for the free plasma electron which is given by Eq.**(17)** and is much shorter than $1/A_n^{Rec}$ for the levels and plasma densities of interest here and is in particular always smaller than the time for elastic collisions $1/\nu_0^c$ for the ion mass and temperature assumed here (see Eq.**(A.2.9)**).

The long time scale associated with the establishment of an equilibrium between the free and bound electron spectrum enables considerable deviations from this equilibrium situation over time scales short compared to this , as indicated above . This could be one of the reasons that one observes for instance sometimes orders of magnitude variations in radar backscatter from the ionosphere within a few minutes or gets an almost instantaneous fading of radio signals transmitted over the ionosphere (short wave fade out) after the onset of strong solar flares (see also Sect.3.4.5).
It is therefore evident that a time dependent approach has to be formulated if one is interested in a time resolution which is better than the characteristic time scales $1/A_n^{Rec}$ and $1/\nu_0^c$. In the context of ionospheric physics this is certainly predominantly the case unless one is dealing with data sets integrated or averaged over several hours or more. In the latter case, the detailed equilibrium theory used in this paper should, apart from giving

general insight into the relationship between the relevant physical quantities, also yield quantitatively correct numerical results (see for instance the discussion of the theoretical and experimental radar scattering coefficients in Sect.3.4.3).

4. Concluding Remarks and Outlook

The results obtained with the present detailed equilibrium approach show that commonly used methods to calculate excited atom densities, which are always related to some kind of LTE- assumption, can not even approximately describe the actual situation which is strongly determined by the quantum mechanical cross sections and time constants of the individual levels. Any theory which does not proceed from these atomic properties (e.g. the usual statistical equilibrium approach) is therefore a priori invalid and must necessarily lead to wrong conclusions. This may be the reason why the process of resonance scattering by high atomic Rydberg states has not yet been considered as a possible mechanism affecting the propagation of radio waves, since the usual Boltzmann distribution underestimates the excited level density dramatically.

The present theoretical work attempts to give a general, complete and detailed coverage of the basic concepts necessary to calculate the efficiency for the scattering of electromagnetic waves by excited atoms without referring to any inconsistent and misleading ad hoc concepts but using only elementary physical laws on a microscopic level and deriving the macroscopic quantities in a logical and deductive way.

A modification of the theory to a time dependent formalism, which is necessary for instance for ionospheric problems if one is interested in a time resolution shorter than a few hours, should in principle be straightforward to accomplish without further basic theoretical work.

With regard to certain situations, it might also become unavoidable to consider inelastic collisions of electrons as an important mechanism affecting the scattering coefficient for radio waves due to the related production rate of electrons at very small energies exceeding the one due to elastic collisions and enhancing therefore the recombination rate into high Rydberg states accordingly. For example, strong increases in the rate of excitation of discrete atomic transitions by electrons are observed during non-linear plasma oscillations in the ionosphere induced by means of high power radio waves (Smid, 1992a) and may in this way explain associated changes in the characteristics of the propagation of radio waves through the affected region.

As a further aspect, future work has to include the problem of the frequency- and angular redistribution of the radiation resonantly scattered by Stark shifted and -broadened levels in the presence of a magnetic field and the task of determining the total spatial interference wave field from the contributions of the individual atoms. With this, one would then for instance be able to calculate the exact frequency dependence of radio wave spectra backscattered from the ionosphere, if additionally the modulation of the wave by the non- linear interaction with the magnetized plasma is taken into account (Smid, 1992b).

In consideration of the addressed theoretical aspects and the numerical results of this paper, it appears to be possible that the concept of resonance scattering by atomic states can generally serve as a basis for a unified theory for the interaction and propagation of electromagnetic waves in arbitrary media, which may replace inconsistent and unphysical

ad hoc theories presently applied to corresponding problems.

Appendix A

Cross Sections and Decay Constants for Atomic Dipole Transitions

A.1 Transitions Between Bound States

The physical parameters for atomic dipole transitions can generally be obtained by considering the power radiated by an oscillator whose dipole moment is given by the quantum mechanical overlap integral

$$\langle r\rangle_{i,k} := r_0 \cdot \int_0^{\infty} d\rho \; \Psi_i(\rho) \cdot \rho \cdot \Psi_k(\rho) \qquad \textbf{(A.1.1)}$$

where Ψ_i and Ψ_k designate the normalized radial wave functions of the energetically lower and upper state respectively (where state k is characterized by the pair of principal quantum number and angular momentum (n,l) and i by (m,l±1)) and ρ is a dimensionless distance parameter which is normalized to the Bohr radius

$$r_0 = h^2/(4\pi^2 m e^2)$$
$$= 5.3 \cdot 10^{-9} \quad [\text{cm}] \quad , \qquad \textbf{(A.1.2)}$$

where h is Planck's constant, m the electron mass and e the elementary charge.

As a result (Smid, 1987), the damping constant related to the transition with the associated frequency $f_{i,k}$ is obtained as

$$A_{i,k} = 16\pi^4 \cdot e^2 \cdot f_{i,k}^3 / 3c^3 h \cdot \langle r\rangle_{i,k}^2 \quad , \qquad \textbf{(A.1.3)}$$

where c is the velocity of light,
and the cross section for resonant absorption or scattering of radiation of frequency f is determined through

$$\sigma_{i,k}(w) = 2\pi^{5/2} \cdot e^2/h \cdot f_{i,k}/c/(\Delta f)_D \cdot \langle r\rangle_{i,k}^2 \cdot H(a,w) \quad , \qquad \textbf{(A.1.4)}$$

with

$$w = (f-f_{i,k})/(\Delta f)_D \qquad \textbf{(A.1.5)}$$

being the difference between the frequency of the radiation and the resonance frequency normalized to the Doppler width

$$(\Delta f)_D = f_{i,k}/c \cdot \sqrt{(2kT/M)} \quad , \qquad \textbf{(A.1.6)}$$

where k is the Boltzmann constant, T the temperature and M the mass of the radiating atoms (ions) which are assumed here to have a Maxwellian velocity distribution.

The frequency dependence of the cross section is determined by the well known Voigt-function

$$H(a,w) = a/\pi \cdot \int_{-\infty}^{\infty} du \; e^{-u^2} / [(w-u)^2+a^2] \quad , \qquad \textbf{(A.1.7)}$$

where

$$a = A_{i,k}/ 4\pi /(\Delta f)_D \quad . \qquad \textbf{(A.1.8)}$$

In most cases of interest, $a<<1$, so that $H(a,w)$ can be approximated by the pure Doppler line profile e^{-w^2}. Note however that **(A.1.7), (A.1.8)** neglects any initial level broadening of the individual atom, since it contains only the apparent ('natural') frequency broadening due to the finite duration $1/A_{i,k}$ of the transition between the two sharp levels involved and the Doppler broadening caused by the Maxwellian velocity distribution of the atoms.
The case of an explicit level broadening is discussed in Sects.2.3 and 2.5, where the resonant cross section including collisional Stark broadening is derived.

Explicit numerical calculations show now that for degenerate l-states (which can be assumed in the case of highly excited atoms), the dipole integral **(A.1.1)** depends primarily upon the principal quantum numbers, in the approximate form

$$\langle r \rangle_{m,n} \approx \langle r \rangle_{m,m+1} \cdot (f_{m,m+1}/f_{m,n})^{1.5} \cdot (m/(n-1))^{1.6} \quad . \qquad \textbf{(A.1.9)}$$

In the case of large m, the Rydberg formula yields the further approximation

$$f_{m,m+1} = f_0 \cdot [1/m^2 - 1/(m+1)^2] \approx$$
$$\approx 2f_0/m^3 \quad , \qquad \textbf{(A.1.10)}$$

with

$$f_0 = 3.2898 \cdot 10^{15} \text{ Hz} \quad , \qquad \textbf{(A.1.11)}$$

and the dipole integral for the mα-transition can be written as

$$\langle r \rangle_{m,m+1} \approx r_0/2 \cdot m^2 \quad , \qquad \textbf{(A.1.12)}$$

so that Eq.**(A.1.9)** becomes (after substituting the explicit Rydberg formula for $f_{m,n}$)

$$\langle r \rangle_{m,n} \approx 1.4 \cdot r_0 \cdot [\, 1/m^2 - 1/n^2 \,]^{-1.5} \cdot m^{-0.9} \cdot (n-1)^{-1.6} \quad . \qquad \textbf{(A.1.13)}$$

With this, one obtains the numerical approximations

$$A_{m,n} \approx 1.3 \cdot 10^9 \cdot m^{-1.8} \cdot (n-1)^{-3.2} \qquad [\text{sec}^{-1}] \qquad (m,n >> 1) \qquad \textbf{(A.1.14)}$$

and

$$\sigma_{m,n}(w) \approx 5.1 \cdot 10^{-12} \cdot [\, 1/m^2 - 1/n^2 \,]^{-3} \cdot m^{-1.8} \cdot (n-1)^{-3.2} \cdot \sqrt{(A/T)} \cdot H(a,w) \qquad [\text{cm}^2] \ ,$$

$$(m,n >> 1) \quad , \qquad \textbf{(A.1.15)}$$

where A is the atomic mass number (=M/M_H with M_H the mass of a hydrogen atom) and T the temperature in ^oK.

The summation of Eq.**(A.1.14)** over m yields the total decay probability for the level n

$$A_n = \sum_{m=1}^{n-1} A_{m,n} \qquad ; \quad (n \geq 2) \quad . \qquad \textbf{(A.1.16)}$$

which can be numerically approximated by

$$A_n \approx 1.1 \cdot 10^9 \cdot (n-1)^{-3.6} \qquad [\text{sec}^{-1}] \quad , \qquad \textbf{(A.1.17)}$$

as it emerges from an explicit numerical evaluation of **(A.1.16)** with **(A.1.14)** including a

correction for the contribution of higher angular momentum values (see Eq.**(20)** and Appendix A.2, Eq.**(A.2.10)** and following) .

It should be noted that the dependence on the angular momentum quantum number, which has been neglected from Eq.**(A.1.9)** onwards, might introduce an error up to about a factor 2 for the absolute values of $A_{m,n}$ and $\sigma_{m,n}$ as obtained by Eq.**(A.1.14)** and **(A.1.15)** (this results from numerical calculations of the dipole integral involving the actual wave functions $\Psi_{(m,l\pm1)}$ and Ψ_{nl}). The relative values for a fixed angular momentum, on the other hand, which determine the branching ratios into the different levels, can be considered to be accurate to within a few percent. Even here, one has nevertheless to exclude very high angular momenta, because the dipole integral turns out to 'collapse' to extremely small values if l comes close in value to the principal quantum number m if m is large. Since those transitions contribute however only a small fraction to the sum of all possible ones (in particular in view of the fact that recombination tends to populate only the lowest angular momenta of a given level, see next Sect. A.2), the error introduced by this circumstance can be neglected for the present purpose.
Furthermore, the explicit numerical calculations show that even for the lowest quantum numbers (for which the approximations **(A.1.10)** and **(A.1.14)** are in principle not valid anymore) Eqs.**(A.1.14)** and **(A.1.17)** are reasonably good approximations to $A_{m,n}$, A_n and $\sigma_{m,n}$.

A.2 Photoionization and Radiative Recombination

The concept outlined in Section A.1 can easily be extended to bound-free transitions by replacing the wave function of the upper state in Eq.**(A.1.1)** by a continuum wave function of the energy ε , i.e.

$$\langle r \rangle_{nl}(\varepsilon) = N_{B,F} \cdot r_0 \cdot \int_0^\infty d\rho \, \Psi_{nl}(r) \cdot \rho \cdot [\, c_l \cdot F_{l-1}(\varepsilon,\rho) + F_{l+1}(\varepsilon,\rho) \,] \quad , \qquad \textbf{(A.2.1)}$$

where $F_{l-1}(\varepsilon,\rho)$ and $F_{l+1}(\varepsilon,\rho)$ are the regular Coulomb wave functions for the two angular momenta allowed by the selection rules for dipole transitions (the angular momentum quantum number l has now been explicitly included because of its greater importance for bound- free transitions (see Eq.**(A.2.10)**).
Note that the dipole integral is evaluated with the sum of the two possible continuous wave functions which are related to the angular momentum l of the bound state by the l-selection rule for dipole transitions, rather than by calculating the dipole integral separately for each l value and adding the results later. This form is assumed here to make more sense for the present case of bound- free transitions, since it is not possible to define the angular momentum of a free electron uniquely before recombination into the bound state nl of a particular ion has taken place. Reversely, the notion of an angular momentum for an electron is in principle meaningless after photoionization out of the atom has occurred (it should be noted that the two indicated methods for calculating the dipole integral produce anyhow only insignificantly (for the present purpose) different results, which are within a factor of 2).

The factor

$$c_l = \begin{cases} 0 \text{ for } l=0 \\ 1 \text{ for } l>0 \end{cases} \qquad \textbf{(A.2.2)}$$

takes the special situation for l=0 into account, where only one transition is allowed by the selection rule,
and the dimensionless normalization constant

$$N_{B,F} = 8.3 \cdot 10^{-6} \qquad \textbf{(A.2.3)}$$

has to be applied here because the integral over $F_l(\varepsilon,r)$ can not be normalized separately like the wave functions for the bound states $\Psi_{nl}(r)$. It is determined from experimental

measurements of the photoionization cross section by comparing it with the unnormalized theoretical result . The latter is obtained by inserting **(A.2.1)** instead of **(A.1.1)** into Eq. **(A.1.4)** and integrating over the atomic line profile H(a,w) with respect to w as (Smid, 1987)

$$\sigma_{nl}^{Ion}(f(\varepsilon)) = 2\pi^3 \cdot e^2/h \cdot \sqrt{(M/2kT)} \cdot \langle r \rangle_{nl}^2(\varepsilon) \cdot N_{B,F} \quad , \qquad \textbf{(A.2.4)}$$

where f(ε) is the frequency of the ionizing radiation which is associated with the continuum energy ε through Eq.**(24)**, Sect.2.1.

The cross section for radiative recombination is obtained from Eq.**(A.2.4)** by means of symmetry arguments, i.e.

$$\sigma_{\eta l}^{Rec}(\varepsilon) = \sigma_{nl}^{Ion}(f(\varepsilon)) \qquad \textbf{(A.2.5)}$$

(note that here and in the following formulae, the index η rather than the (numerically identical) quantum number n is being used with the recombination cross section, indicating that it is strictly to be understood as the cross section for the (collisionfree) recombination into the 'pre-bound' state η from which then the decay into the actual level n occurs if collisions do not interfere during its lifetime $1/A_n^{Rec}$ (see Eq.**(A.2.19)** and Section 2.1, Eq.**(5)** and following)).

Averaging over the angular momentum yields the cross section into the level n

$$\sigma_{\eta}^{Rec}(\varepsilon) = 1/n \cdot \sum_{l=0}^{n-1} \sigma_{\eta l}^{Rec}(\varepsilon) \quad . \qquad \textbf{(A.2.6)}$$

from which the total cross section for recombination of an electron of energy ε into all bound states is obtained as

$$\sigma_{T}^{Rec}(\varepsilon) = \sum_{\eta=1}^{\infty} \sigma_{\eta}^{Rec}(\varepsilon) \quad . \qquad \textbf{(A.2.7)}$$

Explicit numerical calculations of the recombination cross section involving the exact hydrogenic wave functions have been performed for continuum energies $\varepsilon = 10^{-8}$ to 4 Rydberg and bound states n=1....1000 (Smid, 1987 and unpublished work).

As a symmetry property, one observes that for any n, $\sigma_{//}^{Rec}(\varepsilon)$ has its maximum value approximately at an energy

$$\varepsilon_n = 1/n^2 \quad , \qquad \textbf{(A.2.8)}$$

with ε_n in units of Rydberg , and that this peak cross section can be approximated by the power law

$$\sigma_{//}^{Rec}(\varepsilon_n) \approx 3.7 \cdot 10^{-17} \cdot \sqrt{(A/T)} \cdot n^{2.4} \quad [cm^2] \quad , \qquad \textbf{(A.2.9)}$$

where A is the ion mass number and T the ion temperature in ^{o}K (note that for other elements than hydrogen, n has to be interpreted here as designating the effective quantum number (i.e. n=1 for the lowest unoccupied state of the ion) rather than the actual quantum number).
The distribution over the different angular momenta is hereby such that the recombination cross section is only slowly decreasing with l for $l=n^{0.75}$ but drops rapidly if l is greater than this, i.e. one can approximately set (see Eq.**(A.2.6)**)

$$\sigma_{//l}^{Rec}(\varepsilon_n) = \begin{cases} \sigma^{//Rec}(\varepsilon_n) \cdot n_{0.25} & \text{for } l \le n_{0.75} \\ 0 & \text{for } l > n_{0.75} \end{cases} \quad ; \qquad \textbf{(A.2.10)}$$

(note that those electrons which have recombined into the bound state nl are not able to decay directly into a lower lying energy level m in the case l>m because of the l-selection rule for dipole transitions; this circumstance together with **(A.2.10)** leads directly to the correction factor for the transition matrix Eq.**(20)** ,Sect.2.1).

If $\varepsilon<\varepsilon_n$, $\sigma_{//}^{Rec}(\varepsilon)$ turns out to be approximately constant with energy (only for n=1 does one observe a dependence roughly $\sim\sqrt{\varepsilon}$ if $\varepsilon<<1$), whereas for $\varepsilon>>\varepsilon_n$ the cross section decreases rapidly $\sim \varepsilon^{-2.9}$. The transition region is obviously difficult to approximate analytically. Since it occurs however only within a relatively narrow energy band, it is sufficient for the present purpose to approximate the energy dependence of $\sigma_{//}^{Rec}(\varepsilon)$ for fixed n by the schematic function

$$h(\varepsilon,\varepsilon_n) = \begin{cases} 1 & \text{for } \varepsilon \le 2\varepsilon_n \\ (\varepsilon/(2\varepsilon_n))^{-2.9} & \text{for } \varepsilon > 2\varepsilon_n \end{cases} \quad , \qquad \textbf{(A.2.11)}$$

so that

$$\sigma_{\ell}^{Rec}(\varepsilon) = \sigma_{\ell}^{Rec}(\varepsilon_n) \cdot h(\varepsilon,\varepsilon_n) \quad . \qquad \textbf{(A.2.12)}$$

In order to obtain the cross section for a given energy instead of a given quantum number, one transforms the function h by means of Eq.**(A.2.8)** into

$$h(n,\varepsilon) = \begin{cases} 1 \text{ for } n \leq \sqrt{(2/\varepsilon)} \\ (n/\sqrt{(2/\varepsilon)})^{-5.8} \text{ for } n > \sqrt{(2/\varepsilon)} \end{cases} , \qquad \textbf{(A.2.13)}$$

and gets thus the alternative relationship

$$\sigma_{\ell}^{Rec}(\varepsilon) = \sigma_{\ell_\varepsilon}^{Rec}(\varepsilon) \cdot h(n,\varepsilon) \quad , \qquad \textbf{(A.2.14)}$$

where

$$n_\varepsilon = 1/\sqrt{\varepsilon} \qquad \textbf{(A.2.15)}$$

is the inversion of Eq.**(A.2.8)** for continuous energy values and $\sigma_{\ell_\varepsilon}^{Rec}(\varepsilon)$ is the corresponding generalization of the peak cross section Eq.**(A.2.7)** to the continuous quantum number n_ε.

(It should be noted that if $h(\varepsilon,\varepsilon_n)$ (or $h(n,\varepsilon)$) $<<1$, the distribution of the recombination cross section over angular momentum turns out to be even more concentrated towards small l-values than given by the peak cross section scheme **(A.2.10)**. Since those cross sections are however much smaller, their contribution to the recombination rate into level n is only of minor importance, so that **(A.2.10)** can still be assumed to determine the angular momentum correction factor for the decay probability of the bound states (Eq. **(20)**, Sect.2.1)).
By using Eq.**(A.2.14)** and evaluating Eq.**(A.2.7)** numerically, one obtains the total cross section for recombination of an electron of energy ε into all bound states as

$$\sigma_T^{Rec}(\varepsilon) \approx 5.4 \cdot 10^{-17} \cdot \sqrt{(A/T)} \cdot \varepsilon^{-1.7} \qquad [cm^2] \quad (\varepsilon \leq 2) \qquad \textbf{(A.2.16)}$$

with ε again in units of Rydberg (for energies $\varepsilon>2$, $\sigma_T^{Rec}(\varepsilon)$ has to be taken identical to $\sigma_{\ell}^{Rec}(\varepsilon_n)$ (Eq.**(A.2.9)**) for n=1).

In the case of negligible Stark broadening of the bound levels (compared to their energy) ,

i.e. if $\eta_n^{Rec}=1$ (see Sect.2.3, Eq.**(79)**), the related total recombination frequency (see Sect.2.1, Eqs.**(17)** and **(40)**) becomes therewith numerically

$$\begin{aligned}\nu_{\mathcal{I}}^{Rec,0}(\varepsilon) &= \mathcal{N}_p^{\circ} \cdot v_e(\varepsilon) \cdot \sigma_{\mathcal{I}}^{Rec}(\varepsilon) = \\ &= \mathcal{N}_p^{\circ} \cdot v_e(\varepsilon=1) \cdot \sqrt{\varepsilon} \cdot \sigma_{\mathcal{I}}^{Rec}(\varepsilon) \approx \\ &\approx 1.2 \cdot 10^{-8} \cdot \mathcal{N}_p^{\circ} \cdot \sqrt{(A/T)} \cdot \varepsilon^{-1.2} \; [sec^{-1}] \;\; ; \;\; (\eta_n^{Rec}=1;\, \varepsilon \leq 2) \quad , \quad \textbf{(A.2.17)}\end{aligned}$$

where the plasma density $\mathcal{N}_p^{\circ}$ has to be taken in $[cm^{-3}]$ and the superscript 0 has been added to $\nu_{\mathcal{I}}^{Rec}$ in order to emphasize that this quantity describes the collisionfree recombination frequency into the 'pre-bound' state $\mathcal{II}$ (for energies $\varepsilon>2$, $\sigma_{\mathcal{I}}^{Rec}(\varepsilon)$ in the above equation has again to be replaced by $\sigma_{\mathcal{II}}^{Rec}(\varepsilon_n)$ (Eq.**(A.2.9))** for n=1).

The lifetime of the the 'pre-bound' state $\mathcal{II}$ with regard to recombination into the actual bound level n is obtained by generalizing Eq.**(A.1.3)** to bound- free transitions by multiplying the expression with the normalizing factor $N_{B,F}$ (Eq.**(A.2.3)**) (one has to take the same factor here as for the cross section because both quantities depend on the square of the dipole integral (from which the need of a normalization arises ; see below Eq. **(A.2.3)**).
One can therefore write

$$A_{nl}^{Rec}(\varepsilon) = [\, 16\pi^4 \cdot e^2 \cdot f_{nl,\varepsilon}^{\,3} \,/\, 3c^3h \,] \cdot \langle r \rangle_{nl}^{\,2}(\varepsilon) \cdot N_{B,F} \quad , \quad \textbf{(A.2.18)}$$

which (for those angular momenta where the recombination cross section Eq.**(A.2.10)** is different form zero), can be numerically approximated by

$$A_n^{Rec} = 7 \cdot 10^4 \cdot n^{-3.4} \qquad [sec^{-1}] \quad . \qquad \textbf{(A.2.19)}$$

Note that the recombinative decay constant depends only on the bound state n but not the continuous energy ε, which is due to the fact that the energy dependences of $\langle r \rangle_{nl}^{\,2}(\varepsilon)$ and $f_{nl,\varepsilon}^{\,3}$ cancel almost exactly (see Eq.**(A.2.11)**).

Appendix B

Cross Sections and Collision Frequencies for Energy Transfer by Electron-Electron (Coulomb-) Scattering

For particles of arbitrary energy, the calculation of the cross section for Coulomb scattering represents a difficult problem in the laboratory system, which cannot always be solved in closed form or at least leads to complex analytical expressions because of the complicated formula which connects the scattering angles in the laboratory and center of mass system (Landau and Lifshitz, 1982).
With the present problem, however, a great simplification is introduced by the fact that one is primarily interested in electrons which have an energy which is small compared to the energy ε_p of the bulk of the plasma electrons. In this case, the well known Rutherford formula gives to a good approximation the differential scattering cross section, since it just holds for one particle initially resting.
With ε_p being the dimensionless plasma energy (energy of the incident electron) normalized to $E_0 = 1$ Rydberg (in cgs- units) and θ the scattering angle in the center of mass system, the differential cross section for scattering with a low energy electron can thus be written as

$$d\sigma^c(\varepsilon_p,\theta)/d\Omega = e^4 / [\, 16 \cdot E_0^2 \cdot \varepsilon_p^2 \cdot \sin^4(\theta/2) \,] \quad , \qquad \textbf{(B.1)}$$

where e is the elementary charge (in cgs- units) and

$$d\Omega = 2\pi \sin\theta \, d\theta \quad . \qquad \textbf{(B.2)}$$

Even energy changes very small compared to the plasma energy ε_p are fully taken into account by Eq.**(B.1)**, because those can be primarily attributed to small angle scattering of the bulk of higher energetic electrons rather than large angle collisions of the few low energetic electrons.
This is due to the fact that the ratio of the cross section for the latter possibility to the cross section for the former increases more slowly for $\Delta\varepsilon \to 0$ ($\sim \Delta\varepsilon^{-1.5}$) (see Eq.**(B.6)**) than the number of electrons within the energy range $0...\Delta\varepsilon$ decreases ($\sim \Delta\varepsilon^{1.7}$, taking the consistent electron distribution function into account (Figs.3, 4, 5).

The energy change $\Delta\varepsilon$ is generally related to the scattering angle θ through the energy transfer function for particles of equal mass (Landau and Lifshitz, 1982)

$$\Delta\varepsilon/\varepsilon_p = \sin^2(\theta/2) \quad . \qquad \textbf{(B.3)}$$

If one would be interested in the average energy transfer (i.e. scattering about all angles),

the related cross section would be obtained by integrating (from $\theta = 0....\pi$) the product of the differential cross section Eq.**(B.1)**, the energy transfer function Eq.**(B.3)** and a further geometrical weighting function

$$f(\theta) = 1/\pi \cdot \sin(\theta/2) \quad , \qquad \textbf{(B.4)}$$

which takes care of the sphericity of the scattering potential (Smid, 1987).
In the present case, however, one is just interested in those small energy transfers which the function **(B.3)** suppresses, so that only $f(\theta)$ has to be multiplied to the differential cross section. By doing this, changing to the differential (see Eq.**(B.3)**)

$$d(\Delta\varepsilon) = d\theta \cdot \varepsilon_p \cdot \sin(\theta/2) \cdot \cos(\theta/2) \qquad \textbf{(B.5)}$$

and subsequently to $\Delta\varepsilon$ by means of Eq.**(B.3)**, one gets for the differential cross section with regard to a given energy change

$$d\sigma_f^c(\varepsilon_p,\Delta\varepsilon)/d(\Delta\varepsilon) = \sigma_0^c/2 \cdot \varepsilon_p^{-1.5} \cdot (\Delta\varepsilon)^{-1.5} \quad , \qquad \textbf{(B.6)}$$

where

$$\sigma_0^c = 5.6 \cdot 10^{-17} \quad [cm^2] \qquad \textbf{(B.7)}$$

and ε_p and $\Delta\varepsilon$ are in energy units of 1 Rydberg.

Assuming that the energy of an electron within the continuum energy range $\varepsilon_{i-1}, \varepsilon_i$ can be represented by

$$\boldsymbol{\varepsilon_i} = (\varepsilon_{i-1} + \varepsilon_i)/2 \quad , \qquad \textbf{(B.8)}$$

the cross section for scattering from within this range into the given interval $\varepsilon_{k-1}, \varepsilon_k$ is therefore

$$\sigma_{i,k}^c = \sigma_0^c/2 \cdot \varepsilon_p^{-1.5} \cdot \int_{\varepsilon_{k-1}}^{\varepsilon_k} d\varepsilon \; (\pm\varepsilon \mp \boldsymbol{\varepsilon_i})^{-1.5} =$$

$$= \sigma_0^c \cdot \varepsilon_p^{-1.5} \cdot [\pm 1/\sqrt{(\pm\varepsilon_{k-1} \mp \boldsymbol{\varepsilon_i})} \mp 1/\sqrt{(\pm\varepsilon_k \mp \boldsymbol{\varepsilon_i})}] \quad , \qquad \textbf{(B.9)}$$

where the upper sign holds for k>i and the lower for k<i (the exclusion of k=i means that scattering within the interval $\varepsilon_{k-1}, \varepsilon_k$ itself is neglected).

The cross section for collisional loss out of the interval $\varepsilon_{k-1}, \varepsilon_k$ into the whole numerically available energy range $0....\varepsilon_M$ is given by

$$\sigma_{k,L}^c = \sum_{\substack{i=1 \\ \neq k}}^{M} \sigma_{k,i}^c =$$

$$= \sigma_0^c/2 \cdot \varepsilon_p^{-1.5} \cdot \left[\int_0^{\varepsilon_{k-1}} d\varepsilon \ (\boldsymbol{\varepsilon_k} - \varepsilon)^{-1.5} + \int_{\varepsilon_k}^{\varepsilon_M} d\varepsilon \ (\varepsilon - \boldsymbol{\varepsilon_k})^{-1.5} \right] , \qquad \textbf{(B.10)}$$

where, in consistency with Eq.**(B.8)**,

$$\boldsymbol{\varepsilon_k} = (\varepsilon_{k-1} + \varepsilon_k)/2 \quad . \qquad \textbf{(B.11)}$$

Evaluation of the integral yields

$$\sigma_{k,L}^c = \sigma_0^c \cdot \varepsilon_p^{-1.5} \cdot [2\sqrt{2}/\sqrt{(\Delta\varepsilon_k)} - 1/\sqrt{\boldsymbol{\varepsilon_k}} - 1/\sqrt{(\varepsilon_M - \boldsymbol{\varepsilon_k})}] \qquad \textbf{(B.12)}$$

with $\Delta\varepsilon_k$ as defined by Eq.**(41)**.

Furthermore, the cross section for collisional ionization from the bound level n (with energy $-\varepsilon_n$) into the continuum interval $\varepsilon_{k-1}, \varepsilon_k$ is

$$\sigma_{n,k}^c = \sigma_0^c/2 \cdot \varepsilon_p^{-1.5} \cdot \int_{\varepsilon_{k-1}}^{\varepsilon_k} d\varepsilon \ (\varepsilon + \varepsilon_n)^{-1.5} =$$

$$= \sigma_0^c \cdot \varepsilon_p^{-1.5} \cdot [1/\sqrt{(\varepsilon_{k-1} + \varepsilon_n)} - 1/\sqrt{(\varepsilon_k + \varepsilon_n)}] \quad . \qquad \textbf{(B.13)}$$

It has been assumed here that the energy $-\varepsilon_n$, which is a quantum mechanical eigenvalue, is identical with the classical energy of the electron in its orbit, which is at least approximately the case.
The cross section for collisional ionization into the whole (numerically) available continuum energy range $0...\varepsilon_M$ is obtained from Eq.**(B.13)** by setting $\varepsilon_{k-1} = 0$ and $\varepsilon_k = \varepsilon_M$,i.e.

$$\sigma_n^c = \sigma_0^c \cdot \varepsilon_p^{-1.5} \cdot [1/\sqrt{\varepsilon_n} - 1/\sqrt{(\varepsilon_M + \varepsilon_n)}] \quad . \qquad \textbf{(B.14)}$$

In the case $\varepsilon_M >> \varepsilon_n$,this reduces to the simple expression

$$\sigma_n^c = \sigma_0^c \cdot \varepsilon_p^{-1.5} \cdot n \quad . \qquad \textbf{(B.15)}$$

The collision frequency for elastic scattering is generally related to the corresponding cross section by

$$\nu^c = \mathcal{N}_p^* \cdot v_e(\varepsilon_p) \cdot \sigma^c = \\ = \mathcal{N}_p^* \cdot 2.2 \cdot 10^8 \cdot \sqrt{\varepsilon_p} \cdot \sigma^c \qquad [\text{sec}^{-1}] \quad , \qquad \textbf{(B.16)}$$

if ε_p is in units of Rydberg, $\mathcal{N}_p^*$ in $[\text{cm}^{-3}]$ and σ^c in $[\text{cm}^2]$.

From the various cross sections derived in this chapter one gets thus

$$\nu_{i,k}^c = \nu_0^c \cdot [\pm 1/\sqrt{(\pm\varepsilon_{k-1} \mp \boldsymbol{\varepsilon_i})} \mp 1/\sqrt{(\pm\varepsilon_k \mp \boldsymbol{\varepsilon_i})}] \cdot \delta_i \qquad \textbf{(B.17)}$$

$$\nu_{k,L}^c = \nu_0^c \cdot [2\sqrt{2}/\sqrt{(\Delta\varepsilon_k)} - 1/\sqrt{\boldsymbol{\varepsilon_k}} - 1/\sqrt{(\varepsilon_M - \boldsymbol{\varepsilon_k})}] \cdot \delta_k \qquad \textbf{(B.18)}$$

$$\nu_{n,k}^c = \nu_0^c \cdot [1/\sqrt{(\varepsilon_{k-1} + \varepsilon_n)} - 1/\sqrt{(\varepsilon_k + \varepsilon_n)}] \qquad \textbf{(B.19)}$$

$$\nu_n^c = \nu_0^c \cdot [1/\sqrt{\varepsilon_n} - 1/\sqrt{(\varepsilon_M + \varepsilon_n)}] \approx \\ \approx \nu_0^c \cdot n \qquad \text{if } \varepsilon_n << \varepsilon_M \text{ (energy of excited state small compared to the maximum numerical continuum energy)} \qquad \textbf{(B.20)}$$

$$\nu_{\mathit{ll},k}^c = \nu_{n,k}^c \qquad \textbf{(B.21)}$$

$$\nu_{\mathit{ll}}^c = \nu_n^c \quad , \qquad \textbf{(B.22)}$$

where

$$\nu_0^c = 1.2 \cdot 10^{-8} \cdot \mathcal{N}_p^* / \varepsilon_p \qquad [\text{sec}^{-1}] \quad , \qquad \textbf{(B.23)}$$

with $\mathcal{N}_p$ in [cm^{-3}] and ε_p in units of Rydberg, and

$$\delta_k = (\mathcal{N}_p - \mathcal{N}_{e,k}) / \mathcal{N}_p \qquad \textbf{(B.24)}$$

is the fraction of electrons outside the energy interval ε_{k-1}, ε_k (see Sect.2.2, Eq.**(32)**) in consistency with the assumption that scattering within this interval itself is neglected (see below Eq.**(B.9)**) .

From experimental results, it is evident (Smid, 1987) that the cross section for electron impact ionization of neutrals in the ground state by electrons with an energy comparable to the ground state energy is about 4 orders of magnitude smaller as would follow from Eq.**(B.14)** (at least is this true for ionospheric conditions).
For this reason, Eqs.**(B.19)-(B.22)** have been additionally multiplied by the factor

$$\eta_n^c = 10^{-4} \cdot \mathrm{Min}(10^4, \varepsilon_p/\varepsilon_n) \quad . \qquad \textbf{(B.25)}$$

It should be noted that for the present purpose this correction is however only of minor relevance, since electron collisions are only important for large n for which η_n^c is close to 1 (see Sect.3.3).

With regard to the application of the expressions derived in this chapter to the balance equation in Sect.2.2 , one should again realize that in principle they are only strictly valid if the energy transfer is small compared to the bulk plasma energy ε_p . The numerical error introduced by this inconsistency for the highest energies of the electron spectrum is however insignificant for the present purpose, because the high energy bulk of electrons serves only as a background 'pool' for the production of electrons at smaller energies by means of elastic scattering and errors in the assumption for the form of the differential scattering cross section for those energies will more or less average out (this is also the justification for choosing the low numerical resolution of the energy grid for the electron spectrum at high energies (see Sect.3.1)).

References

Boischot, A., Solar radio astronomy, in Solar Physics, edited by J.N. Xanthakis, pp. 465-481, Wiley Interscience, London, New York, Sydney, 1967.

Landau, L.D. and E.M. Lifshitz, Mechanics, Pergamon Press, Oxford, 1976.

Lang, K.R., Astrophysical Formulae, Springer-Verlag, Berlin, Heidelberg, New York, 1974.

Massey, H.S.W., Electronic and Ionic Impact Phenomena, Vol.2, Oxford University Press, 1969.

Mitra, A.P., Ionospheric Effects of Solar Flares, D. Reidel Publishing Company, Dordrecht, Holland, 1974.

Moorcroft, D.R., Estimates of absolute scattering coefficients of radar aurora, J.Geophys.Res. 92, 8723-8732, 1987.

Pankonin, V., The partially ionized medium adjacent to HII regions, in RadioRecombination Lines , edited by P.A. Shaver, pp. 111-125, D. Reidel Publishing Company, Dordrecht, Holland, 1980.

Rees, M.H., Physics and Chemistry of the Upper Atmosphere, Cambridge University Press, 1989.

Smid, T.S., Theoretische Aspekte der Ionosphärenphysik, Ph.D. Thesis, Bonn University, 1987.

Smid, T.S., The resonant excitation of airglow by high power radio waves, submitted to J.Geophys.Res., 1992a.

Smid, T.S., The excitation of oscillations of a magnetized collisionless plasma, submitted to J.Geophys.Res., 1992b.

Unsöld, A., Physik der Sternatmosphären, Springer-Verlag, Berlin, Göttingen, Heidelberg, 1955.

Scattering of Radio Waves by High Atomic Rydberg States

Fig.1:

Scheme illustrating the coupling between the free electron spectrum and the atomic level population in detailed balance equilibrium

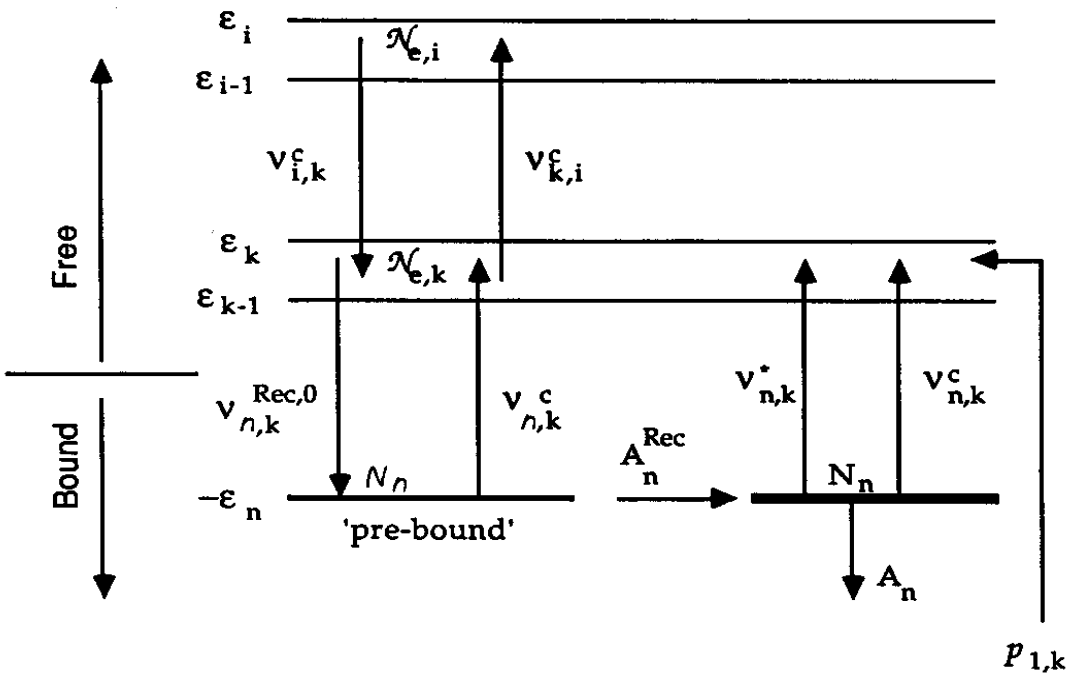

Fig.2:

Effective optical depth for plane-wave radiation of finite field strength (intensity) in an absorbing medium over a pathlength characterized by the field strength independent optical depth depth , for various values of the ratio of the initial wave field strength to the effective plasma fluctuation field.

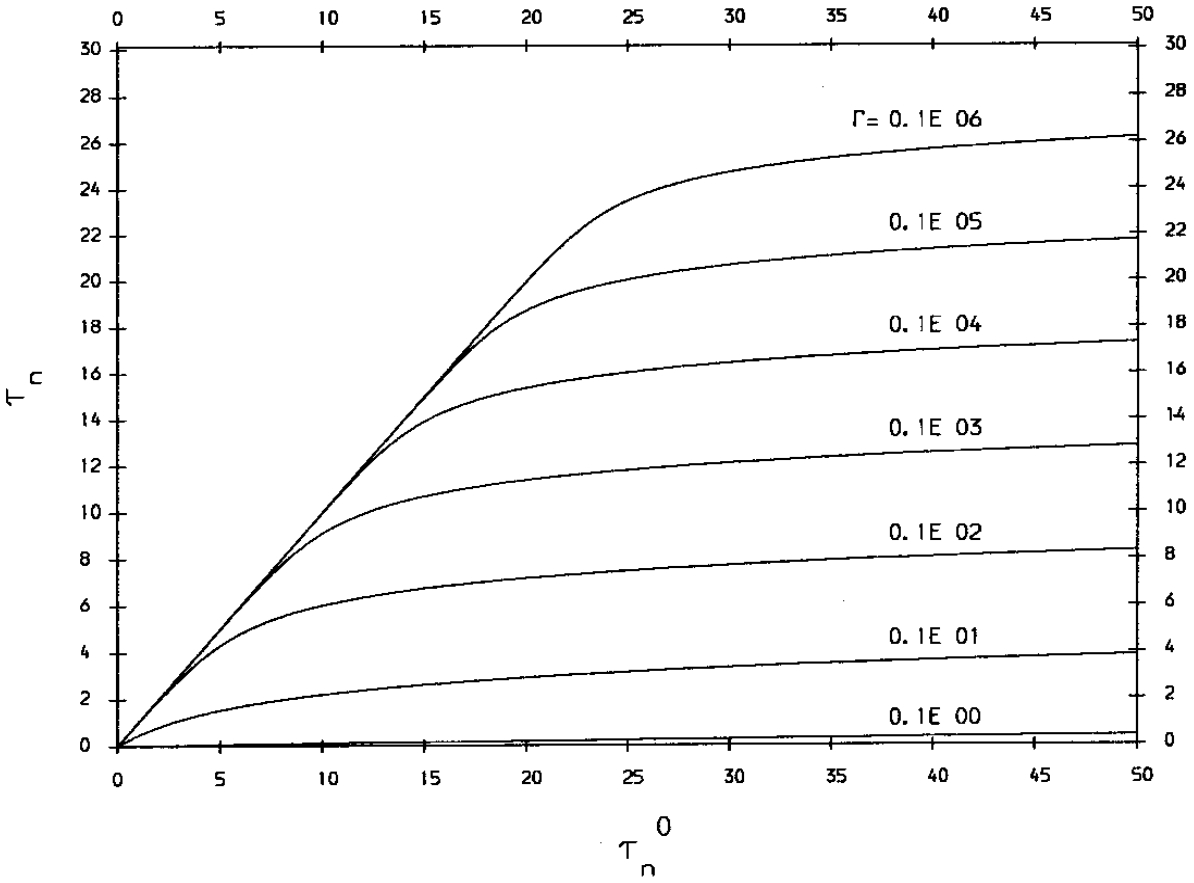

Fig.3:

Free electron distribution function (thick solid step function, right ordinate, lower abscissa) **for a plasma density $N_p=10^5 cm^{-3}$**, an average electron energy of ε = 0.5 Ry , an ion temperature T=300 K and an ion mass number A=32 (the specification of the solar radiation flux is without any significance for the free electron spectrum and can be ignored here). The dashed step function gives the result when all elastic collisions are neglected, that is, only the primary production rate and the recombination frequency $\nu_{T,k}^{Rec,0}$(thin solid curve, left ordinate) are hypothetically assumed to determine the spectrum. The dashed-dotted line shows the recombination constant A_n^{Rec} as a function of the atomic level number n (left ordinate, upper abscissa) and the dashed line the related elastic collision frequency ν_n^c. The point of intersection of the two lines (at n=n*, Eq.(31)) separates the energy region where recombination is unaffected by collisions (the quantum state and energy relate to each other through $\varepsilon = 1/n^2$) from the energy range where collisions interfere with the recombination process (only in the latter regime does $f_e(\varepsilon)$ depend on the total plasma density N_p).

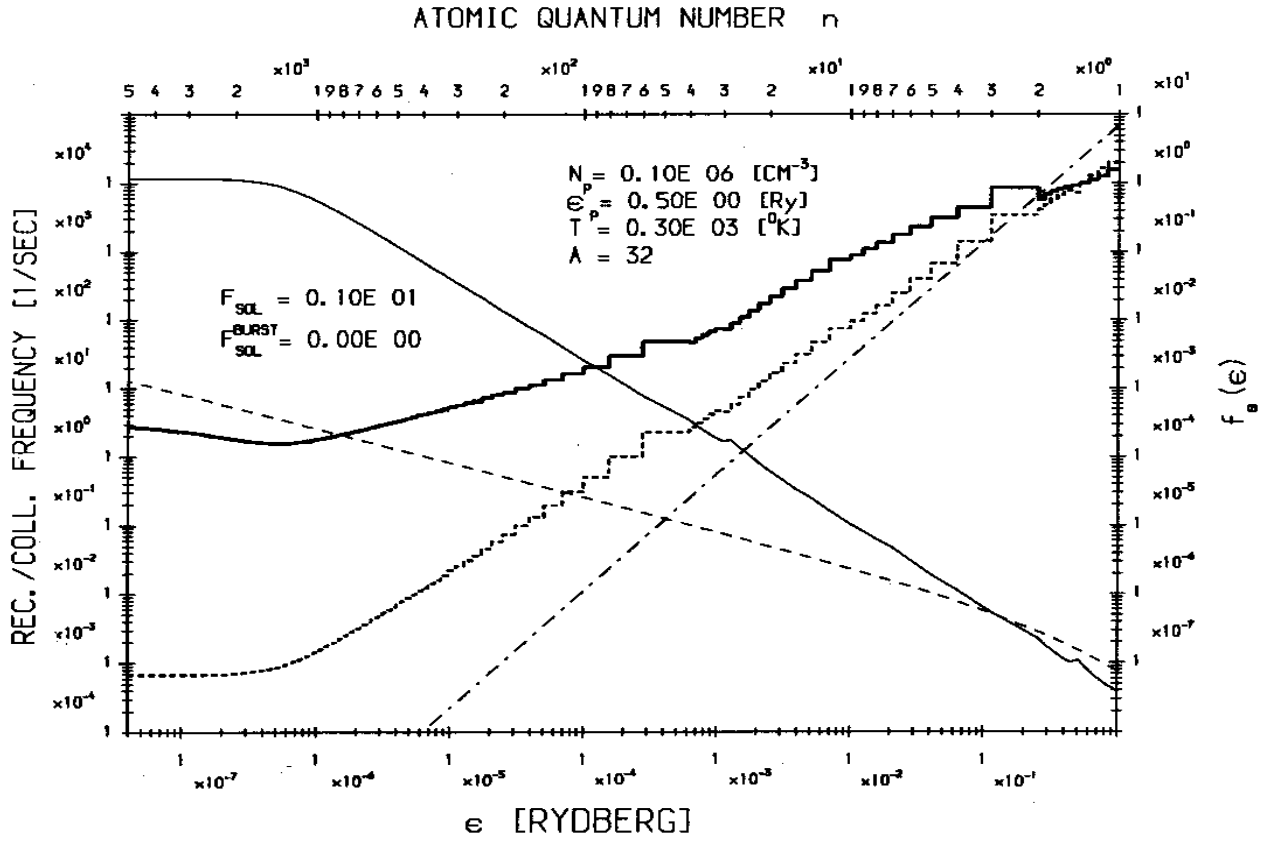

See Fig.4 and Fig.5 for the corresponding results for plasma densities $N_p=10^4 cm^{-3}$ and $N_p=10^6 cm^{-3}$ respectively.

Fig.4:

Free electron distribution function (thick solid step function, right ordinate, lower abscissa) **for a plasma density $N_p=10^4 cm^{-3}$**, an average electron energy of ε = 0.5 Ry , an ion temperature T=300 K and an ion mass number A=32 (the specification of the solar radiation flux is without any significance for the free electron spectrum and can be ignored here). The dashed step function gives the result when all elastic collisions are neglected, that is, only the primary production rate and the recombination frequency $\nu_{T,k}^{Rec,0}$(thin solid curve, left ordinate) are hypothetically assumed to determine the spectrum. The dashed-dotted line shows the recombination constant A_n^{Rec} as a function of the atomic level number n (left ordinate, upper abscissa) and the dashed line the related elastic collision frequency ν_n^c. The point of intersection of the two lines (at n=n*, Eq.(31)) separates the energy region where recombination is unaffected by collisions (the quantum state and energy relate to each other through $\varepsilon = 1/n^2$) from the energy range where collisions interfere with the recombination process (only in the latter regime does $f_e(\varepsilon)$ depend on the total plasma density N_p).

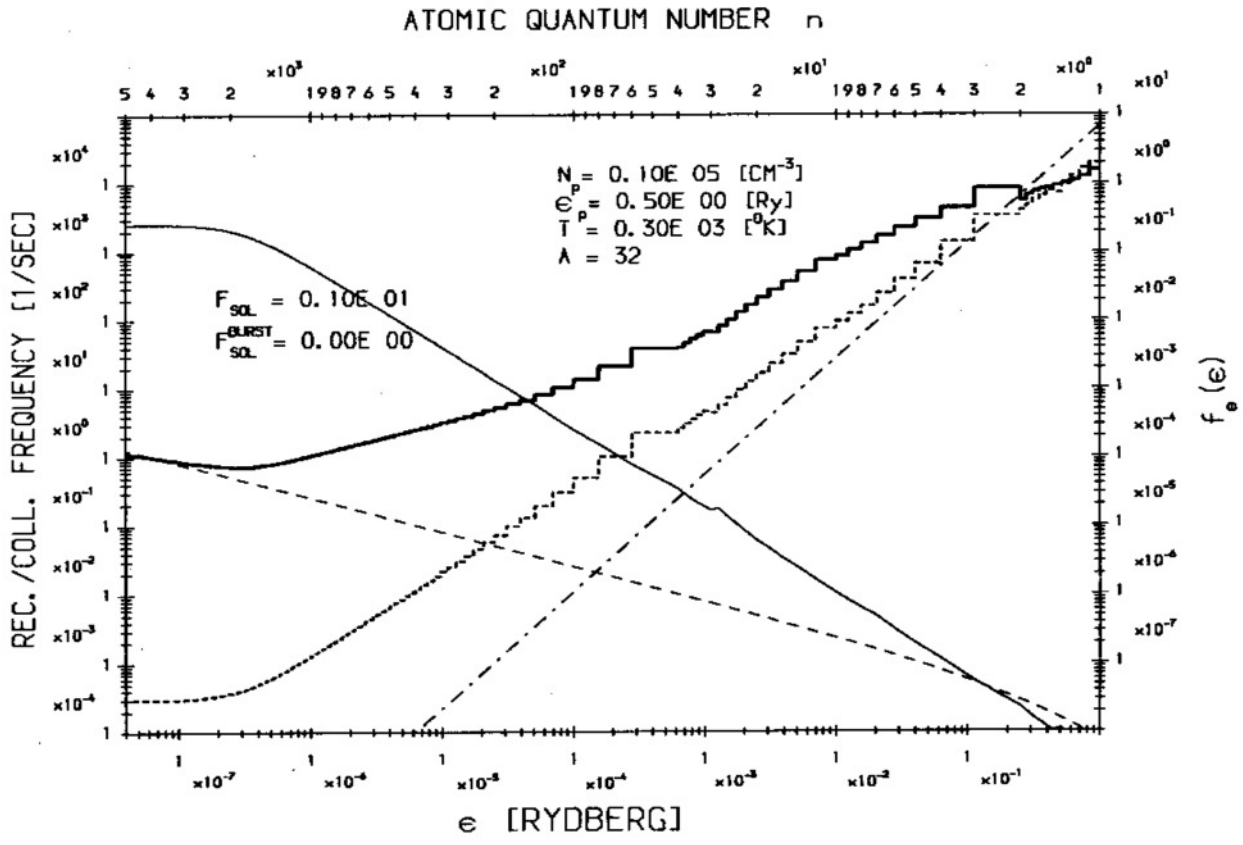

See Fig.3 and Fig.5 for the corresponding results for plasma densities $N_p=10^5 cm^{-3}$ and $N_p=10^6 cm^{-3}$ respectively.

Scattering of Radio Waves by High Atomic Rydberg States

Fig.5:

Free electron distribution function (thick solid step function, right ordinate, lower abscissa) **for a plasma density $N_p=10^6 cm^{-3}$**, an average electron energy of ε = 0.5 Ry , an ion temperature T=300 K and an ion mass number A=32 (the specification of the solar radiation flux is without any significance for the free electron spectrum and can be ignored here). The dashed step function gives the result when all elastic collisions are neglected, that is, only the primary production rate and the recombination frequency $\nu_{T,k}^{Rec,0}$(thin solid curve, left ordinate) are hypothetically assumed to determine the spectrum. The dashed-dotted line shows the recombination constant A_n^{Rec} as a function of the atomic level number n (left ordinate, upper abscissa) and the dashed line the related elastic collision frequency ν_n^c. The point of intersection of the two lines (at n=n*, Eq.(31)) separates the energy region where recombination is unaffected by collisions (the quantum state and energy relate to each other through $\varepsilon = 1/n^2$) from the energy range where collisions interfere with the recombination process (only in the latter regime does $f_e(\varepsilon)$ depend on the total plasma density N_p).

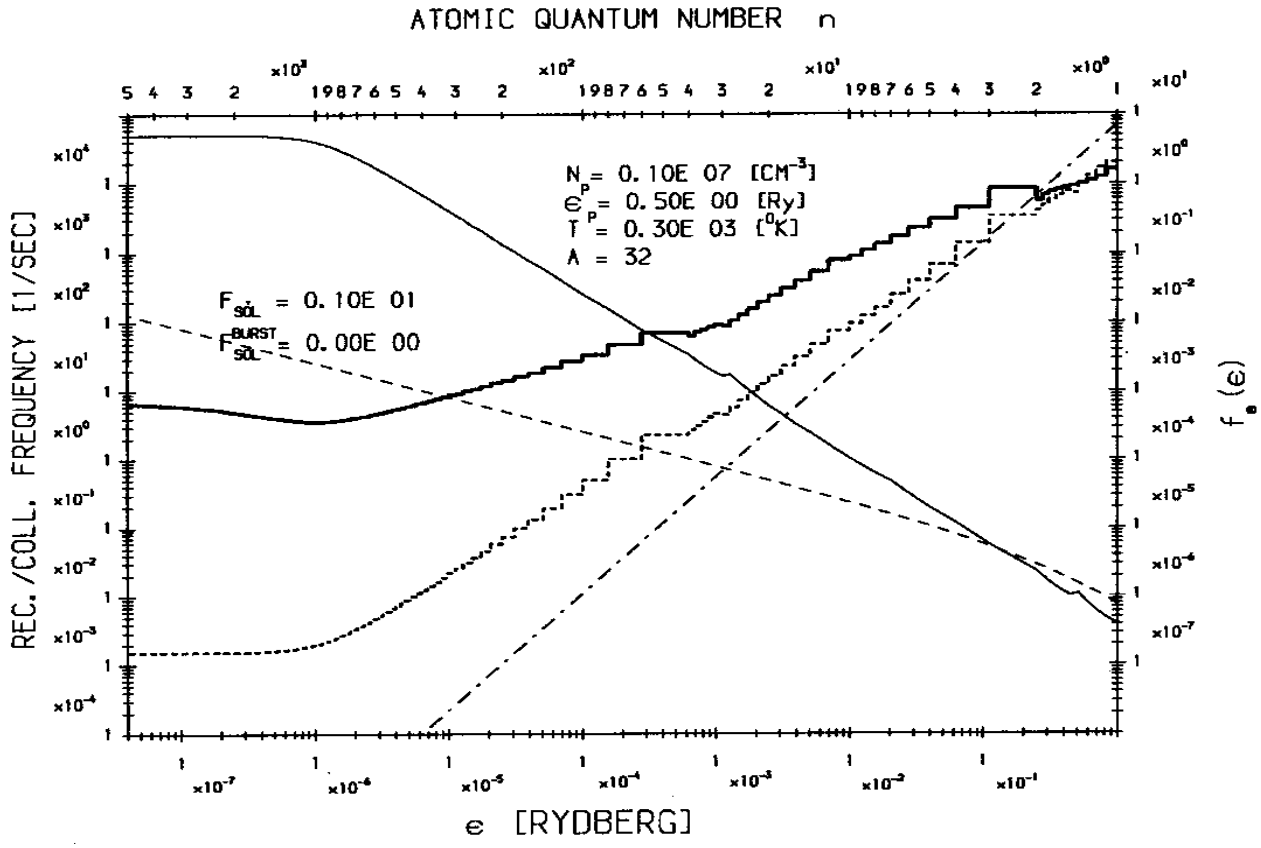

See Fig.3 and Fig.4 for the corresponding results for plasma densities $N_p=10^5 cm^{-3}$ and $N_p=10^4 cm^{-3}$ respectively.

Scattering of Radio Waves by High Atomic Rydberg States

Fig.6:

Density of atoms in excited states (thick solid curve, left ordinate) as a function of the principal quantum number n (lower abscissa) **for a plasma density $N_p=10^5 cm^{-3}$**. The thin solid curve gives the production rate q_n (left ordinate to be multiplied by 10^5) with the close dashed-dotted curve showing the initial recombinative production rate q_n^{Rec} (i.e. neglecting the cascading rate q_n^{casc}). The total loss frequency for each level is given by the sum of the level decay constant A_n (long-dashed curve), the collisional ionization frequency (dashed curve) and the photoionization frequency (dotted curve) where the latter corresponds to an average (quiet conditions) solar flux at the earth ($F_{sol}=1$). The upper abscissa shows the frequency of the n-alpha transition for the quantum number n and gives an approximate idea which levels are responsible for scattering an electromagnetic wave of a certain frequency.

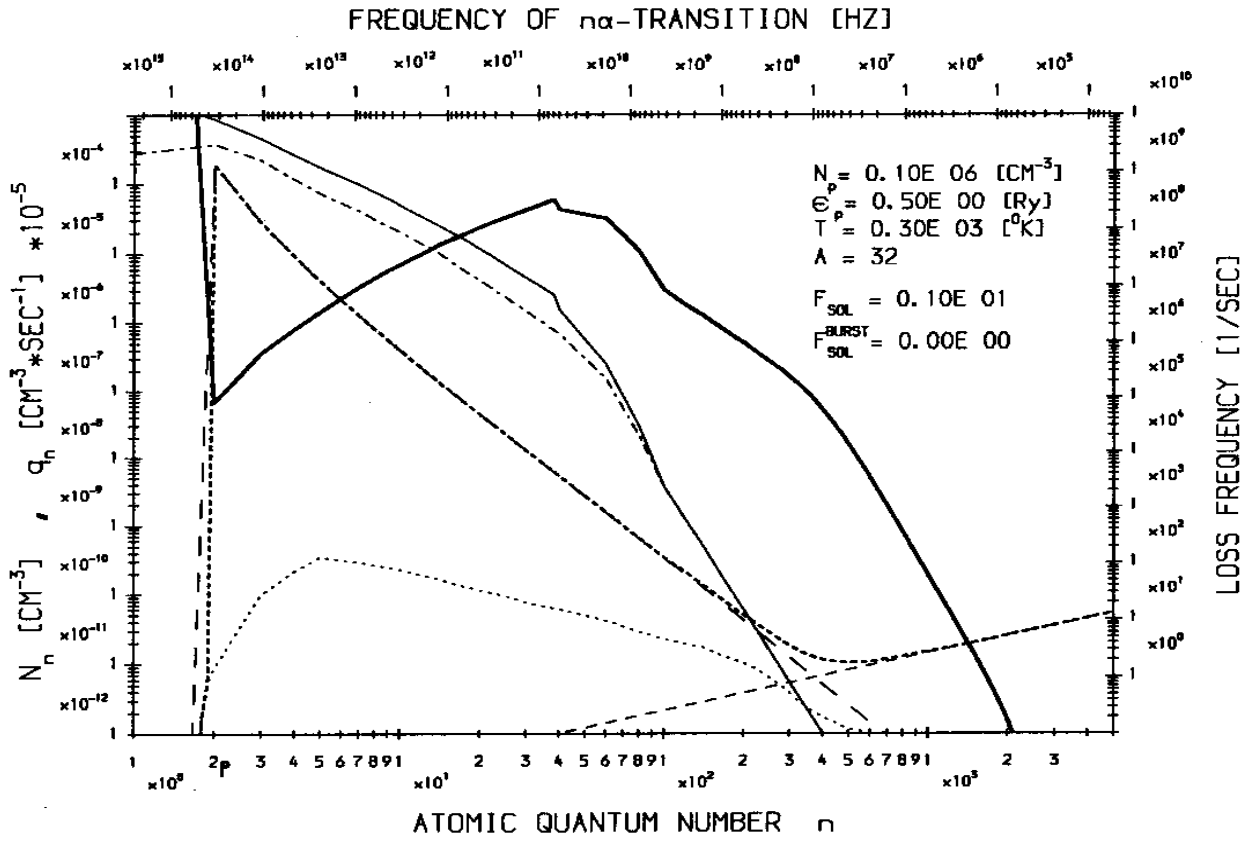

See Fig.7 and Fig.8 for the corresponding results for plasma densities $N_p=10^4 cm^{-3}$ and $N_p=10^6 cm^{-3}$ respectively.

Scattering of Radio Waves by High Atomic Rydberg States

Fig.7:

Density of atoms in excited states (thick solid curve, left ordinate) as a function of the principal quantum number n (lower abscissa) **for a plasma density $N_p=10^4 cm^{-3}$**. The thin solid curve gives the production rate q_n (left ordinate to be multiplied by 10^5) with the close dashed-dotted curve showing the initial recombinative production rate q_n^{Rec} (i.e. neglecting the cascading rate q_n^{casc}). The total loss frequency for each level is given by the sum of the level decay constant A_n (long-dashed curve), the collisional ionization frequency (dashed curve) and the photoionization frequency (dotted curve) where the latter corresponds to an average (quiet conditions) solar flux at the earth ($F_{sol}=1$). The upper abscissa shows the frequency of the n-alpha transition for the quantum number n and gives an approximate idea which levels are responsible for scattering an electromagnetic wave of a certain frequency.

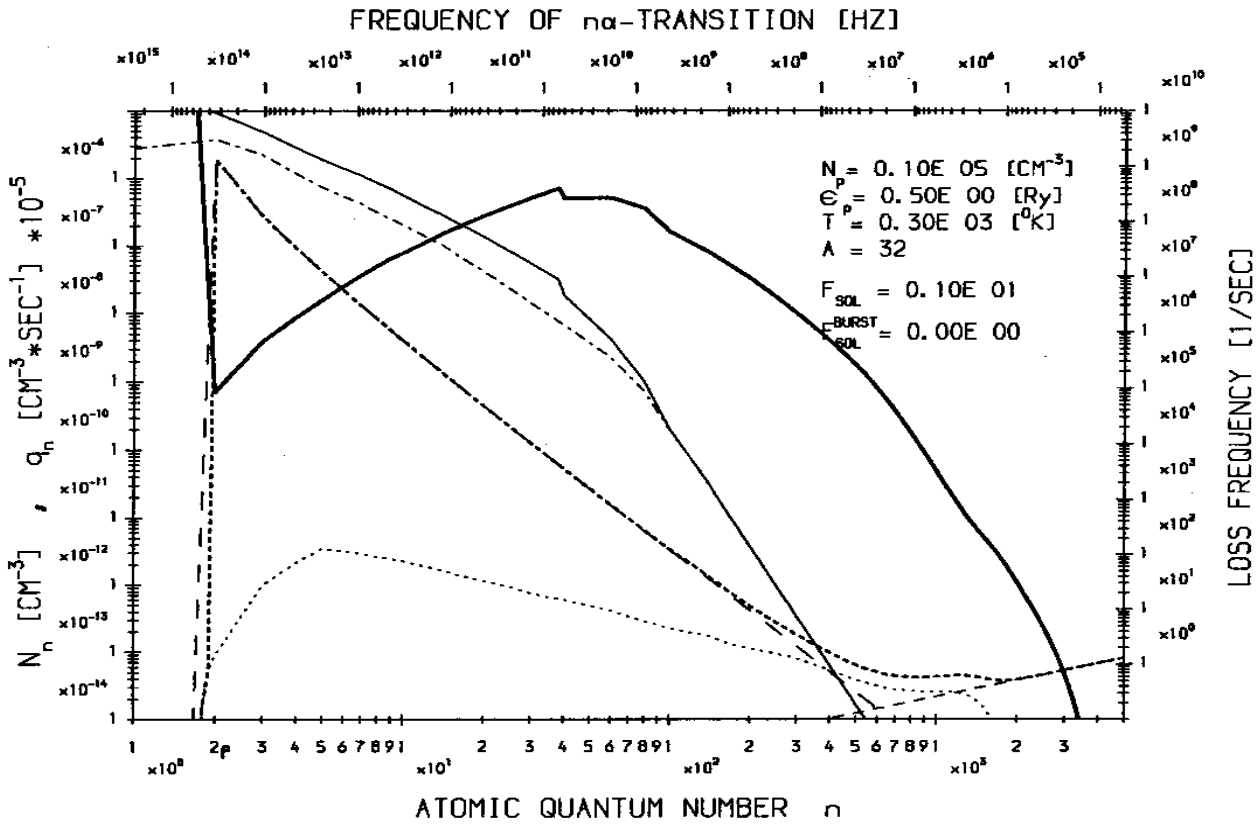

See Fig.6 and Fig.8 for the corresponding results for plasma densities $N_p=10^5 cm^{-3}$ and $N_p=10^6 cm^{-3}$ respectively.

Fig.8:

Density of atoms in excited states (thick solid curve, left ordinate) as a function of the principal quantum number n (lower abscissa) **for a plasma density $N_p=10^6 cm^{-3}$**. The thin solid curve gives the production rate q_n (left ordinate to be multiplied by 10^5) with the close dashed-dotted curve showing the initial recombinative production rate q_n^{Rec} (i.e. neglecting the cascading rate q_n^{casc}). The total loss frequency for each level is given by the sum of the level decay constant A_n (long-dashed curve), the collisional ionization frequency (dashed curve) and the photoionization frequency (dotted curve) where the latter corresponds to an average (quiet conditions) solar flux at the earth ($F_{sol}=1$). The upper abscissa shows the frequency of the n-alpha transition for the quantum number n and gives an approximate idea which levels are responsible for scattering an electromagnetic wave of a certain frequency.

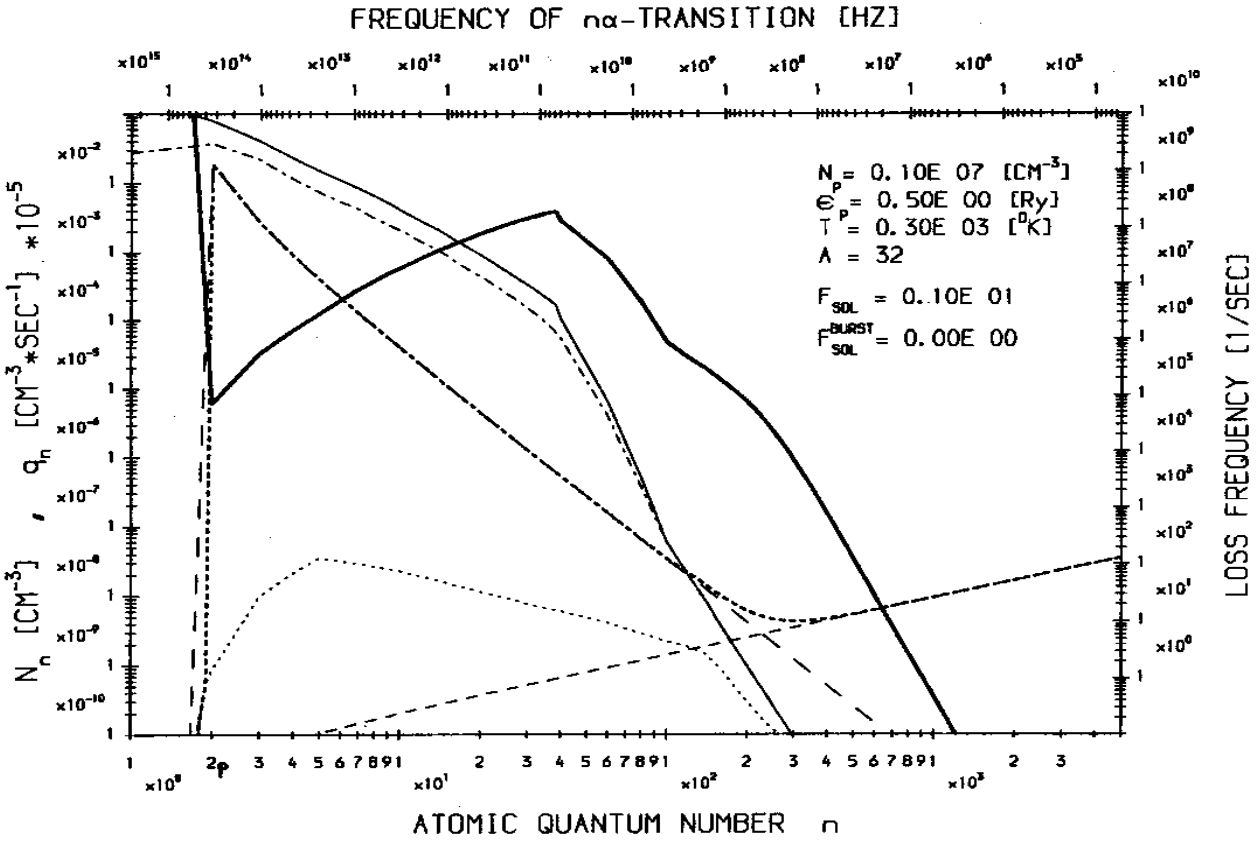

See Fig.6 and Fig.7 for the corresponding results for plasma densities $N_p=10^5 cm^{-3}$ and $N_p=10^4 cm^{-3}$ respectively.

Fig.9:

Density of atoms in excited states (thick solid curve, left ordinate) as a function of the principal quantum number n (lower abscissa) **for a plasma density $N_p=10^5 cm^{-3}$**. The thin solid curve gives the production rate q_n (left ordinate to be multiplied by 10^5) with the close dashed-dotted curve showing the initial recombinative production rate q_n^{Rec} (i.e. neglecting the cascading rate q_n^{casc}). The total loss frequency is given by the sum of the level decay constant A_n (long-dashed curve), the collisional ionization frequency (dashed curve) and the photoionization frequency (dotted curve) where the latter corresponds to an enhanced solar radio flux as appropriate **for a strong ('Type IV') solar burst** (see Fig.10) (F_{sol}=1). (See Fig.6 for normal solar flux conditions, The upper abscissa shows the frequency of the n-alpha transition for the quantum number n and gives an approximate idea which levels are responsible for scattering an electromagnetic wave of a certain frequency.

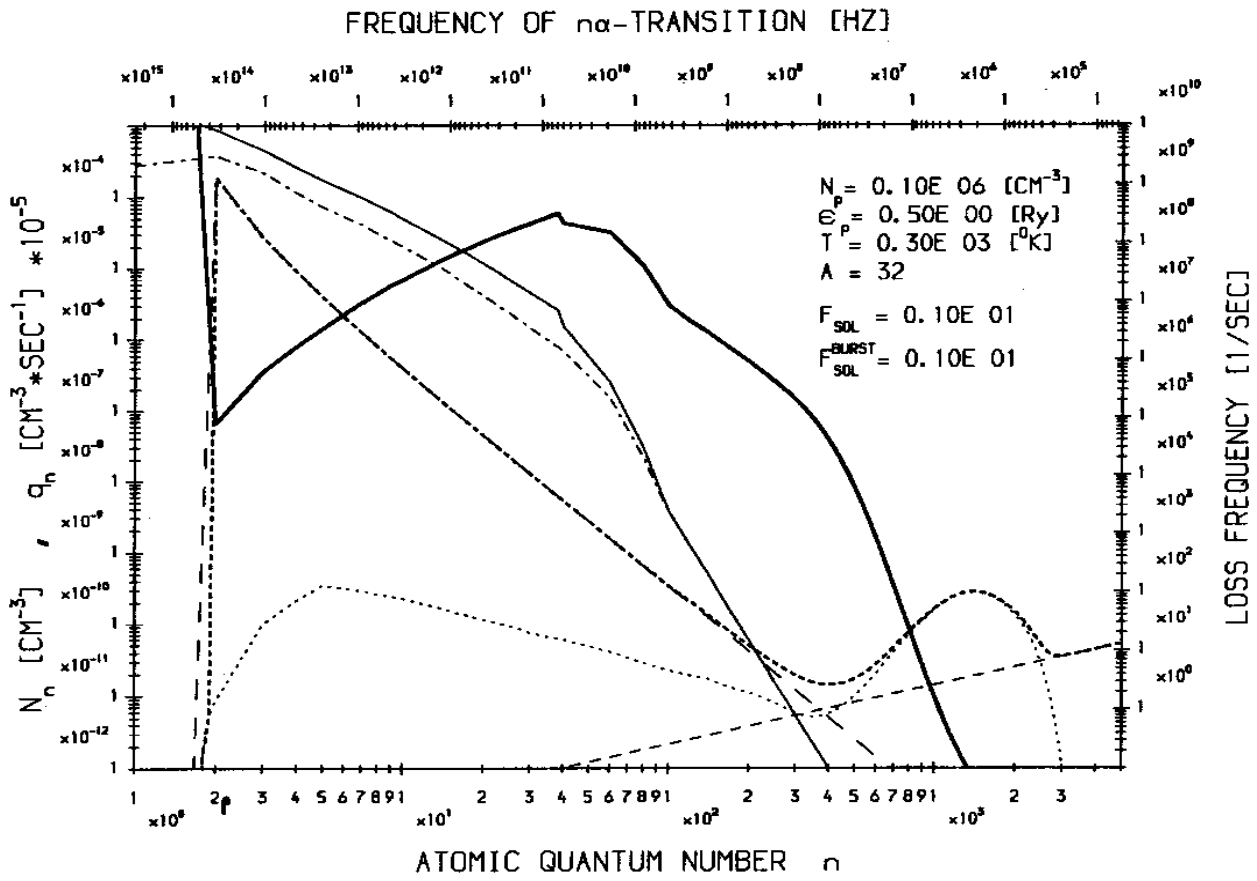

See Fig.23 for the resulting scattering coefficient.

Fig.10:

Measured solar radio flux spectra for quiet conditions and during solar storm (burst) events (the flux for Jovian bursts and the supernova remnant Cassiopeia A is shown additionally) *(after Boischot, A., Solar radio astronomy, in Solar Physics, edited by J.N. Xanthakis, pp. 465-481, Wiley Interscience, 1967; Copyright John Wiley and Sons Ltd., reproduced with permission).*

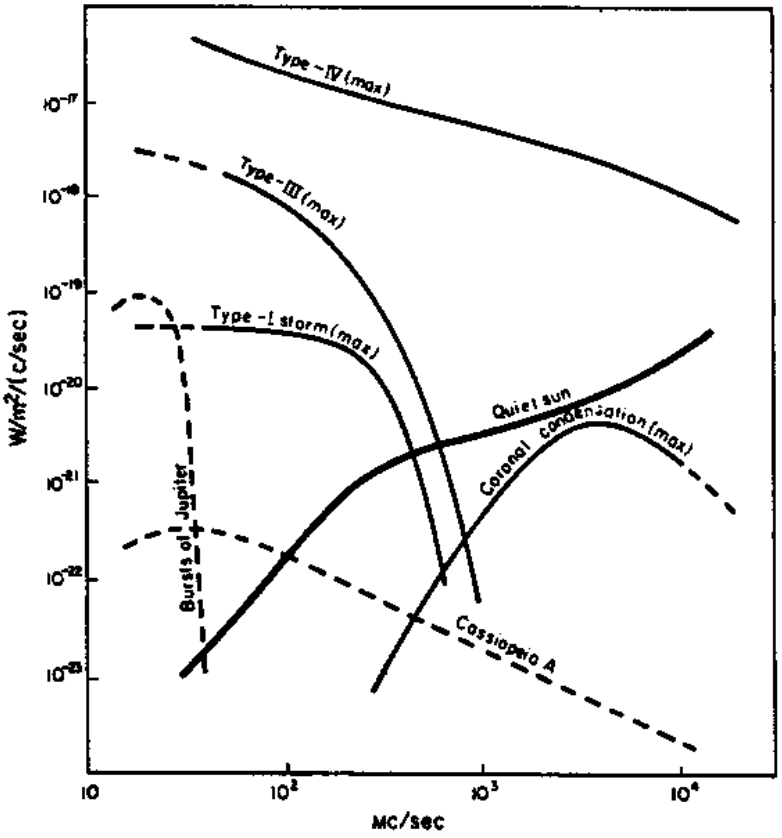

Scattering of Radio Waves by High Atomic Rydberg States

Fig.11:

Theoretical ionospheric scattering coefficient (left ordinate) due to highly excited atomic states (corresponding to the level population in Fig.7, i.e. **for a plasma density of $N_p=10^4 cm^{-3}$**) for radio waves with frequencies from 820 KHz to 1.9 GHz (lower abscissa). The thick short dashed curve gives the atomic (incoherent) coefficient, whereas the thick solid curve includes an enhancement due to phase coherent ('specular') scattering. The thin solid curve shows the broadening of the n-alpha lines in units of [Hz] (right ordinate) as a function of the level number n (upper abscissa) which relates to the frequency scale through $f=f_0*[1/n^2-1/(n+1)^2]$ with $f_0=3.29*10^{15}$ Hz. The points of intersection of this curve with the lines for the frequency separation of two neighbouring levels (dashed-dotted) and the frequency separation of two neighbouring lines (nα, (n+1)α) (long-dashed) determine the 3 different regions for the scattering coefficient

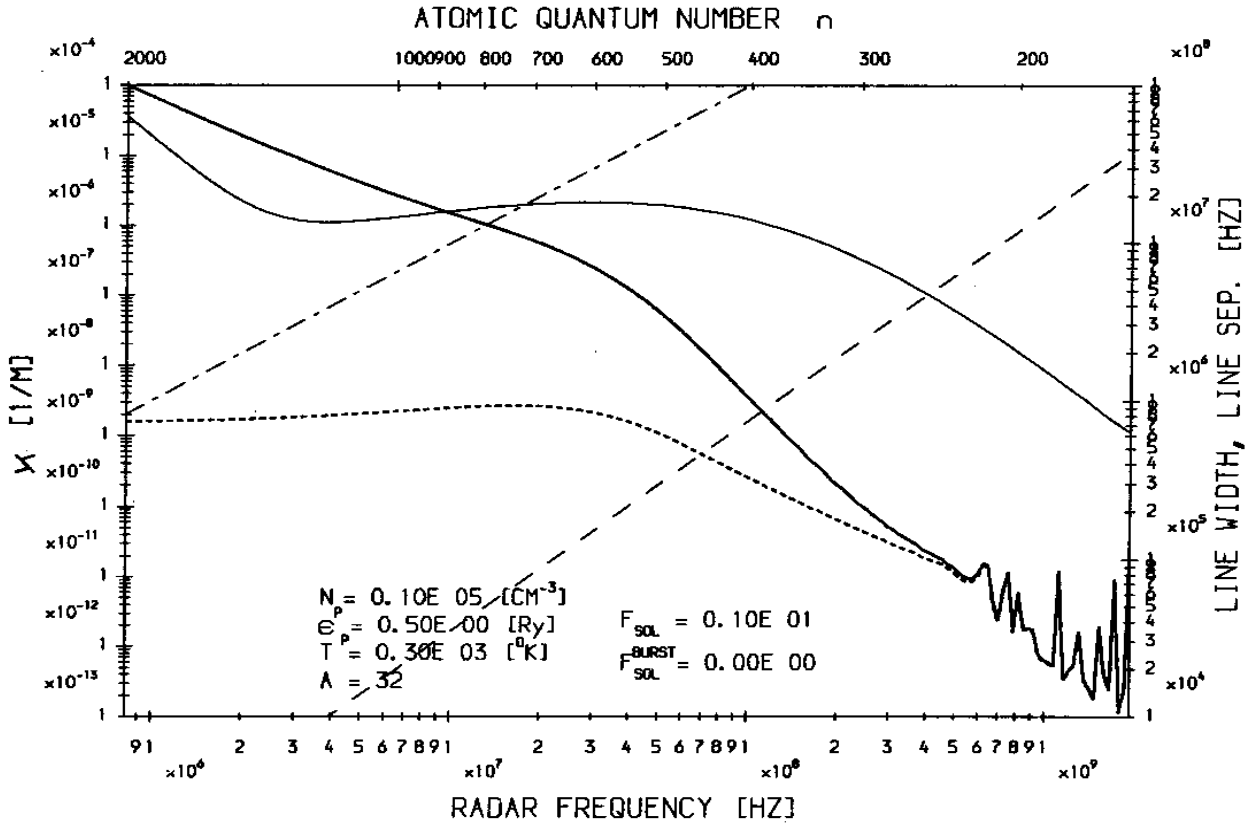

See Fig.12 and Fig.13 for the corresponding results for plasma densities $N_p=10^5 cm^{-3}$ and $N_p=10^6 cm^{-3}$ respectively.

Scattering of Radio Waves by High Atomic Rydberg States

Fig.12:

Theoretical ionospheric scattering coefficient (left ordinate) due to highly excited atomic states (corresponding to the level population in Fig.6, i.e. **for a plasma density of $N_p=10^5 cm^{-3}$**) for radio waves with frequencies from 820 KHz to 1.9 GHz (lower abscissa). The thick short dashed curve gives the atomic (incoherent) coefficient, whereas the thick solid curve includes an enhancement due to phase coherent ('specular') scattering. The thin solid curve shows the broadening of the n-alpha lines in units of [Hz] (right ordinate) as a function of the level number n (upper abscissa) which relates to the frequency scale through $f=f_0*[1/n^2-1/(n+1)^2]$ with $f_0=3.29*10^{15}$ Hz. The points of intersection of this curve with the lines for the frequency separation of two neighbouring levels (dashed-dotted) and the frequency separation of two neighbouring lines (nα, (n+1)α) (long-dashed) determine the 3 different regions for the scattering coefficient.

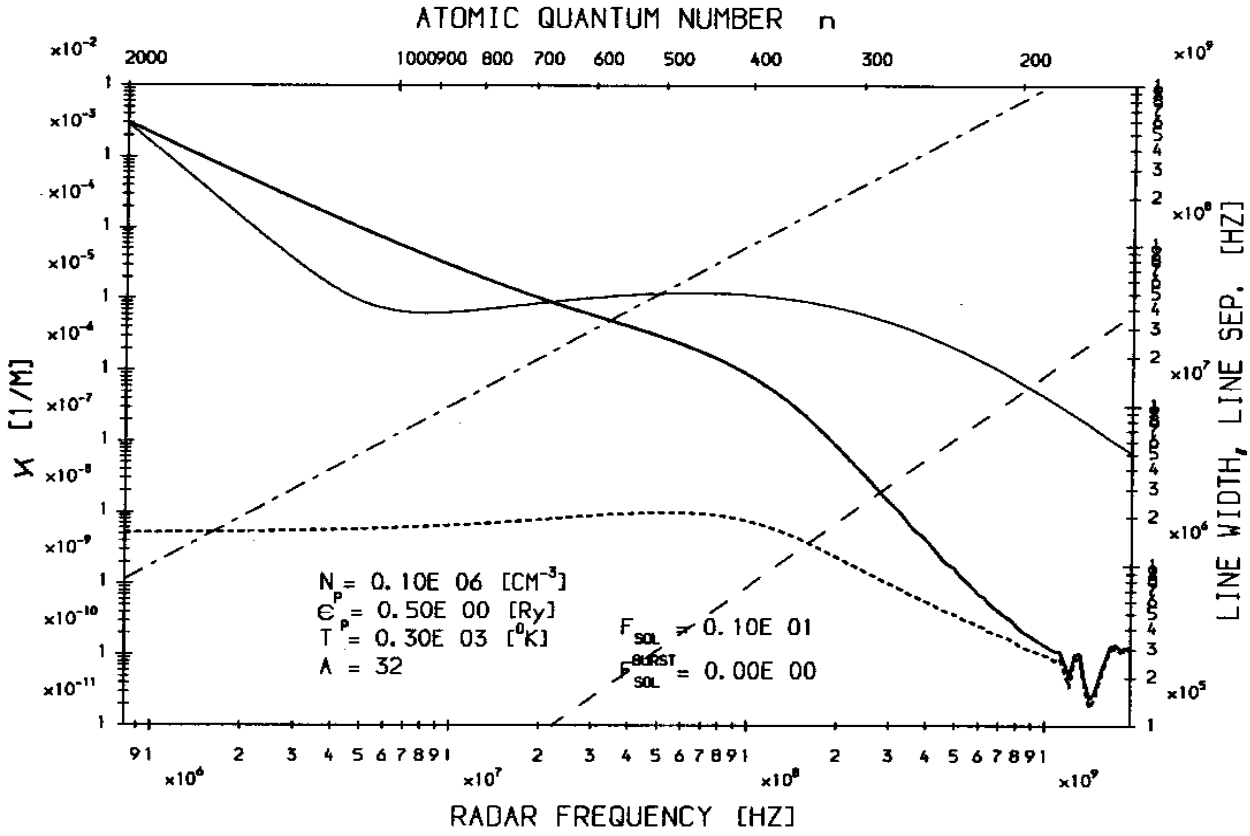

The result shows good agreement with experimentally obtained values (see Fig.20; units can be compared directly).

See Fig.11 and Fig.13 for the corresponding results for plasma densities $N_p=10^4 cm^{-3}$ and $N_p=10^6 cm^{-3}$ respectively.

Scattering of Radio Waves by High Atomic Rydberg States

Fig.13:

Theoretical ionospheric scattering coefficient (left ordinate) due to highly excited atomic states (corresponding to the level population in Fig.8, i.e. **for a plasma density of $N_p=10^6 cm^{-3}$**) for radio waves with frequencies from 820 KHz to 1.9 GHz (lower abscissa). The thick short dashed curve gives the atomic (incoherent) coefficient, whereas the thick solid curve includes an enhancement due to phase coherent ('specular') scattering. The thin solid curve shows the broadening of the n-alpha lines in units of [Hz] (right ordinate) as a function of the level number n (upper abscissa) which relates to the frequency scale through $f=f_0*[1/n^2-1/(n+1)^2]$ with $f_0=3.29*10^{15}$ Hz. The points of intersection of this curve with the lines for the frequency separation of two neighbouring levels (dashed-dotted) and the frequency separation of two neighbouring lines (nα, (n+1)α) (long-dashed) determine the 3 different regions for the scattering coefficient.

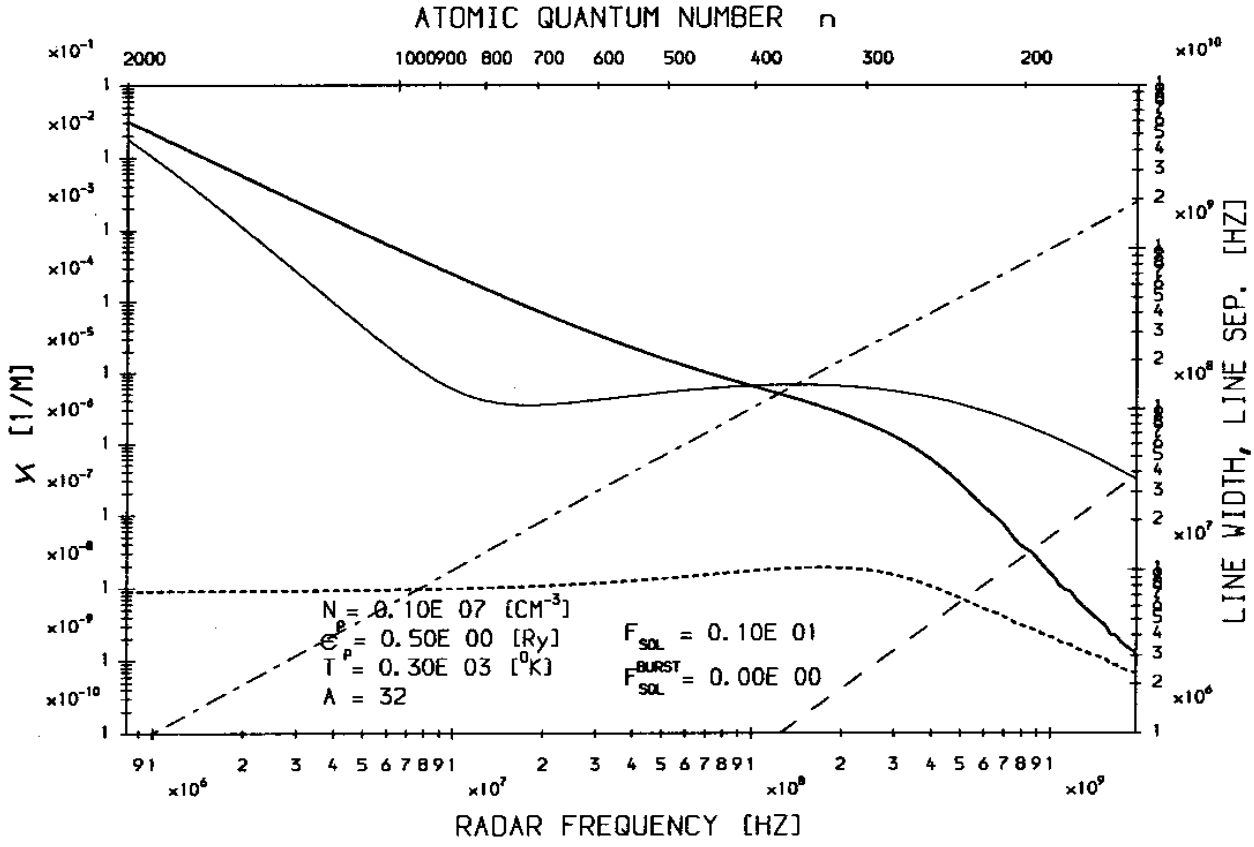

See Fig.11 and Fig.12 for the corresponding results for plasma densities $N_p=10^4 cm^{-3}$ and $N_p=10^5 cm^{-3}$ respectively.

Fig.14:

Theoretical scattering coefficient between 900 and 1000 MHz for a plasma density of $N_p=10^4 cm^{-3}$ ($\kappa(f)$ and $\kappa_0(f)$ coincide).

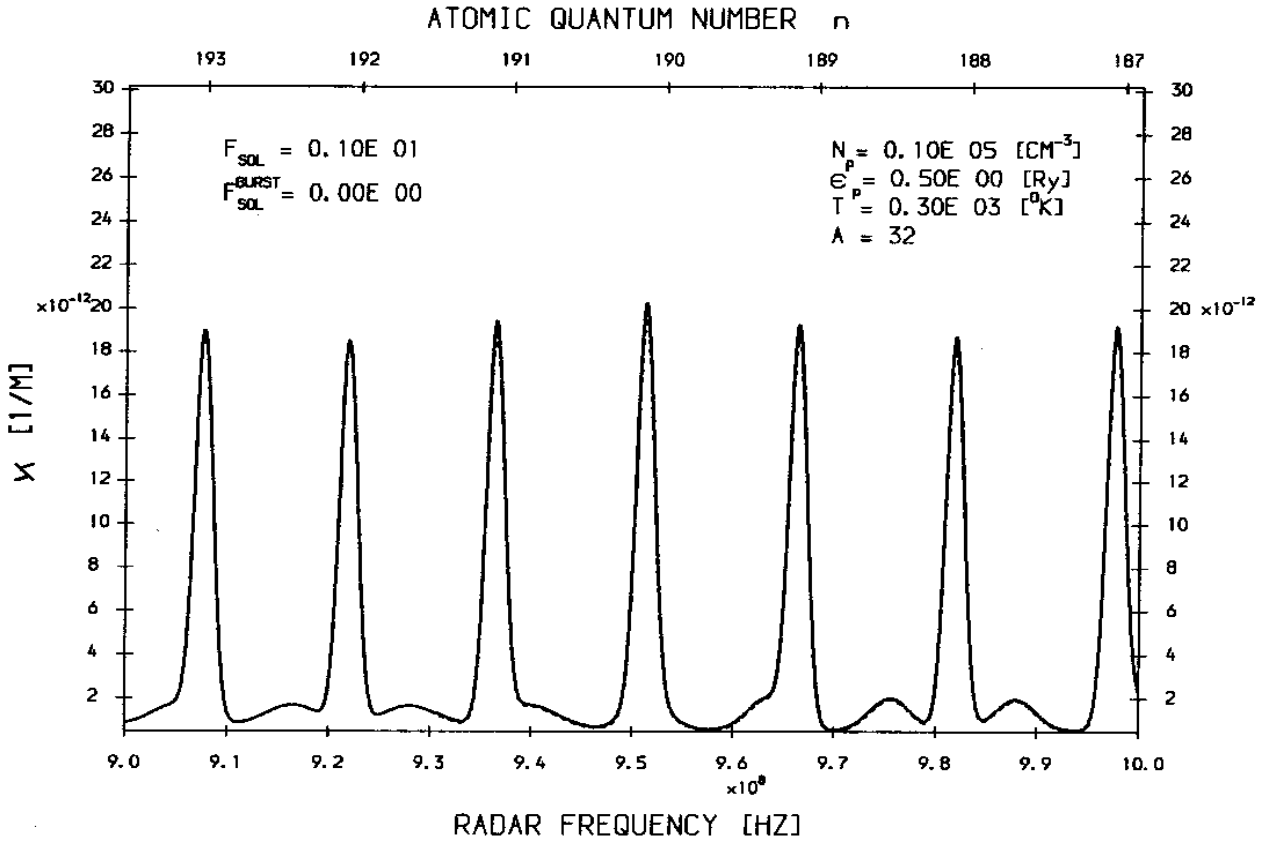

See Fig.15 for the corresponding result for a plasma density $N_p=10^5 cm^{-3}$.

Scattering of Radio Waves by High Atomic Rydberg States

Fig.15:

Theoretical scattering coefficient between 900 and 1000 MHz for a plasma density of $N_p=10^5 cm^{-3}$ (solid curve: $\kappa(f)$, dashed curve: $\kappa_0(f)$).

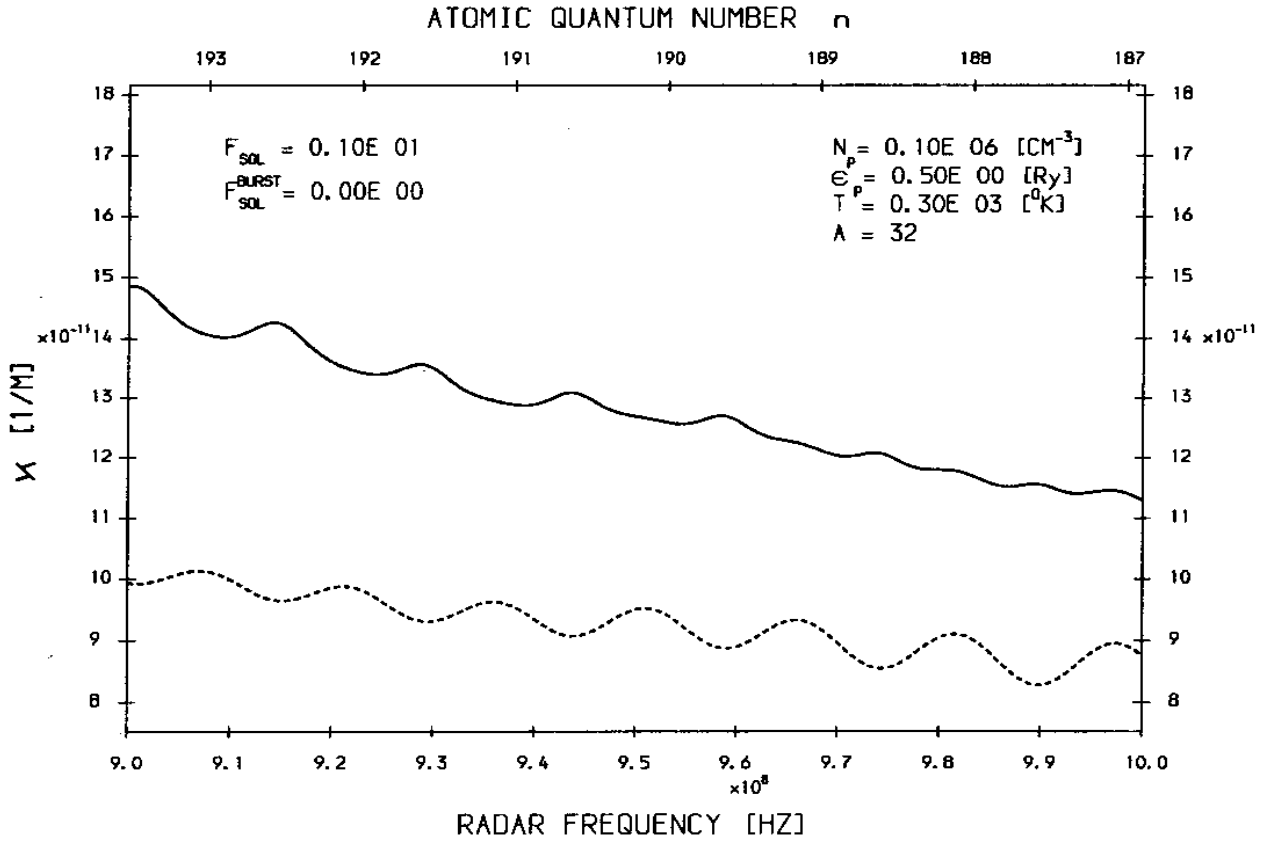

See Fig.14 for the corresponding result for a plasma density $N_p=10^4 cm^{-3}$.

Fig.16:

Same as Fig.12, but showing only the contribution due to transitions between neighboring levels (nα-transitions).

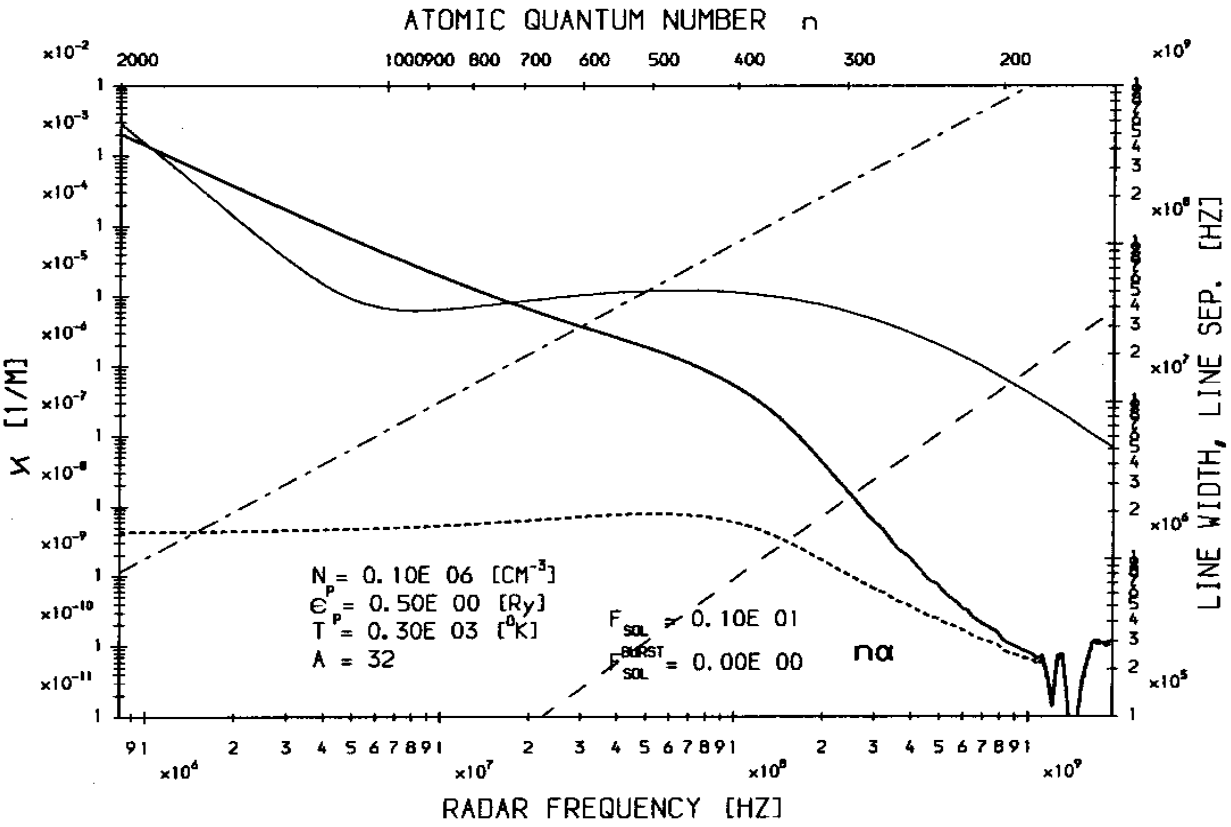

Fig.17:

Effective density N_{eff} of scattering atoms (thick solid curve, left ordinate) as a function of radar frequency f (lower abscissa) resulting from the atomic scattering coefficient $\kappa_0(f)$ in Fig.11) ($\mathbf{N_p=10^4 cm^{-3}}$) . For comparison, the thin solid curve shows the density of excited atoms N_n as a function of the level number n (upper abscissa). The dashed curve gives the ratio $\delta(f)$ of the radar wavelength to the average distance of scattering atoms related to N_{eff} (right ordinate) (see Eq.110). The quantity $1+\delta^2(f)$ transforms $\kappa_0(f)$ into $\kappa(f)$ in Fig.11.

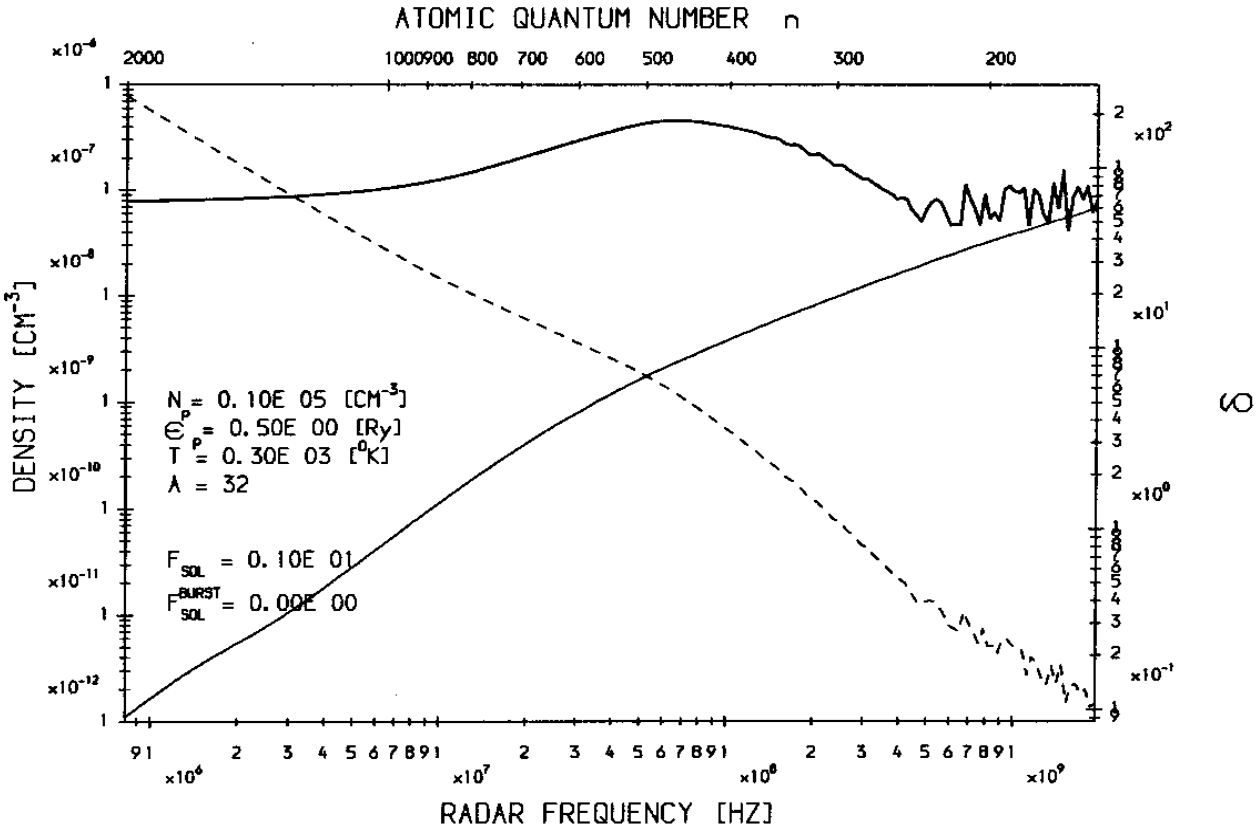

See Fig.18 and Fig.19 for the corresponding results for plasma densities $N_p=10^5 cm^{-3}$ and $N_p=10^6 cm^{-3}$ respectively.

Fig.18:

Effective density N_{eff} of scattering atoms (thick solid curve, left ordinate) as a function of radar frequency f (lower abscissa) resulting from the atomic scattering coefficient $\kappa_0(f)$ in Fig.12) ($\mathbf{N_p=10^5 cm^{-3}}$) . For comparison, the thin solid curve shows the density of excited atoms N_n as a function of the level number n (upper abscissa). The dashed curve gives the ratio $\delta(f)$ of the radar wavelength to the average distance of scattering atoms related to N_{eff} (right ordinate) (see Eq.110). The quantity $1+\delta^2(f)$ transforms $\kappa_0(f)$ into $\kappa(f)$ in Fig.11.

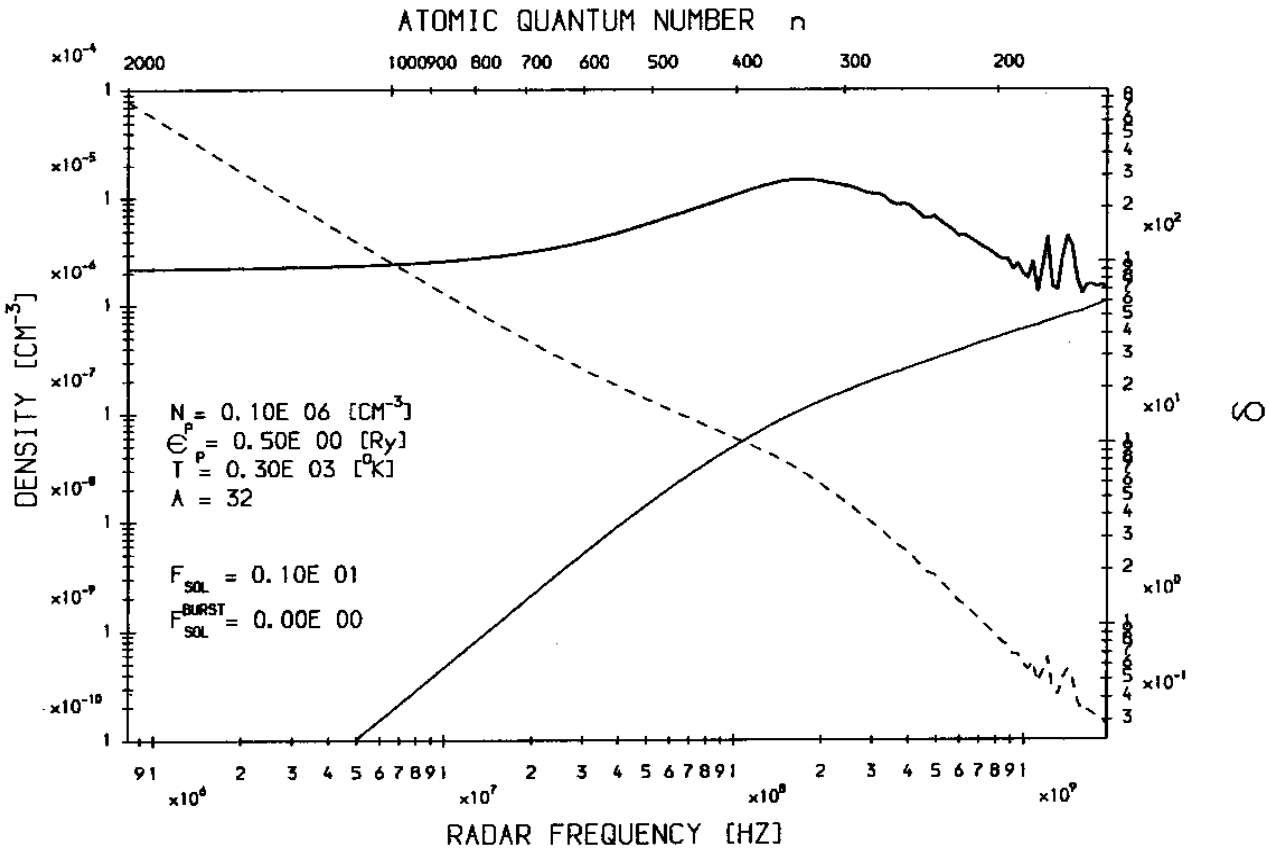

See Fig.17 and Fig.19 for the corresponding results for plasma densities $N_p=10^4 cm^{-3}$ and $N_p=10^6 cm^{-3}$ respectively.

Fig.19:

Effective density N_{eff} of scattering atoms (thick solid curve, left ordinate) as a function of radar frequency f (lower abscissa) resulting from the atomic scattering coefficient $\kappa_0(f)$ in Fig.13) ($\mathbf{N_p=10^6 cm^{-3}}$) . For comparison, the thin solid curve shows the density of excited atoms N_n as a function of the level number n (upper abscissa). The dashed curve gives the ratio $\delta(f)$ of the radar wavelength to the average distance of scattering atoms related to N_{eff} (right ordinate) (see Eq.110). The quantity $1+\delta^2(f)$ transforms $\kappa_0(f)$ into $\kappa(f)$ in Fig.11.

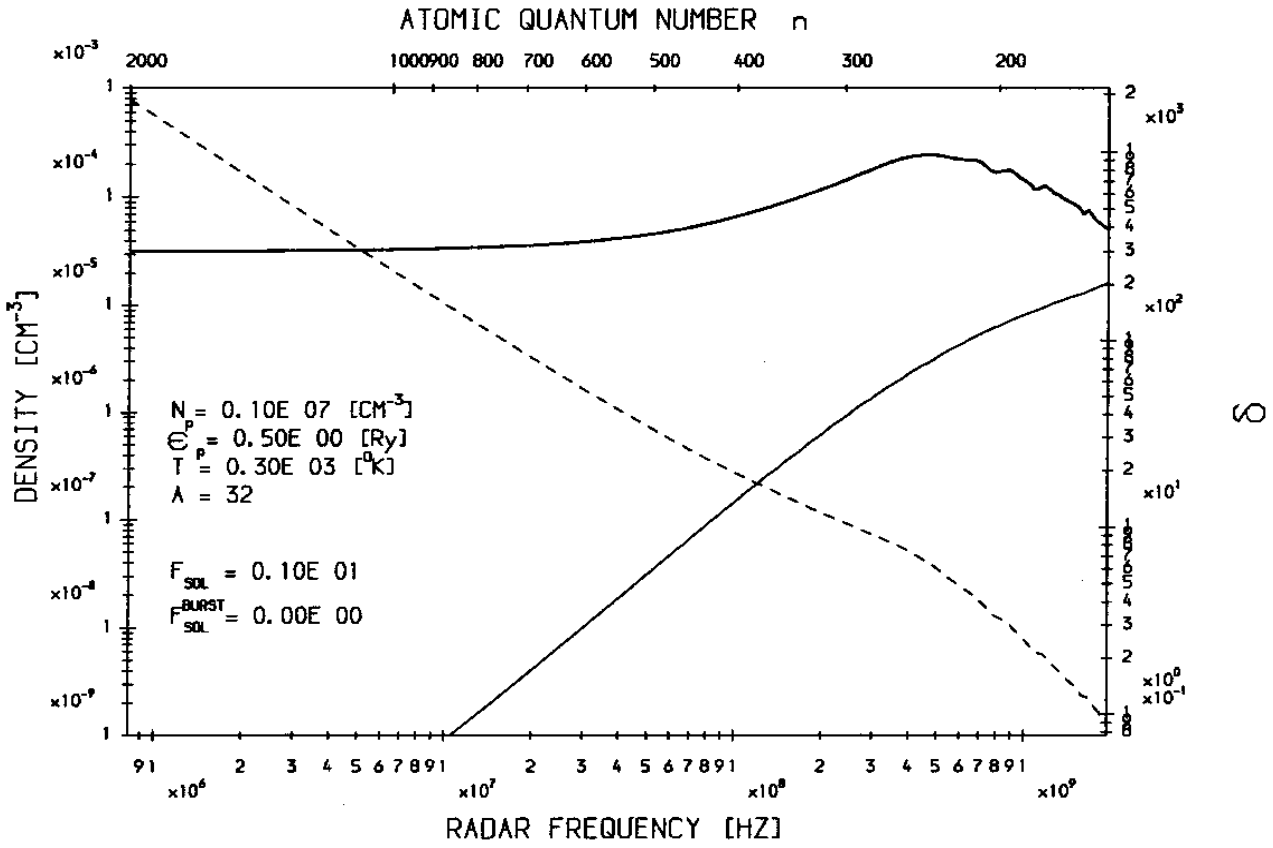

See Fig.17 and Fig.18 for the corresponding results for plasma densities $N_p=10^4 cm^{-3}$ and $N_p=10^5 cm^{-3}$ respectively.

Fig.20:

Experimental estimate of the scattering coefficient as a function of radar frequency for the auroral ionospheric region *(after Moorcroft, D.R., Estimates of absolute scattering coefficients of radar aurora, J.Geophys.Res. 92, 8723-8732, 1987; Copyright American Geophysical Union, reproduced with permission).*

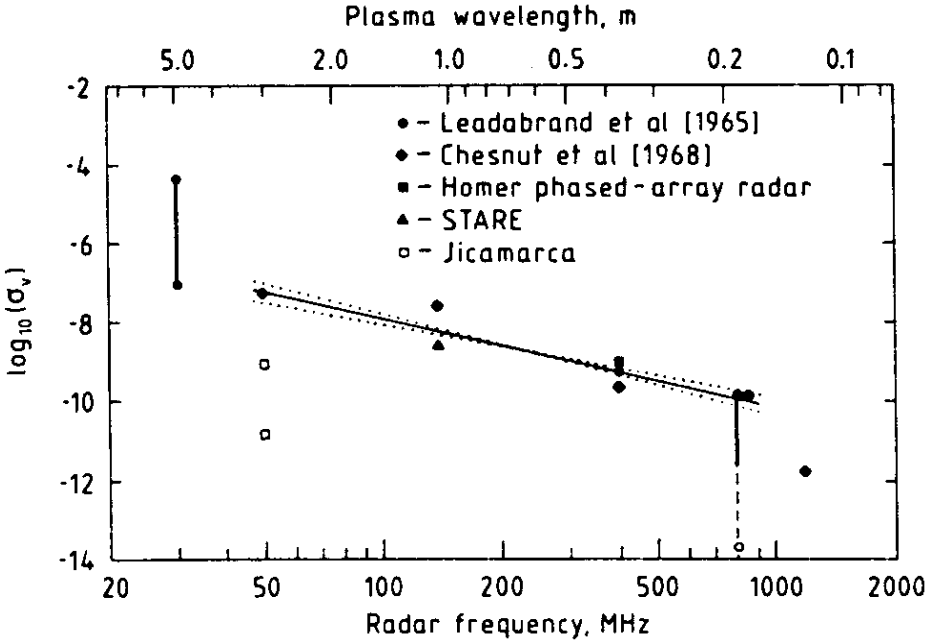

Fig.21:

Radio astronomical measurement of the H157a - (1.6832 GHz) line profile emitted from the Orion nebula (after Pankonin (1980), p.121).

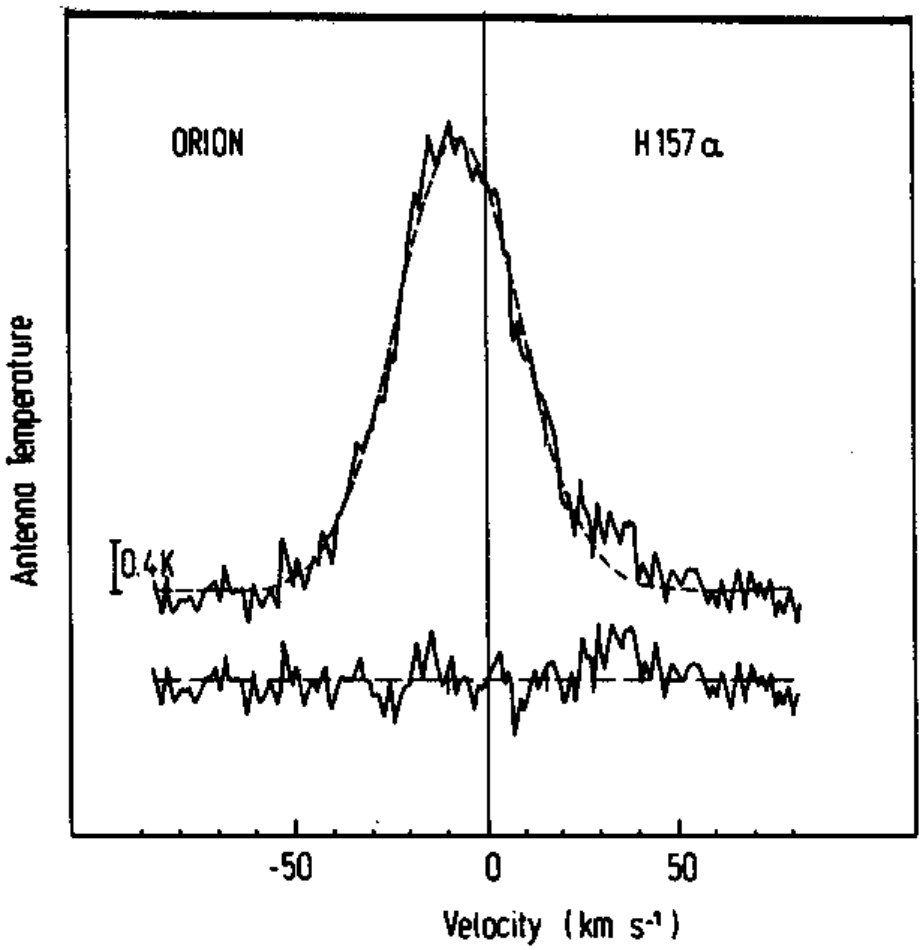

See Fig.22 for the corresponding theoretical profile.

Fig.22:

Theoretical H157a- line profile due to Stark broadening in a plasma of density $N_p=2\cdot10^3 cm^{-3}$.

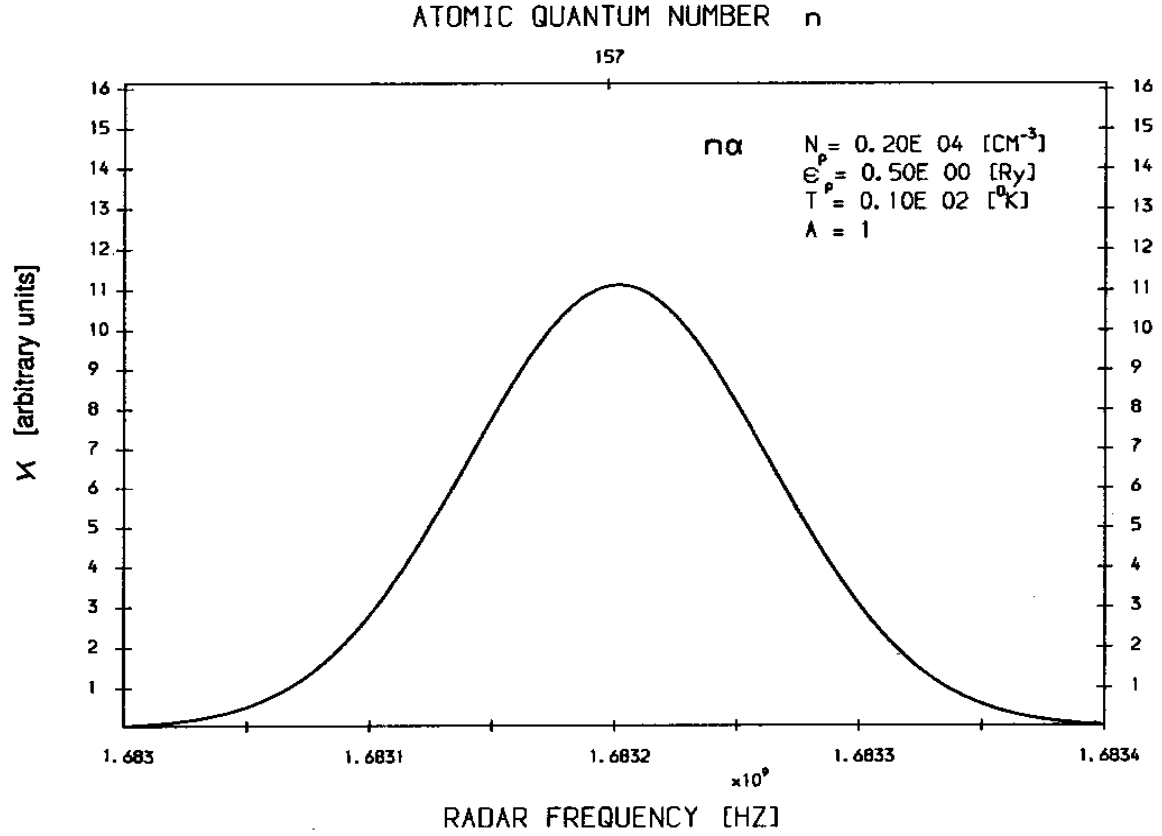

See Fig.21 for the corresponding experimental profile.

Fig.23:

Scattering coefficient for a plasma density $N_p=10^5 cm^{-3}$ and a solar radio flux corresponding to a strong ('Type IV', see Fig.10) **solar burst** ($F_{sol}^{Burst}=1$; compare to the quiet conditions ($F_{sol}^{Burst}=0$) of Fig.12) .

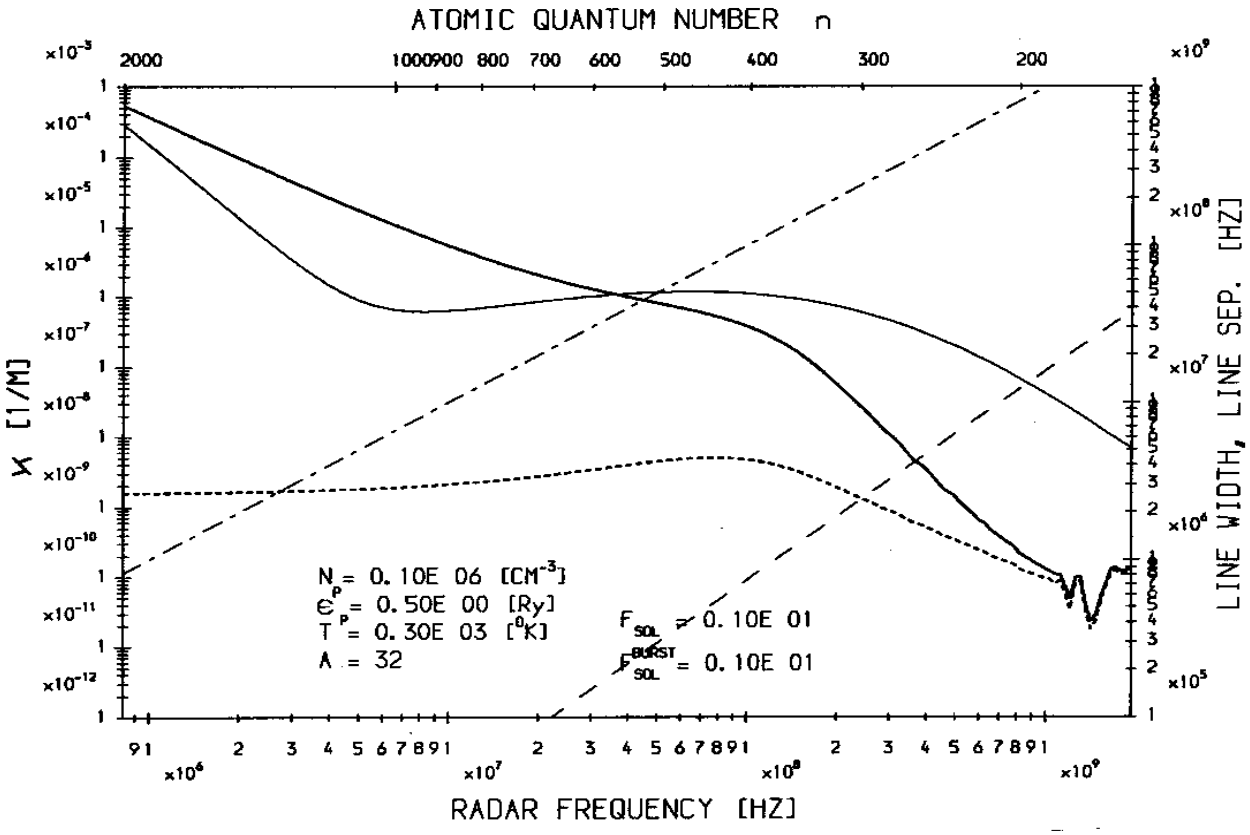

See Fig.24 for the corresponding result for a plasma density $N_p=10^4 cm^{-3}$.

Scattering of Radio Waves by High Atomic Rydberg States

Fig.24:

Scattering coefficient for a plasma density $N_p=10^4 cm^{-3}$ and a solar radio flux corresponding to a strong ('Type IV', see Fig.10) **solar burst** ($F_{sol}^{Burst}=1$; compare to the quiet conditions ($F_{sol}^{Burst}=0$) of Fig.11) .

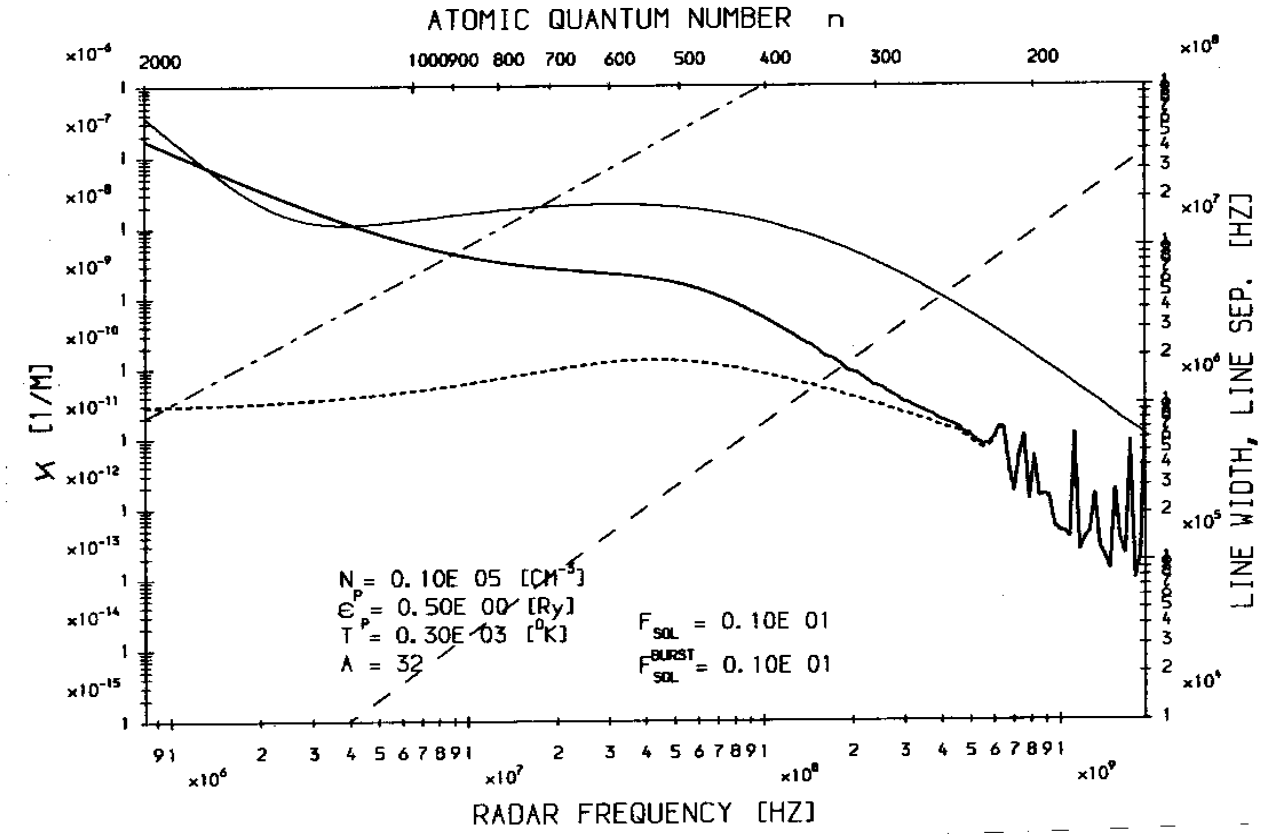

See Fig.23 for the corresponding result for a plasma density $N_p=10^4 cm^{-3}$.

Fig.25:

Experimental measurements of the enhancement of the solar radio flux at various frequencies during a strong solar burst and the simultaneous fading of a short wave signal transmitted over the ionosphere (after Unsöld (1955), p.744).

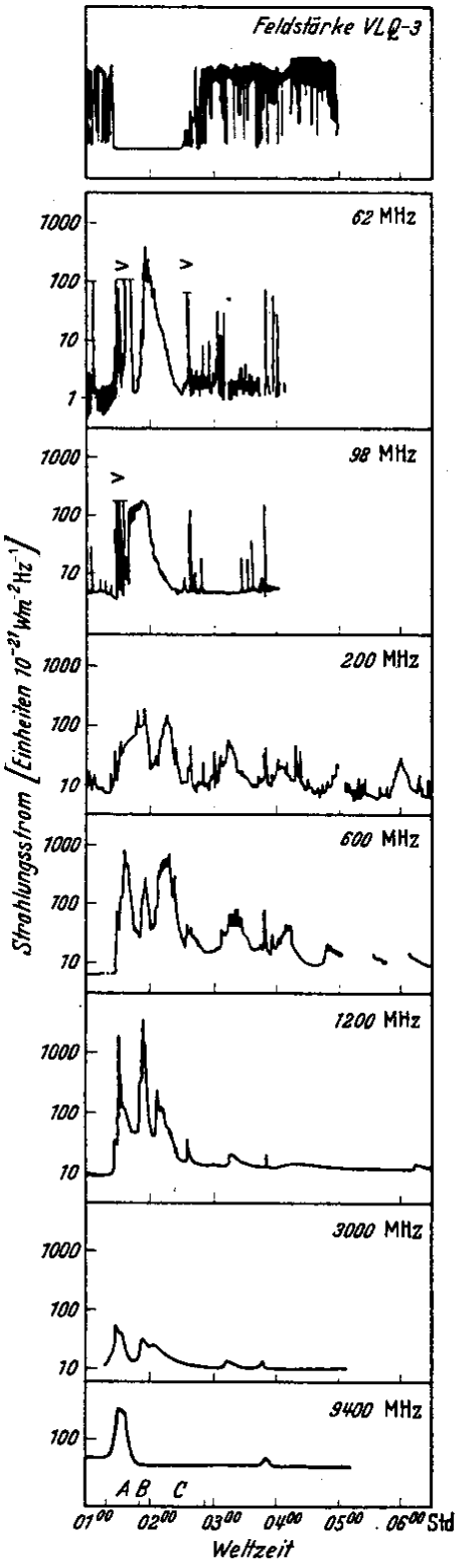

Scattering of Radio Waves by High Atomic Rydberg States

Fig.26:

Scattering coefficient for a plasma density $N_p=10^5 cm^{-3}$ and quiet solar conditions (that is, corresponding to Fig.12) but **an additional (artificial) radio flux** at 35 GHz with a field strength of 0.2 V/m.

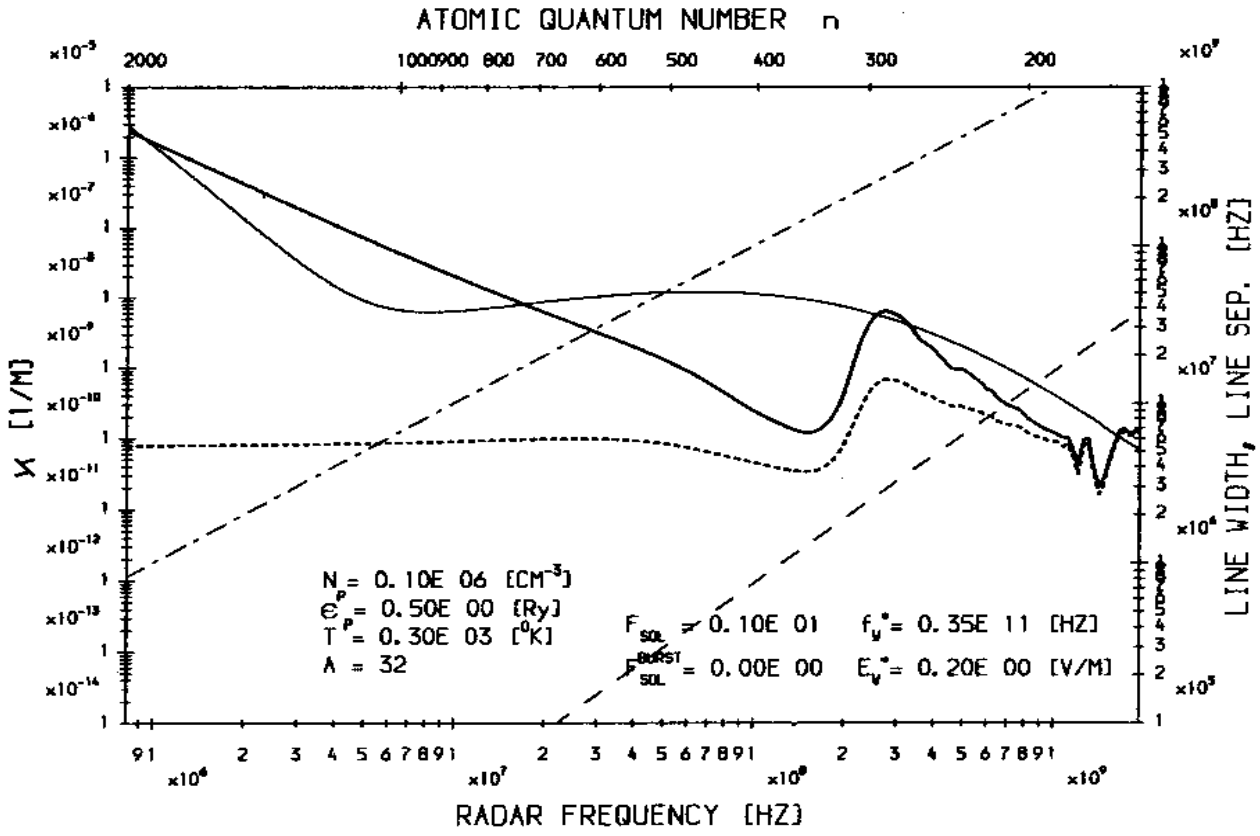

See Fig.27 for the corresponding atomic level population..

Fig.27:

Reduction of the level population N_n (thin solid curve), left ordinate) for states n=300 **due to the ionizing microwave flux considered for** Fig.26 and the related decrease of the effective density $N_{eff}(f)$ (thick solid curve) (the small scale variation of N_n for n=300 is not real but a numerical effect) (compare to the undisturbed case shown in Fig.18 which also gives a full explanation of the curves and scales).